2004

Quantum chemistry, an eclectic mix: from silicon carbide to size consistency

Jamie Marie Rintelman
Iowa State University

Quantum chemistry, an eclectic mix: from silicon carbide to size consistency

by

Jamie Marie Rintelman

A dissertation submitted to the graduate faculty

in partial fulfillment of the requirements for the degree of

DOCTOR OF PHILOSOPHY

Major: Physical Chemistry

Program of Study Committee:
Mark S. Gordon, Major Professor
Patricia Thiel
James Evans
Nicola Pohl
Gordon Miller

Iowa State University

Ames, Iowa

2004

Graduate College
Iowa State University

This is to certify that the doctoral dissertation of

Jamie Marie Rintelman

has met the dissertation requirements of Iowa State University

Signature was redacted for privacy.
Committee Member

Signature was redacted for privacy.
Committee Member

Signature was redacted for privacy.
Committee Member

Signature was redacted for privacy.
Committee Member

Signature was redacted for privacy.
Major Professor

Signature was redacted for privacy.
For the Major Program

TABLE OF CONTENTS

CHAPTER 1. GENERAL INTRODUCTION 1

CHAPTER 2. STRUCTURE AND ENERGETICS OF THE SILICON CARBIDE CLUSTERS SiC_3 AND Si_2C_2 8

CHAPTER 3. ADSORPTION OF ACETYLENE ON SI(100)-(2×1) 35

CHAPTER 4. MULTI-REFERENCE SECOND-ORDER PERTURBATION THEORY: HOW SIZE CONSISTENT IS "ALMOST SIZE CONSISTENT"? 63

CHAPTER 5. EXCHANGE REPULSION IN THE GENERAL EFFECTIVE FRAGMENT POTENTIAL (EFP) METHOD 83

CHAPTER 6. GENERAL CONCLUSIONS 104

ACKNOWLEDGMENTS 106

CHAPTER 1: GENERAL INTRODUCTION

Chemistry is a field of great breadth and variety. It is this diversity that makes for both an interesting and challenging field. My interests have spanned three major areas of theoretical chemistry: applications, method development, and method evaluation. The topics presented in this thesis are as follows: (1) a multi-reference study of the geometries and relative energies of four atom silicon carbide clusters in the gas phase; (2) the reaction of acetylene on the Si(100)-(2x1) surface; (3) an improvement to the Effective Fragment Potential (EFP) solvent model to enable the study of reactions in both aqueous and nonaqueous solution; and (4) an evaluation of the size consistency of Multireference Perturbation Theory (MRPT). In the following section, I briefly discuss two topics central to, and present throughout, this thesis: Multi-reference methods and Quantum Mechanics / Molecular Mechanics (QM/MM) methods.

Computational section

a. Multi-Reference Methods:

When molecular bonding cannot be described by one simple Lewis dot structure, that is, several resonance structures are required, a single configuration or single reference wave function is no longer appropriate, since each Lewis structure corresponds to a different arrangement of electrons (electronic configuration). In such cases, the use of many configurations, or a multi-reference wave function, is demanded.

The exact wave function is provided by full configuration interaction (Full-CI)[1], which includes all possible excitations of electrons. This approach gives the exact energy for a chemical system within a given atomic basis set. While this is the most reliable method available, it is impractical in all but the smallest cases since the computational effort grows factorially with the size of the system.

MCSCF. Fortunately, many chemical situations are dominated by a handful of important configurations. However, the suitability of the chosen configurations is critically dependent on the quality of the orbitals used to construct them. The multi-configuration self-consistent field (MCSCF) wave function is the most reliable method in these situations since it permits

both the orbitals and the CI coefficients to be optimized together. Two further problems arise when specifying the configurational space for a problem: 1) it may be tedious to list them all, 2) it may not be easy to predict which will be important. Several automatic methods for generating the list of configurations have been devised. Notable among these is the fully optimized reaction space MCSCF (FORS-MCSCF) method due to Ruedenberg and co-workers[2].

The FORS-MCSCF (alternatively called complete active space SCF, or CASSCF [3]) method aims to capture the flexibility of Full-CI without its expense by restricting the so-called *active* orbitals, those that generate the configurations, to just those involved in the chemical process of interest. With a suitable choice of active orbitals and electrons, collectively referred to as the *active space*, it is possible to describe changes in chemical bonding smoothly through all molecular conformations. The chief advantage of FORS-MCSCF is that it reduces the problem of choosing configurations to one of choosing an active space. However, once the active space is defined, the problem of finding a suitable set of starting orbitals still remains. Moreover, like Full-CI, the expense of FORS-MCSCF grows factorially with the size of the active space.

Though the FORS-MCSCF wave function can provide qualitatively correct descriptions of electronic structure, it is less suited to accounting for the instantaneous effects of electron correlation that bring about a quantitative improvement in the wave function and its properties. Such effects may be described by excitations outside the active space and are sometimes referred to as dynamic or external correlation.

1) Choice of Active Space. In general, the active space must be tailored to each specific problem. A consideration of such chemically intuitive matters as valence electrons, bonding orbitals, lone pairs, and so on, is only one part of active space selection. The biggest problem usually comes from the practical matter of generating starting orbitals from a preliminary calculation, often Hartree-Fock, and then choosing from these, the orbitals which encompass the relevant chemistry. Constructing the active space is usually cited as the reason MCSCF is not more popular. In response to this, new approaches to generating active orbitals are being developed which are intuitive and based on the orbitals of the separated atoms[4].

2) Factorial Problem. The computational cost of the FORS-MCSCF problem grows factorially with the active space, presenting a significant bottleneck to accessing larger problems. However, recent progress in theory and algorithm development may offer solutions. One solution is to exploit the explosive growth in parallel supercomputing, particularly if the data storage demands can be distributed[5,6]. Much larger Full-CI problems become feasible if the aggregate memory of many thousands of processors can be harnessed[7].

   On the other hand, rather than attempt the full problem, one may consider breaking it down into several smaller ones that are more manageable. This forms the basis of the occupationally restricted multiple active space (ORMAS) method. ORMAS allows more than one active space to be defined, such that the active subspaces interact via a restricted set of excitations between them[8].

3) Dynamic correlation. Finally, two general approaches to incorporating dynamic correlation involve applying second order perturbation theory, or truncated CI expansions, to the already multi-reference FORS-MCSCF wave function. Multi-reference perturbation theory (MRPT) is neither variational nor size consistent, but it is computationally efficient and has been shown to give good results while requiring resources that are comparable to that of the FORS-SCF itself. Multi-reference singles and doubles CI (MR(SD)CI)[9], on the other hand, is variational, but not size consistent, as is the case with any truncated CI. MRCI yields very accurate results, but at considerably greater computational expense than MRPT. Thus, MRPT has proved to be a popular method for determining barrier heights and relative energies.

Multi-reference Perturbation Theory. MRPT is not uniquely defined, and several 'flavors' have emerged. The most well known are CASPT2[10], MROPT[11], MRMP2[12], and MCQDPT2[13]. It is notable that while energies produced by the various methods differ, relative energies are very close. We concern ourselves with MCQDPT2. MCQDPT is a multi-state theory, equivalent to MRMP2 when applied to a single state. It is used both as a single- and multi-state theory in this thesis. When applied to multiple states it belongs to the so-called 'perturb-then-diagonalize' class of methods (in contrast to other methods described as 'diagonalize-then-perturb'), that is, perturbation theory is first applied to an

'effective' Hamiltonian. A subsequent diagonalization of the effective Hamiltonian has the additional advantage of guaranteeing that unwanted interactions between states of the same symmetry, such as 'avoided crossings', are avoided.

Given the success of MRPT methods, it would seem worthwhile to assess whether their lack of size extensivity and size consistency has any affect on the results. Surprisingly, beyond the liberal use of the phrase 'almost size consistent'[14], the literature is largely silent on this topic. Thus, we are motivated toward a systematic study of exactly how significantly MRMP deviates from size consistency. Our results are striking (see Chapter 4).

b. QM/MM

i. SIMOMM

The calculations on the reaction of acetylene on the Si(100)-(2x1) surface were performed using the surface integrated molecular orbital/molecular mechanics (SIMOMM) method. SIMOMM is an extension of the integrated molecular orbital molecular mechanics (IMOMM)[15] method. The SIMOMM method removes all user imposed constraints on bond lengths and angles present in the IMOMM method. This degree of flexibility is critical to studying the silicon surface.

SIMOMM was developed with an important principle in mind: while edge effects, or the errors introduced by removing the steric constraints of a bulk solid, are important to avoid, chemical reactions are local. Because of this locality, a 'bulk' region not far from the reaction may be approximated very cheaply with insignificant loss of accuracy.

SIMOMM is implemented in the quantum chemistry package GAMESS[5,14,16] (General Atomic and Molecular Electronic Structure System). The user defines an ab initio region where the 'chemistry' is occurring. The ab initio wave function describes the bond breaking or forming region, and is surrounded by a molecular mechanics region that accounts for bulk behavior. The geometries of both regions are fully optimized, by computing the gradients of each region in the traditional way, and then summing and minimizing the forces.

ii. Effective Fragment Potential (EFP)

The EFP method[17] is a discrete solvent/liquid model that was originally developed and implemented as a potential for water in order to study aqueous solvation. The success of this implementation prompted the development of a generalized version enabling a potential for any molecule, from a single ab initio calculation or a small number of calculations for very large molecules, to be generated.

Although it is a classical potential, the EFP method has its roots in quantum mechanics. The original method, EFP1, contains terms that represent Coulomb, polarization, and exchange repulsion+charge transfer, as well as higher order effects. The Coulomb and polarization terms can be generated from a single ab initio calculation, and thus any parameters in these terms can be stored and used as needed or generated on the fly. The exchange repulsion + charge transfer and higher order terms (remainder term) are obtained by fitting to the potential generated from a number of calculations on the water dimer. All of these effects are added as one-electron terms to the ab initio Hamiltonian. There are currently two additional implementations of the EFP1 method, one based on density functional theory (DFT)[18] and a second based on second order Moeller-Plesset Perturbation theory (MP2)[19]. These methods both include dynamic correlation effects and are therefore more accurate, though they still require fitting of the remainder term.

The work in this thesis concerns the extension of the EFP method to replace a fitted repulsion term with an approximate analytical term, thereby avoiding the inconvenience of a fitting procedure. In the original EFP1 method, the fitted term was considered a 'remainder', since it incorporated all effects not accounted for in the Coulomb and polarizability terms (and the dispersion term in the MP2-EFP implementation). Thus, more than one term is needed to include all of the remaining effects, of which exchange repulsion is the dominant contribution, followed by charge transfer. This thesis describes the coding and testing of the approximate exchange repulsion interaction term between the EFP and ab initio regions.

References:

1 C. W. Bauchlicher, S. R. Langhoff, and P. R. Taylor, Advances in Chemical Physics **77**, 103 (1990); S. Boys, Advances in Chemical Physics **A201**, 125 (1950); I. Shavitt, in *Modern Theoretical Chemistry*, edited by H. F. Schaefer III (Plenum Press, New York, 1977), Vol. 3, pp. 189.

2 K. Ruedenberg, M. W. Schmidt, M. M. Gilbert, and S. T. Elbert, Chemical Physics **71** (1), 41 (1982).

3 B. O. Roos, P. Taylor, and P. E. Siegbahn, Chemical Physics **48**, 157 (1980).

4 W. C. Lu, C. Z. Wang, M. W. Schmidt, L. Bytautas, K. M. Ho, and K. Ruedenberg, Journal of Chemical Physics **120** (6), 2629 (2004); W. C. Lu, C. Z. Wang, M. W. Schmidt, L. Bytautas, K. M. Ho, and K. Ruedenberg, Journal of Chemical Physics **120** (6), 2638 (2004).

5 G. D. Fletcher, M. W. Schmidt, B. M. Bode, and M. S. Gordon, Computer Physics Communications **128** (1-2), 190 (2000).

6 G. D. Fletcher, M. W. Schmidt, and M. S. Gordon, Advances in Chemical Physics **110**, 267 (1999).

7 Z. T. Gan, Y. Alexeev, M. S. Gordon, and R. A. Kendall, Journal of Chemical Physics **119** (1), 47 (2003).

8 J. Ivanic, Journal of Chemical Physics **119** (18), 9377 (2003).

9 H.-J. Werner, Advances in Chemical Physics **69**, 1 (1987).

10 B. O. Roos, K. Andersson, M. K. Fulscher, P.-A. Malmqvist, L. Serrano-Andres, K. Pierloot, and M. Merchan, Advances in Chemical Physics **93**, 219 (1996).

11 P. M. Kozlowski and E. R. Davidson, Journal of Chemical Physics **100**, 3672 (1994).

12 K. Hirao, Chemical Physics Letters **190**, 374 (1992); K. Hirao, Chemical Physics Letters **196**, 397 (1992); K. Hirao, International Journal of Quantum Chemistry **S26**, 517 (1992); K. Hirao, Chemical Physics Letters **201**, 59 (1993).

13 H. Nakano, Journal of Chemical Physics **99** (10), 7983 (1993); H. Nakano, Chemical Physics Letters **207**, 372 (1993).

[14] H. A. Witek, H. Nakano, and K. Hirao, Journal of Chemical Physics **118** (18), 8197 (2003).

[15] F. Maseras and K. Morokuma, Journal of Computational Chemistry **16**, 1170 (1995).

[16] M. W. Schmidt, K. K. Baldridge, J. A. Boatz, S. T. Elbert, M. S. Gordon, J. H. Jensen, S. Koseki, N. Matsunaga, K. A. Nguyen, S. J. Su, T. L. Windus, M. Dupuis, and J. A. Montgomery, Journal of Computational Chemistry **14** (11), 1347 (1993).

[17] P. N. Day, J. H. Jensen, M. S. Gordon, S. P. Webb, W. J. Stevens, M. Krauss, D. Garmer, H. Basch, and D. Cohen, Journal of Chemical Physics **105** (5), 1968 (1996); M. S. Gordon, M. A. Freitag, P. Bandyopadhyay, J. H. Jensen, V. Kairys, and W. J. Stevens, Journal of Physical Chemistry A **105** (2), 293 (2001); W. Chen and M. S. Gordon, Journal of Chemical Physics **105** (24), 11081 (1996).

[18] I. Adamovic, M. A. Freitag, and M. S. Gordon, Journal of Chemical Physics **118** (15), 6725 (2003).

[19] J. Song and M. S. Gordon, in preparation; C. Moller and S. Plesset, Phys. Rev. **46**, 618 (1934).

CHAPTER 2: STRUCTURE AND ENERGETICS OF THE SILICON CARBIDE CLUSTERS SIC_3 AND SI_2C_2

A paper published in the *Journal of Chemical Physics*

Reprinted with permission. *Journal of Chemical Physics* **2001,** *115*, 1795.

Jamie M. Rintelman and Mark S. Gordon

Abstract

A comprehensive *ab initio* study of the four atom silicon carbide clusters SiC_3 and Si_2C_2 using multiconfigurational self-consistent field wave functions is presented. In contrast to previous studies the global minimum isomer for SiC_3 is predicted to be a $C_{\infty v}$ linear triplet with a terminal silicon atom. For Si_2C_2 the global minimum is a rhombic structure, in accordance with previous studies, while the linear triplet Si-C-C-Si is just 1.0 kcal·mol^{-1} higher in energy.

I. Introduction

Understanding the reactivity of silicon carbide under extreme environments is of current interest. In order to understand the properties of such a material it is useful to study smaller clusters of the bulk material. Information on the nature of bonding and electronic structure can be gained when studying these smaller units at a level of theory that would not be possible for the bulk material. Such calculations then provide a baseline for future calculations on larger species. This is the focus of the present study.

The work presented in this paper has been additionally stimulated by recent experiments performed by the Lineberger group, who are studying silicon carbide clusters of three to ten atoms. Because the recent experiments by Lineberger, Davico and Schwartz[1] find primarily carbon-dominated species, SiC_3 and Si_2C_2 are considered here. In order to compare

fully with the results of the photodetachment experiments it will ultimately be necessary to look at both the neutral and anion species. This paper presents results for the neutral species.

There have been a number of previous studies of SiC_3 and Si_2C_2, all of which used single reference wave functions. Albers, Grev and Schaefer studied SiC_3 using configuration interaction with single and double excitations (CISD) at Hartree Fock geometries [2]. They found the lowest energy isomer to be a singlet rhombic C_{2v} structure with the silicon terminated linear $^3\Sigma^-$ structure 4.1 kcal·mol^{-1} higher and a second rhombic C_{2v} structure 4.3 kcal·mol^{-1} higher than the global minimum (Fig. 1). In 1997, Gomei et. al. conducted a study of SiC_n clusters [3]. They also found a C_{2v} rhombic structure to be the SiC_3 global minimum at the CCSD(T)/aug-cc-pVDZ//MP2/6-31G(d) level of theory with the $^3\Sigma^-$ silicon terminated linear isomer 6.9 kcal·mol^{-1} higher. Hunsiker and Jones examined mixed silicon carbide clusters using density functional theory (DFT) and found the SiC_3 global minimum again to be the singlet rhombic structure, with the linear triplet and second rhombic structure just 0.2 and 1.8 kcal·mol^{-1} higher, respectively [4].

Trucks and Bartlett performed SDTQ-MBPT[4] calculations on Si_2C_2 [5], and later Fitzgerald and Bartlett performed MBPT(4) calculations [6]. Both studies found the D_{2h} rhombic structure to be the global minimum with a silicon terminated linear $^3\Sigma_u^-$ isomer ~12 kcal·mol^{-1} higher (12.3 and 11.9 kcal·mol^{-1} respectively). The second study, however, also located a distorted trapezoid 4.0 kcal·mol^{-1} above the global minimum. Lamertsma et al's MP2 study of Si_2C_2 located the same rhombic ground state with the distorted trapezoid 10.1 kcal·mol^{-1}and the $^3\Sigma_u^-$ structure 15.5 kcal·mol^{-1} higher than the global minimum [7]. Hunsiker and Jones' DFT study found the same ordering although the three isomers were found to be closer in energy [4]. The Hunsiker and Jones results indicate that the distorted trapezoid and $^3\Sigma_u^-$ isomers are just 4.2 kcal·mol^{-1} and 8.3 kcal·mol^{-1} above the global minimum, respectively. Presilla-Márquez et al optimized the rhombic global minimum structure with CCSD(T) and found its energy to be 6.5 kcal·mol^{-1} lower than the distorted trapezoid and 7.7 kcal·mol^{-1} lower than the linear triplet, with single points for the latter two structures calculated using CCSD(T) at the MBPT(2) optimized structures [8].

Because all of the previous calculations were performed with single reference wave functions, some potentially low-lying states were not studied. In this paper we present the

results of a comprehensive *ab initio* study of the SiC_3 and Si_2C_2 systems utilizing a multiconfigurational self consistent field (MCSCF) wave function. Energies, equilibrium geometries, and vibrational frequencies are presented for each isomer. We also evaluate the need for the application of a multireference wave function in this investigation.

II. Computational Details

(a) Basis Set. In this investigation the 6-31G(d) basis set[9] was used for all geometry optimizations. Future calculations on anion structures are planned. Therefore, in the interest of using a consistent basis set throughout, the aug-cc-pVDZ basis [10-12] was chosen. This basis set includes necessary diffuse functions, yet remains tractable enough to apply to these systems. This basis set was used in calculating single point energies subsequent to geometry optimization.

(b) Wave functions. A fully optimized reaction space (FORS)-MCSCF wavefunction [13-15] (also referred to as CASSCF [16]) was used as the reference function for all calculations in this study. An active space of 12 electrons in 10 orbitals was used for geometry optimization of nonlinear structures and a 12 electrons in 11 orbitals active space was used for geometry optimization of all linear structures. This difference in active space is necessary in order to include all eight π orbitals formed by all combinations of valence p_x and p_y orbitals on silicon and carbon. As will be discussed later, the calculation and inspection of natural orbital occupation numbers (NOONs) for each isomer confirms this choice. For single point energies the larger (12,11) active space was used for all species.

In the case of the linear species studied here, it is impossible to represent the correct singlet wave function without including at least two determinants. Because the highest occupied molecular orbital (HOMO) and lowest unoccupied molecular orbital (LUMO) are degenerate π MOs, the correct wave function must include partial and equal occupation of each of these orbitals. This is true of both the $^1\Sigma_g^+$ and $^1\Delta_g$ states of Si_2C_2 and the $^1\Sigma^+$ and $^1\Delta$ states of SiC_3. Due to these group theoretical considerations, it is necessary to use a multi-determinant description in order to construct a qualitatively correct wavefunction for the linear singlet species. It is straightforward to determine that this is an even-odd phenomenon,

that is, at least two configurations will be necessary to construct a wavefunction for the singlet species of any linear silicon carbide cluster constructed from an even number of atoms. Likewise a similar approach is required when describing a linear triplet silicon carbide cluster containing an odd number of atoms. One can determine this by considering the bonding using a minimal basis model. In the case of four atom clusters there are 16 valence electrons, 10 of which reside in either σ or lone pair orbitals. The remaining six electrons must reside in π orbitals. Since each π orbital is one of a degenerate pair of orbitals, the first four π electrons go in the two fully bonding (no nodes) π orbitals. The next two must go into a degenerate pair of orbitals, so that to construct a correct singlet wave function one must include a combination of $(\pi_{xz}^2 + \pi_{yz}^0)$ and $(\pi_{xz}^0 + \pi_{yz}^2)$. Of course, this applies only to fully unsaturated species.

Generally, for a given spin and symmetry, only the lowest electronic state is considered for each isomer.

(c) Methods. Starting with preliminary Hartree Fock structures, geometry optimizations were performed using a 12 electrons in 10 orbitals (11 orbitals for linear structures) FORS – MCSCF wavefunction with the 6-31G(d) basis set[9]. Unless otherwise stated any discussion of optimized structures or nature of stationary points implies this level of theory. Some structures with very high energies (e.g., structures **2a**, **6a**, **2b** in Figures 1 and 2) were optimized with only a six electrons in six orbitals active space. Stationary points were characterized by the calculation and diagonalization of the energy second derivative matrix (hessian). No negative eigenvalues indicates a minimum on the potential energy surface, one negative eigenvalue indicates a transition state, and more than one negative root indicates a higher order saddle point of little chemical interest.

External correlation effects (sometimes referred to as dynamic correlation effects) were included by carrying out second order multiconfigurational quasi degenerate perturbation theory (MCQDPT) [17] calculations at the MCSCF (12,10 or 12,11) optimized geometries. For these single point calculations the aug-cc-pVDZ basis set was used[10-12].

All calculations were done using the electronic structure code GAMESS [18,19].

III. Results and Discussion

For both the SiC_3 and the Si_2C_2 system all structures considered chemically reasonable and interesting were investigated and optimized. Each isomer was then characterized as a minimum, transition state, or higher order stationary point. Results are presented first for SiC_3 followed by results for Si_2C_2. Each isomer is given an alphanumeric label. The number refers to the geometric structure; an 'a' or 'b' designates SiC_3 or Si_2C_2, respectively; and 's' and 't' refer to singlet and triplet spin states, respectively.

SiC_3. Six basic structures were optimized and identified as stationary points on the SiC_3 potential energy surface (PES). Geometries are shown in Figure 1. Vibrational frequencies can be found in Table 1. All energies, summarized in Table 2, are given in relation to 1ta, the SiC_3 global minimum, unless otherwise stated.

Linear. There are two possible linear ($C_{\infty v}$) SiC_3 isomers, for which $^1\Sigma^+$, $^1\Delta$, and $^3\Sigma^-$ states can be calculated. These linear isomers differ in the location of the Si, either terminal (**1a**) or internal (**2a**). Since unsaturation at C is preferred, and silylenes are more stable than carbenes, **1a** is likely to be lower in energy than **2a**.

2a. The FORS(12,11)/6-31G(d) energy of the $^3\Sigma^-$ state of isomer **2a** is very high (86 kcal·mol^{-1}) at the FORS(6,6) geometry [FORS(12,11)/6-31G(d)//FORS(6,6)/6-31G(d)]. The energies of the $^1\Sigma^+$and $^1\Delta$ states are 101 kcal·mol^{-1} and 104 kcal·mol^{-1}, respectively, at the triplet geometry using the same level of theory described above. Because of the high energies of these species, they are not discussed further.

1a. More important than isomer **2a**, from an energetic point of view, is the silicon terminated linear isomer **1a**. The $^3\Sigma^-$ state, **1ta**, is a minimum on the FORS(12,11)/6-31G(d) potential energy surface. In fact, it is the global minimum among all SiC_3 isomers at the MCQDPT(12,11)/aug-cc-pVDZ// MCSCF(12,11)/6-31G(d) level of theory. Examination of natural orbitals and bond lengths indicates a strong double bond between each pair of carbons. The internal C-C bond (1.29Å) is slightly shorter than the terminal C-C bond (1.31 Å) [20]. Likewise, the C-Si bond length of 1.74 Å is comparable to the double bond length of 1.69Å in silene [21].

In the $^3\Sigma^-$ state the unpaired electrons are in degenerate π orbitals. These orbitals have a node between the two central carbons, and bonding interaction between the terminal

carbon and its nearest neighbor carbon and between the terminal silicon and its nearest neighbor carbon.

Examination of NOONs reveals considerable electron density outside those orbitals which would be occupied in the Hartree-Fock reference (for the sake of brevity, in subsequent discussions we will refer to this as "outside the HF reference"). The first two such orbitals are degenerate π orbitals with two nodes and bonding interactions between the two middle carbons. The corresponding NOONs are both 0.097. It is likely that this makes a contribution to the strength of this central C-C bond. The remaining two active orbitals are a degenerate pair of completely antibonding π orbitals. The corresponding NOONs are both 0.044. Thus the total deviation from the RHF reference is 0.282 electrons.

Hund's rule predicts the triplet to be lower in energy than the singlet, and our results are consistent with that prediction. However, since singlet configurations, $^1\Sigma^+$ and $^1\Delta$, have energies within 11 kcal·mol^{-1} of the triplet state, it is important to consider these two singlet states. In the $^3\Sigma^-$ state, the two unpaired electrons are in degenerate π orbitals, π_x and π_y. To generate a singlet spin state the electrons must be paired, and will occupy a degenerate pair of π orbitals. Therefore, one must use a minimum of two determinants to correctly describe the qualitative nature of the singlet states. Conceptually, the $^1\Sigma^+$ state can be characterized by the orbital occupation ($\pi_x^0\,\pi_y^2 + \pi_x^2\,\pi_y^0$), the two dominant determinants. The $^1\Delta$ state consists of two degenerate states ($\pi_x^0\,\pi_y^2 - \pi_x^2\,\pi_y^0$) and $\pi_x^1\,\pi_y^1$ such that in the latter the electrons are singlet coupled. The $^1\Sigma^+$ and $^1\Delta$ energies are 9.3 kcal·mol^{-1} and 10.6 kcal·mol^{-1}, respectively, above the $^3\Sigma^-$ global minimum at the MCQDPT/ aug-cc pVDZ//CASSCF / 6-31G(d) level. All subsequent SiC_3 energies are likewise given in reference to the above-mentioned global minimum (1ta $^3\Sigma^-$). The geometries of the linear singlets differ only slightly from the geometry of the triplet.

Four membered ring. Isomers **3a** and **4a** (Fig. 1) have very similar four membered ring structures. Conceptually, they can be interconverted simply by lengthening the transannular C-C bond while simultaneously shortening the transannular carbon-silicon bond. The bond stretch isomerism of these two species has been examined in depth in a previous study [22].

3a. Both singlet and triplet states were examined for isomer **3a**. The $^1A_1$ structure is lower in energy than the $^3B_2$ structure by 21.9 kcal·mol^{-1}. The transannular C-C bond is slightly shorter in the $^1A_1$ structure (1.46Å) than in the $^3B_2$ structure (1.53Å). The two equivalent C-C bonds are slightly longer in the singlet (1.42Å) than in the triplet (1.35Å), while the two equivalent C-Si bonds are shorter in the singlet (1.82Å) than in the triplet (1.95Å). Relative energies (Table 2) for **3sa** and **3ta** are 4.4 kcal·mol^{-1} and 26.2 kcal·mol^{-1} above the global minimum, respectively.

4a. Structure **4a** is related to **3a** by a lengthening of the C-C bond, and a corresponding shortening of the Si-C transannular bond. In **4ta** the singly occupied orbitals are b_1 and a_2 giving a $^3B_2$ state.

It has been proposed [2] that **4a** can be viewed as a silicon atom complexed to a linear C_3 unit. While the C-C-C bond angles of 154.9° and 138.1° for **4sa** and **4ta**, respectively, may suggest this, examination of natural orbitals, and the corresponding density matrix over active MCSCF orbitals gives no indication of this type of bonding situation. For both the $^1A_1$ and $^3B_2$ states silicon participates in σ bonding with each of the three carbons, with the majority of the remaining electron density around silicon located in a lone pair orbital. There is a bonding π orbital on the C_3 unit that has no bonding overlap with the π orbital or the σ lone pair orbital on silicon.

The C-C bonds are intermediate between single and double bonds in both **4sa** and **4ta**. The transannular C-Si bond length in **4sa** indicates single bonding, while peripheral C-Si bond lengths indicate weak single bonding [23]. In **4ta**, however, the three C-Si bonds are almost equivalent, with the transannular bond only .02 Å longer than the peripheral C-Si bonds. The MCSCF bond order analysis[24,25] is consistent with this picture. The three C-Si bond orders are virtually identical for **4ta** (0.691, 0.691, and 0.684), while in **4sa** the transannular Si-C bond is a bit stronger than the peripheral Si-C bonds (0.736, 0.595, and 0.595).

4sa and **4ta** are very close in energy, 7.8 and 5.9 kcal·mol^{-1} above the global minimum, respectively.

Three membered ring structures. Two C_{2v} structures containing one three membered ring were examined. Isomer **5a** (Fig. 1) consists of a ring of three carbons with a silicon bonded to one of the vertices. Isomer **6a** has a ring containing two carbons and one silicon with an exocyclic carbon bonded to the silicon.

5a and 6a. Both the $^1A_1$ and $^3A_2$ states of isomer **6a** are very high in energy ($^1A_1$ 103.4 kcal, $^3A_2$ 82.1 kcal) at the MCQDPT(12,10)/6-31G(d) level. Thus, this isomer was not examined extensively for quantitative information on energetics. Clearly it is not relevant in a search for the most stable isomers, those isomers most likely to be observed experimentally; however, when seeking to understand the characteristics of the most stable clusters, it is helpful to contrast these with the properties of the least stable structures. Note that isomer **5a** maximizes C-C bonding while minimizing Si-C bonding. Isomer **6a** represents the three-membered ring structure with the maximum possible number of Si-C bonds and the minimum possible number of C-C bonds (one). Since silicon avoids multiple bonding, it is not surprising that the π bond in **6a** is located almost completely between the two equivalent carbons of the ring, whereas in isomer **5a**, the analogous π bond is much more delocalized throughout the ring. In **5a** the $^1A_1$ energy is 25.2 kcal·mol^{-1}, while that of the triplet is 30.8 kcal·mol^{-1}.

SiC_3 Relative Energies. The lowest energy isomer is predicted to be the $^3\Sigma^-$ state of the linear molecule with a terminal silicon atom (Si-C-C-C). The $^1\Sigma^+$ and $^1\Delta$ states are both within 11 kcal·mol^{-1} of the global minimum, 9.3 and 10.6 kcal·mol^{-1} respectively. The linear isomer with an internal silicon atom is found to be much higher in energy. The second lowest energy structure, rhombic **3sa**, with a silicon at the vertex of the long axis, is 4.4 kcal·mol^{-1} above the global minimum. The previous CISD study by Alberts, Grev, and Schaefer [2] predicts the reverse order of the two lowest isomers. This may be due to the multi-configurational nature of these clusters, since these earlier calculations were done using single reference wave functions. The occupation numbers in the virtual orbitals for **3sa** are all greater than 0.05, with the largest being 0.076. Those for 1ta are (2x) 0.097 and (2x) 0.044. The singlet and triplet states of isomer **4a**, **4sa** and **4ta**, are also quite low in energy at 7.8 and 5.9 kcal·mol^{-1}, respectively (see Table 2).

Somewhat intermediate in energy, at 25.2 and 30.8 kcal·mol^{-1} are **5sa** and **5ta**. In the context of trends observed in this system this is most likely due to ring strain and Si-C multiple bonding.

High energy structures include singlet and triplet **6a** and **2a,** all at least 80 kcal·mol^{-1} above the global minimum. Isomer **6a** has the maximum number of Si-C bonds, with very little C-C bonding, and an exocyclic carbene. Isomer **2a** forces silicon to participate in π bonding, and also has an additional C-Si bond instead of a C-C bond, and a terminal carbene carbon.

Si_2C_2. Ten basic structures were optimized and identified as stationary points on the Si_2C_2 PES. Singlet and lowest energy triplet configurations were examined for all isomers when possible. Geometries are shown in Figure 2. Vibrational frequencies are presented in Table 3.

$D_{\infty h}$ structures. Two (linear) $D_{\infty h}$ isomers of Si_2C_2 have been considered. Isomer **1b** has two terminal silicon atoms, while in isomer **2b** the carbon atoms are terminal. Both isomers have $^3\Sigma_g^-$, $^1\Sigma_g^+$, and $^1\Delta$ states to be considered.

1b. The $^3\Sigma_g^-$ configuration of isomer **1b**, **1tb**, has an energy of 1.0 kcal·mol^{-1} relative to the rhombic global minimum. Before the addition of dynamic correlation via MCQDPT2, the $^3\Sigma_g^-$ state is lowest in energy; however, as is frequently the case, the addition of external correlation preferentially stabilizes the singlet with respect to the triplet.

A C-C bond length of 1.28 Å in **1tb** indicates that there is a double bond interaction between these two atoms [20]. The silicon-carbon bond length of 1.77Å also indicates a double bond [21]. The Mayer bond order analysis is consistent with this picture [19,24,25].

The $^1\Sigma_g^+$ and $^1\Delta$ states of **1b**, **1sb-Σ** and **1sb-Δ**, are just 8.9 and 5.8 kcal·mol^{-1}above the global minimum, respectively. Since Si_2C_2 and SiC_3 are isovalent, the electron occupations for linear singlet species are quite similar. The $^1\Delta$ state can be described schematically as having ($\pi_x^0\,\pi_y^2 - \pi_x^2\,\pi_y^0$) and $\pi_x^1\,\pi_y^1$ occupation in the HOMO and LUMO π orbitals, while **1sb-Σ** can be described by ($\pi_x^0\,\pi_y^2 + \pi_x^2\,\pi_y^0$).

Bond lengths in **1sb-Σ** and **1sb-Δ** are quite similar to those in **1tb**; the C-C bonds are the same length, 1.27 Å, while the C-Si bonds are slightly longer in the $^1\Sigma_g^+$ and $^1\Delta$ states (Fig. 2). Thus, bonds again appear to be double bonds.

2b. The calculated states of isomer **2b** are all significantly higher in energy ($\approx$ 200 kcal·mol^{-1}) than isomer **1b**. Thus, these states were not studied extensively. It is worthwhile to briefly consider the qualitative differences between **1b** and **2b**. Especially significant is the observation that in **2b** the silicons are forced to multiple bond with each other. This is highly unfavorable; the C-C multiple bonds in **1b** are preferred.

D_{2h} structures. The two D_{2h} structures considered in this investigation each consist of four membered rings of alternating silicons and carbons (Fig. 2). Isomer **5b** has a transannular C-C bond, and a long Si-Si distance. In isomer **7b**, the Si-Si bond is short, while the C-C bond distance is much longer than that of **5b**.

5b. The ^1A_g state of rhombic structure **5b** is a minimum on the PES.

The C-C bond in ^1A_g (**5sb**) is intermediate between typical single and double bond lengths at 1.48Å. In agreement with this, the Mayer bond order analysis indicates a C-C bond order of 1.45. The HOMO is a σ bonding orbital, between the two carbons, with additional electron density extending outside the ring from the two carbons. The HOMO-1 is a π bonding orbital with Mulliken populations indicating that approximately 80% of the electron density is located on the carbons. Additionally, there is a low lying σ orbital that is bonding throughout the molecule. These are the only orbitals contributing to C-C bonding in this molecule. Si-C bond distances are 1.82 Å, with bond orders of 1.061. The Si-Si distance is 3.33Å. Examination of NOONs shows 0.19 electrons outside the RHF reference for **5b** ^1A_g.

The lowest triplet state of isomer **5b**, $^3B_{1g}$, is 43.0 kcal·mol^{-1} above the $^1A_1$ state, the Si_2C_2 global minimum. $^3B_{1g}$ is also a minimum on the FORS(12,10)/6-31G(d) PES. The C-C bond distance is slightly shorter than that of the singlet, 1.44Å ($^1A_1$ = 1.48Å), while the Si-C bond distance is slightly longer at 1.86Å compared to 1.82Å in $^1A_1$.

7b. Relative to **5b** the second D_{2h} isomer, **7b**, has a longer C-C distance and a shorter Si-Si distance. Both the ^1A_g and the lowest triplet, ^3A_u, are rather high in energy; 76.8 and 47.3 kcal·mol^{-1} higher than the global minimum, respectively (Table 4).

The **7b** ^1A_g state (**7sb**) is a minimum on the PES. It is interesting to compare the **7b** ^1A_g π bonding MO with the analogous **5b** ^1A_g π MO. In **5b** ^1A_g this orbital is located

primarily between the two carbons; in **7b** ^1A_g, the electron density is almost equally distributed among all atoms.

Now consider the ^3A_u state of isomer **7b, 7tb**. Not only is **7tb** much lower in energy than **7sb**, there is also a significant change in geometry. The Si-Si bond distance is more than 0.5 Å longer in **7tb** than **7sb** (^1A_g 2.304, $^3B_{1g}$ 2.835Å) while the C-C distance is more than 0.5 Å shorter in the triplet than the singlet (^1A_g 2.967, $^3B_{1g}$ 2.329Å). Examination of molecular orbitals shows σ bonding between the carbons of **7tb**, whereas there is virtually no C-C σ bonding in **7sb**.

The $^3B_{1g}$ state is a transition state on the PES. When this structure is distorted along the imaginary normal mode, subsequent optimization leads to the $^3A_2$ state of C_{2v} symmetry (***10tb***).

C_{2v} structures. Four C_{2v} structures have been studied (Fig. 2). Two of these (**3b, 4b**) consist of three-membered rings with an exocyclic carbon or silicon. The third C_{2v} structure (**10b**) is a butterfly shaped four membered ring generated from **7b** $^3B_{1g}$ by following the normal mode with the imaginary frequency, as discussed above. The fourth (**8b**) is a trapezoidal planar structure.

3b. The lowest energy C_{2v} structure is isomer **3b**. The $^1A_1$ state is slightly lower in energy than the $^3B_2$ state, by 1.8 kcal·mol^{-1} (Table 4). In both **3sb** and **3tb** Si-Si and Si-C bond lengths are very close to typical single bond lengths [21]. The Mayer bond order analysis indicates that the Si-Si bond orders for the singlet and triplet are 1.145 and 1.269, while the Si-C bond orders are 0.815 and 0.803, respectively. For both states there is very strong bonding between the carbons. C-C bond lengths of 1.29 Å for the $^1A_1$ structure and 1.30 Å for the $^3B_2$ structure indicate strong double bonding. Examination of natural orbitals is consistent with this: There are two π bonding orbitals between the carbons, one of them perpendicular to the plane of the molecule and the other in the plane of the molecule. The NOONs in the singlet are 1.940 and 1.914; in the triplet they are 1.938 and 1.925, respectively. The π bond perpendicular to the plane is very localized between the two carbons such that it is analogous to the bonding observed in the linear species where there are two degenerate π bonds. Of course, in this case the two orbitals are not degenerate. The singlet and the triplet are 26.4 and 28.2 kcal·mol^{-1} above the global minimum.

4b. Isomer **4b** consists of a three-membered ring with an exocyclic silicon bonded to the silicon vertex. There is very little difference between the $^1A_1$ structure, **4sb**, and that of $^3A_2$, **4tb**. The largest difference in bond lengths is 0.06 Å; bond angles are the same to within 1°. The bonding is quite similar. The bond lengths indicate strong double bonding between the carbons, Si-C bonding slightly stronger than single, and a Si-Si bond intermediate between single and double bonding.

The lowest energy state for this isomer is $^3A_2$, in which the two unpaired electrons reside in the b_1 Si-Si π bonding orbital and a b_2 π orbital that is primarily localized on the exocyclic silicon. Strictly speaking, this b_2 orbital is anti-bonding between the cyclic silicon and the two carbons; however, there is so little electron density on the carbons that there is little anti-bonding character. **4tb** and **4sb** are 44.8 and 70.2 kcal·mol^{-1} above the global minimum, respectively.

10b. The butterfly C_{2v} isomer, **10tb**, is closely related to its D_{2h} precursor **7tb**. In **10tb** the molecular plane of **7tb** is broken. **7sb** is not a low energy species, with a relative energy more than 80 kcal·mol^{-1} higher than the global minimum.

Although the transannular C-C distance is 2.35Å, natural orbitals indicate that the carbons participate in both σ bonding and banana shaped, π like bonding, both with diradical character on the carbons. Lone pairs are located on the silicons.

Attempts to isolate the singlet with this geometry (**10sb**) were not successful. Optimizations starting from the triplet geometry in attempt to find an isomer **10sb** all lead back to the global minimum structure **5sb**.

8b. Isomers **8sb** and **8tb** are trapezoidal structures. Although the singlet and triplet are only 33.5 and 25.5 kcal·mol^{-1} above the global minimum, both structures have two imaginary frequencies. For isomer **8sb**, the modes corresponding to the two imaginary frequencies lead to isomers **6sb** and **9sb**. For isomer **8tb**, the two imaginary frequencies connect this structure to isomers **6tb** and **9tb**. Both **9sb** and **9tb** are C_2 transition states on the PES.

Isomer **9sb** (23.0 kcal·mol^{-1} above the global minimum) has one imaginary frequency at 271i cm^{-1}. Distortion along this normal mode followed by optimization of the geometry leads to isomer **6sb**.

For **9tb**, distortion along the mode with imaginary frequency 142i cm^{-1}, followed by geometry optimization produces isomer **6tb**. **9tb** is 21.6 kcal·mol^{-1} higher than the global minimum **5sb**.

C_s structures. 6b. Isomer **6b** is a distorted trapezoidal structure with C_s symmetry. Both the singlet and the triplet are minima on the MCSCF/6-31G(d) potential energy surface.

6sb is 4.2 kcal·mol^{-1} higher than the global minimum. The Si-Si bond distance is 2.455Å compared with 2.342Å in disilane [26], indicating a weak bond. On the other hand, qualitative examination of natural orbitals reveals five orbitals with some amount of bonding interaction between the two silicons, and one with anti-bonding character. MCSCF bond order analysis indicates a Si-Si bond order of 0.819, and Edmiston-Ruedenberg energy localized orbitals [27] indicate weak Si-Si interaction. The 4c-2e- π bond is mostly localized on the two carbon atoms, with Mulliken populations of 1.083 on the central carbon and 0.520 on the other carbon atom. The populations on the silicons are 0.226 and 0.113. Between each carbon atom and silicon-1 there is nearly a single bond; the third C-Si bond is much stronger, with a bond order of 1.406. The C-C MCSCF bond order is 1.547.

6tb is higher in energy than **6sb**, 15.0 kcal·mol^{-1} above the global minimum. The Si-Si distance is 2.62Å in **6tb** compared to 2.46 Å in **6sb**. The transannular C-Si bond is slightly longer in **6tb** than that in **6sb**, while the peripheral carbon distance to the same silicon is shorter by 0.06 Å. The Si-Si bond length here is much shorter than the 2.971 Å obtained in a previous study that employed UHF with the 6-31G* basis set [7].

Si_2C_2 relative energies. The lowest energy isomer is predicted to be **5sb**, just 1.0 kcal·mol^{-1} lower than the $^3\Sigma_g^-$ state of **1b**, **1tb**. Although the relative ordering of these two isomers is in agreement with most previous studies[5-7], we find them to be much closer in energy than the 11.9 kcal·mol^{-1} found by Fitzgerald and Bartlett (MP4/DZP) or the 15.5 kcal·mol^{-1} found by Lammertsma and Güner (MP2/6-31G(d)). As with SiC_3 the linear singlets are also quite low in energy. The $^1\Sigma_g^+$ state has a relative energy of 8.9 kcal·mol^{-1}, while the $^1\Delta_g$ state has an energy of only 5.8 kcal·mol^{-1} at the $^1\Sigma_g^+$ geometry. Also very low

in energy is the distorted trapezoid structure **6b**; the singlet is only 4.2 kcal·mol^{-1} and the triplet is 15.0 kcal·mol^{-1} above the global minimum.

A number of structures have somewhat higher energy, ~20 – 30 kcal·mol^{-1}. These have some C-C bonding, but suffer either from some degree of ring strain associated with the incorporation of a three-membered ring, or from some C-Si bonding at the expense of C-C bonding. Very high energy isomers (> 40 kcal·mol^{-1}) allow very little C-C bonding, **7b**, or suffer from a great deal of ring strain, as in **4b** where Si-C-C bond angles are 69° and the C-Si-C bond angle is 41°.

IV. Wave functions.

Now consider the importance of using MCSCF wave functions for these compounds. The unsaturated nature of these molecules, combined with the presence of a large number of negative virtual orbital energies at the Hartree Fock level suggests the need for a multi-reference wave function.

Since our primary interest is in predicting the lowest energy structures, and characterizing these and other structures which might be observed experimentally, we will focus on those isomers whose energy is ≤ 10 kcal·mol^{-1} above the global minimum. Within these isomers we will focus on those orbitals which would be unoccupied by a single reference wave function. We will refer to these orbitals as "unoccupied" orbitals, although clearly they are not completely unoccupied in an MCSCF wave function. These low energy isomers all have at least one "unoccupied" natural orbital occupation number (U-NOON) greater than 0.07. **1ta** has two U-NOONs of 0.097, with total electron density outside the Hartree-Fock configuration of 0.281 e$^-$. **1sa-Σ** and **1sa-Δ** both have U-NOONs above 0.1 and total electron density in "unoccupied" orbitals of more than 0.3. It has been suggested previously [28-31] that an occupation number for a virtual orbital of 0.1 or as low as 0.07 indicates that a single determinant wavefunction is suspect.

The situation is similar for Si_2C_2. The wavefunction of the rhombic structure **5sb** is the most dominated by the Hartree-Fock configuration. Its largest U-NOON is 0.070, with 0.189 e$^-$ total electron density outside the RHF reference. The linear species more clearly

require a multiconfigurational representation. **1tb** has two U-NOONs of .117 and total electron density in "unoccupied" orbitals is 0.339. **1sb-Σ** has two U-NOONs of 0.170 and total electron density in "unoccupied" orbitals of 0.463, nearly half an electron.

These occupation numbers indicate that a multi-reference wave function is most appropriate. This may explain the difference between relative energies found in this study and those in previous studies.

V. Conclusions

A comprehensive study of singlet and triplet isomers of SiC_3 and Si_2C_2 has been presented, including examination of structures, bonding, relative energies and vibrational modes. The SiC_3 global minimum is predicted to be a silicon terminated $^3\Sigma^-$ structure, **1ta**, with a singlet rhombic structure, **3sa**, 4.4 kcal·mol^{-1} higher. This is in contrast to previous predictions that the rhombic structure is the global minimum. The Si_2C_2 global minimum is predicted to be a singlet rhombic structure, **5sb**, with a $^3\Sigma_u^-$ silicon terminated linear isomer, **1tb**, 1.0 kcal·mol^{-1} higher in energy. Although the rhombic structure has previously been predicted to be the global minimum, we find the $^3\Sigma_u^-$ structure to be much lower in energy than had previously been expected.

It has also been determined that the use of a multireference wavefunction is important for studying these systems.

Acknowledgements. This work was supported by grants from the Air Force Office of Scientific Research. JR was supported in part by a grant from the Basic Energy Sciences Division of the Department of Energy, administered by the Ames Laboratory. The authors have benefited greatly from discussions with Professor Larry Burggraf, Professor Carl Lineberger, Dr. Gustavo Davico, and Dr. Rebecca Schwartz. Some of the calculations were performed on an IBM Power3 cluster, obtained in part from an IBM SUR grant and in part from a grant from the Department of Energy MICS Division.

References:

[1] C. Lineberger, G. Davico, and R. Schwartz (private communication).

[2] I. L. Alberts, R. S. Grev, and H. F. Schaefer III, *Journal of Chemical Physics* **93,** 5046-5052 (1990).

[3] M. Gomei, R. Kishi, A. Nakajima, S. Iwata, and K. Kaya, *Journal of Chemical Physics* **107,** 10051-10060 (1997).

[4] S. Hunsiker and R. O. Jones, *Journal of Chemical Physics* **105,** 5048-5060 (1996).

[5] G. W. Trucks and R. J. Bartlett, *Journal of Molecular Structure (Theochem)* **135,** 423-428 (1986).

[6] G. B. Fitzgerald and R. J. Bartlett, *International Journal of Quantum Chemistry* **XXXVIII,** 121-128 (1990).

[7] K. Lammertsma and O. F. Güner, *Journal of the American Chemical Society* **110,** 5239-5245 (1988).

[8] J. D. Presilla-Márquez, S. C. Gay, C. M. L. Rittby, and W. R. M. Graham, *Journal of Chemical Physics* **102,** 6354-6361 (1995).

[9] M. S. Gordon, *Chemical Physics Letters* **76,** 163-168 (1980).

[10] T. H. Dunning Jr., *Journal of Chemical Physics* **90,** 1007-1023 (1989).

[11] R. A. Kendall, T. H. Dunning Jr., and R. J. Harrison, *Journal of Chemical Physics* **96,** 6796-6806 (1992).

[12] D. E. Woon and T. H. Dunning Jr., *Journal of Chemical Physics* **98,** 1358 (1993).

[13] L. M. Cheung, K. R. Sunberg, and K. Ruedenberg, *International Journal of Quantum Chemistry* **5,** 1103-1139 (1979).

[14] K. Ruedenberg, M. W. Schmidt, M. M. Gilbert, and S. T. Elbert, *Chemical Physics* **71,** 41-49 (1982).

[15] K. R. Sundberg and K. Ruedenberg, in *Quantum Science*, edited by J. L. Calais, O. Goscinski, J. Linderberg, and Y. Ohrn (Plenum, New York, 1976), pp. 505.

[16] B. O. Roos, P. Taylor, and P. E. Siegbahn, *Chemical Physics* **48,** 157-173 (1980).

[17] H. Nakano, *Journal of Chemical Physics* **99,** 7983-7992 (1993).

[18] G. D. Fletcher, M. W. Schmidt, and M. S. Gordon, *Advances in Chemical Physics* **110,** 267-294 (1999).

[19] M. W. Schmidt, K. K. Baldridge, J. A. Boatz, S. T. Elbert, M. S. Gordon, J. J. Jensen, S. Koseki, N. Matsunage, K. A. Nguyen, S. Su, T. Windus, M. Dupuis, and J. A. Montgomery, *Journal of Computational Chemistry* **14,** 1347-1363 (1993).

[20] *CRC Handbook of Chemistry and Physics*, Vol., edited by R. C. Weast, M. J. Astle, and W. H. Beyer (CRC Press, Boca Raton, FL, 1983).

[21] G. Raabe and J. Michl, *Chemical Reviews* **85,** 419-509 (1985).

[22] P. V. Sudhakar and K. Lammertsma, *Journal of Physical Chemistry* **96,** 4830-4834 (1992).

[23] L. Pierce and R. W. Kilb, *Journal of Chemical Physics* **27,** 108-112 (1957).

[24] G. Chung, M. V. Pak, D. R. Reed, S. R. Kass, and M. S. Gordon, *Journal of Physical Chemistry A* **104,** 11822-11828 (2000).

[25] I. Mayer, *Chemical Physics Letters* **97,** 270-274 (1983).

[26] M. S. Gordon, T. Truong, and Bonderson, *Journal of the American Chemical Society* **108,** 1412-1427 (1986).

[27] C. Edmiston and K. Ruedenberg, *Reviews of Modern Physics* **35,** 457-465 (1963).

[28] J. M. Bofill and P. Pulay, *Journal of Chemical Physics* **90,** 3637-3646 (1989).

[29] M. S. Gordon, M. W. Schmidt, G. M. Chaban, K. R. Glaesemann, W. J. Stevens, and C. Gonzalez, *Journal of Chemical Physics* **110,** 4199-4207 (1999).

[30] P. Pulay and T. P. Hamilton, *Journal of Chemical Physics* **88,** 4926-4933 (1988).

[31] K. Wolinski and P. Pulay, *Journal of Chemical Physics* **90,** 3647-3659 (1989).

Table 1. SiC_3 vibrational frequencies

vibration	symmetry	intensity debeye^{2}amu^{-1}Å^{-2}	frequency
1sa-delta			
1,4 bend	π	0.05	153 (2x)
1,3 bend	π	0.14	397 (2x)
Si-C stretch	σ	0.31	612
1,3 C-C stretch	σ	1.99	1350
C-C stretch	σ	4.70	1982
1sa-sigma			
1,4 bend	π	0.04	150 (2x)
1,3 bend	π	0.14	382 (2x)
Si-C stretch	σ	0.45	613
1,3 C-C stretch	σ	2.45	1342
C-C stretch	σ	4.19	1959
1ta			
1,4 bend	π	0.08	160 (2x)
1,3 bend	π	0.15	410 (2x)
Si-C stretch	σ	0.10	619
1,3 C-C stretch	σ	0.66	1369
C-C stretch	σ	5.04	2055
3sa			
out of plane bend	b_2	0.11	316
in plane bend	b_1	0.89	509
breathing	a_1	1.28	720
symmetric Si-C stretch	a_1	1.51	984
in plane ring distortion	b_1	0.06	1120
symmetric C-C stretch	a_1	5.63	1504
3ta			
in plane ring distortion	b_1	0.84	272
out of plane bend	b_2	0.00	395
symmetric Si-C stretch	a_1	1.24	502
breathing	a_1	0.13	747
asymmetric C-C stretch	b_1	0.01	1255
symmetric C-C stretch	a_1	0.23	1651

vibration	symmetry	Intensity debeye^{2}amu^{-1}Å^{-2}	Frequency
4sa			
out of plane bend	b_2	0.58	279
in plane ring distortion	b_1	0.00	420
symmetric Si-C stretch	a_1	0.51	538
transannular Si-C stretch	a_1	1.08	852
symmetric C-C stretch	a_1	0.10	1254
asymmetric C-C stretch	b_1	4.72	1603
4ta			
in plane ring distortion	b_1	2.69	363
out of plane bend	b_2	0.09	479
symmetric C-Si stretch	a_1	1.60	674
transannular C-Si stretch	a_1	0.47	755
breathing	a_1	0.19	1234
asymmetric C-Si stretch	b_1	1.57	1380
5sa			
in plane rocking	b_1	2.56	373i
out of plane bend	b_2	0.09	257
asymmetric C-C stretch	b_1	1.81	527
C-Si stretch	a_1	0.00	559
C-C-C bend	a_1	0.08	1254
C_3 ring breathing	a_1	1.31	1508
5ta			
asymmmetric C-C stretch	b_1	82.03	1475i
in plane rocking	b_1	0.02	115
out of plane bend	b_2	0.04	326
C-Si stretch	a_1	0.90	536
C-C-C in-plane bend	a_1	0.96	1124
C_3 ring breathing	a_1	0.08	1685

Table 2. SiC_3 Relative Energies

isomer	state	MCQDPT/6-31G(d) //FORS(12,10/11)/6-31G(d)	MCQDPT/aug-cc pVDZ //FORS(12,10/11)/6-31G(d) (zero point corrected energies in parentheses)
1sa	$^1\Delta$	6.6	10.6 (10.4)
1sa	$^1\Sigma^+$	10.0	9.3 (9.0)
1ta	$^3\Sigma^-$	0.0	0.0 (0.0)
2sa	$^1\Delta$	94.1	
2sa	$^1\Sigma^+$	97.9	
2ta	$^3\Sigma^-$	79.5	
3sa	A_1	0.7	4.4 (4.3)
3ta	$^3B_2$	20.4	26.2 (25.7)
4sa	A_1	6.8	7.8 (7.4)
4ta	$^3B_2$	12.7	5.9 (5.4)
5sa	A_1	28.1	25.2 (24.7)
5ta	$^3A_2$	30.1	30.8 (28.8)
6sa	A_1	103.4	
6ta	$^3A_2$	82.1	

Table 3. Si_2C_2 vibrational frequencies

vibration	symmetry	intensity debeye^{2}amu^{-1}Å^{-2}	frequency cm^{-1}
1sb-sigma			
symmetric bend	π_g	0.01	128(2x)
asymmetric bend	π_u	0.00	344(2x)
symmetric C-Si strech	σ_g^+	0.00	460
asymmetric C-Si stretch	σ_u^+	3.82	898
C-C stretch	σ_g^+	0.00	1782
1sb-delta			
symmetric bend	π_g	0.12	130(2x)
asymmetric bend	π_u	0.00	357(2x)
symmetric C-Si strech	σ_g^+	0.00	467
asymmetric C-Si stretch	σ_u^+	2.88	893
C-C stretch	σ_g^+	0.00	1800
1tb			
symmetric bend	π_g	0.00	137 (2x)
asymmetric bend	π_u	0.00	371 (2x)
symmetric C-Si stretch	σ_g^+	0.00	474
asymmetric C-Si stretch	σ_u^+	0.21	922
C-C stretch	σ_g^+	0.00	1860
3sb			
in plane distortion	b_1	0.04	224i
out of plane bend	b_2	0.04	86
Si-C-Si bend in plane	a_1	0.55	418
C-Si asymmetric stretch	b_1	0.29	528
ring breathing	a_1	1.68	647
C-C stretch	a_1	14.24	1881
3tb			
in plane distortion	b_1	0.07	47
out of plane bend	b_2	0.00	233
Si-C-Si bend	a_1	0.59	386
asymmetric C-Si stretch	b_1	0.76	397
ring breathing	a_1	1.30	643
C-C stretch	a_1	10.64	1759

vibration	symmetry	Intensity debeye^{2}amu^{-1}Å^{-2}	frequency
4sb			
out of plane bend	b_2	0.00	77i
in plane distortion	b_1	0.59	126
asymmetric C-Si stretch	b_1	1.37	361
Si-Si stretch	a_1	0.57	412
symmetric C-Si stretch	a_1	6.20	892
C-Si-C bend	a_1	1.81	1783
4tb			
in plane distortion	b_1	0.39	126
out of plane bend	b_2	0.28	136
C-Si asymmetric stretch	b_1	1.53	345
Si-Si stretch	a_1	0.02	394
C-Si symmetric stretch	b_1	9.24	895
C-Si-C bend	a_1	0.80	1803
5sb			
out of plane bend	b_{2u}	0.13	224
in plane ring distortion	b_{1u}	1.34	424
breathing	a_g	0.00	543
C-C stretch	a_g	0.00	1013
C-Si asymmetric stretch	b_{2g}	0.00	1026
C-Si symmetric stretch	b_{3u}	9.74	1066
5tb			
out of plane bend	b_{2u}	0.04	269
in plane ring distortion	b_{1u}	0.29	411
breathing	b_{3u}	6.03	474
C-Si symmetric stretch	b_{3u}	33.35	623
C-C stretch	a_g	0.97	1150
Si-C asymmetric stretch	b_{2g}	0.01	2686

vibration	symmetry	Intensity debeye^{2}amu^{-1}Å^{-2}	Frequency
6sb			
out of plane bend	a"	0.22	244
Si-Si stretch	a'	0.06	358
peripheral C-C-Si bend	a'	0.08	484
transannular C-Si stretch	a'	1.31	627
breathing	a'	0.98	735
C-C stretch	a'	0.52	1676
6tb			
Si-C-Si bend	a'	0.11	173
out of plane bend	a"	0.01	341
transannular C-Si stretch	a'	1.25	527
Si_2-C_4 stretch	a'	0.21	593
Si_1-C_3 stretch	a'	1.21	747
C-C stretch	a'	0.49	1619
7sb			
out of plane bend	b_{2u}	3.00	177
Si-C symmetric stretch	b_{1u}	0.01	537
Si-Si stretch	a_g	0.00	570
in plane ring distortion	b_{2g}	0.00	600
Si-C asymmetric stretch	b_{3u}	0.78	715
breathing	a_g	0.00	803
7tb			
out of plane bend (to **10tb**)	b_{2u}	0.06	261i
Si-Si stretch	a_g	0.00	404
Si-C asymmetric stretch	b_{3u}	0.49	519
in plane ring distortion	b_{2g}	0.00	625
Si-C symmetric stretch	b_{1u}	0.59	752
breathing	a_g	0.00	794

vibration	symmetry	Intensity debeye^{2}amu^{-1}Å^{-2}	Frequency
8sb			
in plane distortion to **6sb**	b_1	0.02	445i
out of plane twist to **9sb**	a_2	0.00	330i
Si-Si stretch	a_1	0.03	316
C-Si asymmetric stretch	b_1	0.63	557
C-Si symmetric stretch	a_1	3.89	722
C-C stretch	a_1	1.43	1909
8tb			
in plane distortion to **6tb**	b_1	2109.50	1333i
out of plane twist to **9tb**	a_2	38.51	919i
Si-Si stretch	a_1	0.27	625
out of plane twist	a_2	23.43	705
C-Si asymmetric stretch	b_1	705.41	937
C-C stretch	a_1	1.83	1813
9sb			
C-Si asymmetric stretch	B	0.58	272i
Si-Si stretch	A	0.04	287
twist	A	0.18	305
C-Si asymmetric stretch	B	1.04	623
C-Si symmetric stretch	A	2.71	709
C-C stretch	A	0.21	1721
9tb			
C-Si asymmetric stretch	B	0.06	142i
twist	A	0.15	296
Si-Si stretch	A	0.08	342
C-Si asymmetric stretch	B	0.31	459
C-Si symmetric stretch	A	2.30	725
C-C stretch	A	0.11	1713
10sb			
symmetric butterfly bend	a_1	0.23	262
C-C stretch	a_1	0.29	419
C-Si asymmmetric stretch	b_1	0.45	573
C-Si asymmmetric stretch	a_2	0.00	702
C-Si symmetric stretch	a_1	0.34	762
breathing	a_1	0.03	806

Table 4. Si_2C_2 Relative Energies

Isomer	state	MCQDPT/6-31G(d) //FORS(12,10/11)/6-31G(d)	MCQDPT(12,11)/aug-cc pVDZ //FORS(12,10/11)/6-31G(d)
1sb-Δ	$^1\Delta$	6.2	5.8 (5.6)
1sb-Σ	$^1\Sigma_g^+$	9.2	8.9 (8.6)
1tb	$^3\Sigma_g^-$	1.0	1.0 (1.0)
3sb	$^1A_1$	34.8	26.4 (25.4)
3tb	$^3B_2$	33.4	28.2 (27.0)
4sb	$^1A_1$	68.2	70.2 (69.2)
4tb	$^3A_2$	58.8	44.8 (43.9)
5sb	^1A_g	0.0	0.0 (0.0)
5tb	$^3B_{1g}$	51.4	43.0 (44.9)
6sb	$^1A'$	6.0	4.2 (4.0)
6tb	$^3A''$	24.8	15.0 (14.6)
7sb	^1A_g	82.2	76.8 (75.5)
7tb	^3A_u	55.6	47.3 (45.6)
8sb	$^1A_1$	46.4	33.5 (32.4)
8tb	$^3B_2$	35.5	25.5 (25.2)
9sb	^1A	40.8	23.0 (22.1)
9tb	^3B	23.5	21.6 (20.6)
10tb	$^3A_2$	52.2	47.1 (46.0)

Figure 1. Optimized MCSCF geometries for the singlet and triplet isomers of SiC_3. Triplet bond lengths are given in parentheses.

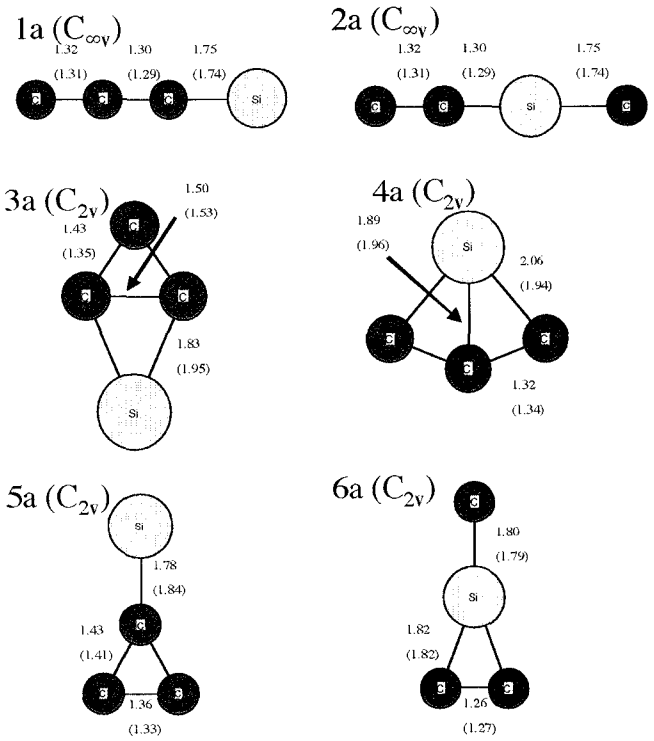

Figure 2. Optimized MCSCF geometries for the singlet and triplet isomers of Si_2C_2. Triplet bond lengths are given in parentheses.

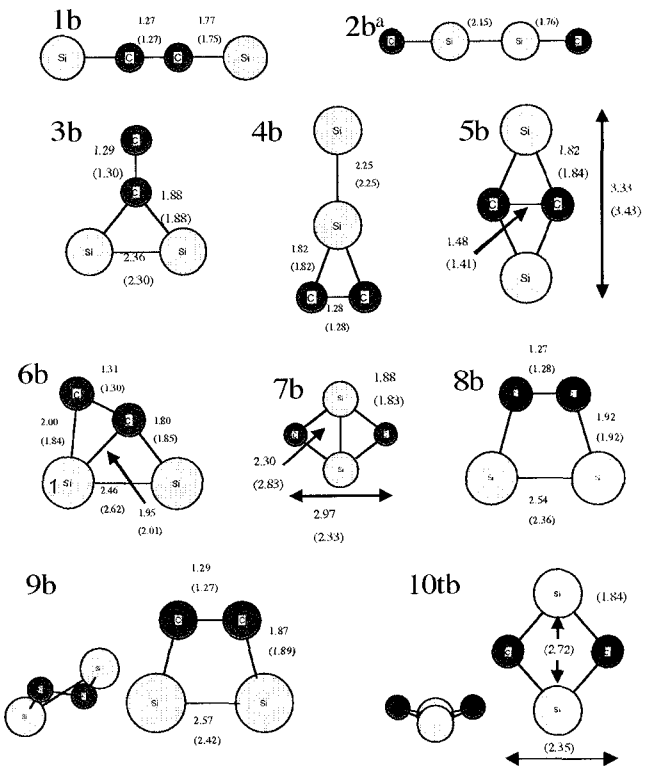

CHAPTER 3: ADSORPTION OF ACETYLENE ON SI(100)-(2×1)

A paper published in the *Journal of Physical Chemistry B*
Reprinted with permission. *Journal of Physical Chemistry B* **2004,** *108*, 7820.

Jamie M. Rintelman and Mark S. Gordon

Abstract

A study of a single acetylene adsorbed onto the Si(100)-(2x1) surface is presented. A MCSCF+MRMP2 wave function is used to study this system, which is shown to be significantly multiconfigurational over large sections of the potential energy surface. The lowest energy isomer is shown to have the acetylene adsorbed directly above a single dimer, di-σ, where the silicon-silicon dimer bond remains intact. These results are compared with those from a previous DFT study.

I. Introduction

There is a great deal of interest in the interaction of organic molecules with the 2x1 reconstructed silicon(100) surface. The primary motivation for this interest is a desire to combine the vast amounts of knowledge about the Si(100)-(2x1) surface, with the even more expansive field of organic chemistry. As the methods for manipulating and machining silicon wafers have become quite sophisticated, surface scientists are increasingly able to create micron sized gears, engines, and many other structures from silicon[1]. The centuries old field of organic chemistry encompasses the study of an extensive collection of molecules spanning nearly every kind of functionality known to chemists. It is not difficult to understand, therefore, why there is a great deal of interest in combining these two fields. If organic molecules can be reacted with and attached to the Si(100)-(2x1) surface in such a way that they retain their functionality, the utility of silicon-based materials would be greatly expanded. Many advances have been made in this direction[2,3], and continue to be explored.

In recent years our group has been interested in modeling the interactions of small molecules with the Si(100)-(2x1) surface. It was established early on [4] that saturated hydrocarbons do not react with the surface; it is necessary that the hydrocarbon contain at least one multiple bond as a reaction center to react with the surface dimers. Acetylene is the simplest hydrocarbon containing a carbon-carbon triple bond. It is therefore an important prototype molecule, as well as being an interesting system in its own right.

The 2x1 reconstruction of the Si(100) surface leads to rows of surface Si-Si dimers that are trivalent. Because Si-Si π bonds are very weak, these dimers have a significant amount of diradical character. Consequently, many recent studies[5-7] of the Si(100)-(2x1) surface and its reactions have suggested that a multi-reference wave function is essential for a correct description of these dimers and their reactions. This study was initiated to assess the impact of multi-reference calculations on the predicted results for the Si(100)/acetylene system.

Early experimental studies of the Si(100)-(2x1)/C_2H_2 system disagreed initially about whether the silicon dimer bond was broken [8]or remained intact [9] upon chemisorption of an acetylene molecule. It was soon resolved that upon addition of an acetylene to the dimer, a σ bond remained between the silicons. Most *ab initio* and DFT calculations that have been performed on this system agree that in the di-σ (see Fig. 1), or on top configuration, the dimer bond remains intact [10-12]. Subsequent experimental studies observed two additional adsorption configurations: (1) endbridge, (the acetylene carbons coordinated to one silicon each on the same side of adjacent dimers); (2) another structure that is postulated to be a tetracoordinated species, with the acetylene coordinated to adjacent dimers either perpendicular (rbridge) or parallel (pbridge), to the surface dimers[3,13] (see Fig. 1). It is universally agreed[3,4,10,11,13,14] that the tetracoordinated species are higher in energy than either the di-σ or endbridge configurations; however, it has been suggested[3] that the observed tetracoordinated species sit in adsorption sites that are more kinetically accessible. The acetylene, therefore, can presumably be trapped in such sites. It has also been suggested that the observation of so-called tetracoordinated species are actually misinterpretations of two acetylenes adsorbed in the endbridge fashion [14].

II. Computational Details

When studying surface chemistry using quantum mechanics, one must develop a model of the surface that is able to capture both the local properties of the surface and the bulk behavior. Eliminating edge effects is important, but it must be feasible to perform the calculations using available computational resources. To study surface chemistry in this manner, it must be possible to construct a model cluster of reasonable size that captures the essential features of the surface. In the case of Si(100)-(2x1), the cluster must accurately represent the dimerized structure of the surface. The smallest reasonable one and two dimer clusters are Si_9H_{12} and $Si_{15}H_{16}$, respectively (see Fig. 2). These clusters model the behavior of the surface well, yet are small enough to study with a reasonably high level of theory. A more sophisticated approach is to use an embedded cluster model, in which the quantum mechanics (QM) cluster is embedded into a larger bulk region represented by a lower level of theory. This approach diminishes edge effects while allowing the "action region" to be described by the highest levels of theory. In the present study, a $Si_{15}H_{16}$ QM cluster is surrounded by a larger molecular mechanics (MM) cluster, in order to adequately treat several isomers in which the acetylene molecule is interacting with two dimers in the same dimer row. The details of this model are as follows.

(a) Bulk Model: Bulk effects are taken into account using the hybrid quantum mechanics/molecular mechanics (QM/MM) approach called Surface Integrated Molecular Orbital/ Molecular Mechanics (SIMOMM) [15]. This method, implemented in the quantum chemistry package GAMESS[16] (General and Atomic Molecular Electronic Structure System), employs MM3[17] parameters in the Tinker program[18]. Tinker is linked to GAMESS to perform the MM portion of the calculation. The interface between the QM and MM regions is handled by terminating the severed Si-Si bonds with Hydrogens as link atoms. The bulk model includes 333 atoms, comprising 5 layers of silicon. The surface includes 18 dimers; 3 dimer rows wide by 6 dimers long (Fig. 3).

(b) Ab Initio Region. The atomic basis set employs a mixture of all electron and effective core potential (ECP) basis functions. Each silicon atom has the Hay-Wadt[19] ECP supplemented with the d function from the 6-31G(d) basis set[20], giving each silicon a

double zeta plus polarization basis in the valence. Carbons and hydrogens have the 6-31G(d)[21] all electron basis set. This basis set will henceforth be referred to as Mixed HW(d),6-31G(d).

It has been established that the bare Si(100) – (2x1) surface has considerable multireference character, and therefore should be studied using a multireference method [6,7]. Often, when the surface has been saturated with adsorbates, it acquires more single reference character [22]. This is not surprising, since the unpaired electrons (or dangling bonds) from which the multireference character arises, have bonded with the substrate on the surface. Thus, when beginning a study of the acetylene on Si(100)-(2x1) system, it is necessary to determine the extent to which multireference wave functions are a necessary zeroth order description.

Preliminary Fully Optimized Reaction Space (FORS)-MCSCF calculations revealed natural orbital occupation numbers (NOONs) for some isomers that deviate significantly from the Hartree-Fock values of 2.0 and 0.0 for occupied and virtual orbitals, respectively. As expected, the most significant deviation occurs when the surface dimers are not fully saturated. Although some isomers, particularly the tetracoordinated species, are well described by single-reference wave functions, our intention to study a significant portion of the surface in a continuous manner precludes any possibility of using single reference methods to study some isomers and multireference methods for others.

Due to these considerations the QM region is represented by a FORS-MCSCF[23] wave function with an eight electrons in eight orbitals active space. Active orbitals include both π bonds on acetylene, the π bond on each Si-Si dimer and the four corresponding antibonds (see Fig. 4).

(c) Geometry Optimizations. Geometries are fully optimized in both the QM and MM regions [15]. Minima and transition states are characterized by the calculation and diagonalization of the energy second derivative matrix (hessian). A positive definite hessian indicates that a local minimum has been found, one negative eigenvalue indicates that the stationary point is a transition state (first order saddle point). No higher order saddle points were encountered in this study.

Minimum energy paths [24]are performed to connect minima and transition states, using the second order Gonzalez-Schlegel (GS2) method[25], employing a step size of 0.15 $(amu)^{1/2}$·bohr.

Multireference second order perturbation theory [26](MRMP2) calculations are performed at all stationary points to provide accurate relative energies and reaction barriers.

III. Ground State Potential Energy Surface

In order to include all surface minima that may be relevant to the interpretation of experimental data on the acetylene on Si(100) – (2x1) surface, five minima have been examined, the di-σ (also called on top dimerized), endbridge, pbridge, rbridge, and cross configurations (see Fig. 1). Other possible adsorption configurations are not included, since previous studies have suggested that they are much higher in energy [10].

A. Relative Energies and Adsorption Energies. The energies discussed in this section have been obtained at the MRMP2//FORS(8,8)/ Mixed HW(d),6-31G(d) level of theory. Adsorption energies are defined as E_{ads}= E(surface+acetylene)-E(complex). E(surface+acetylene) is obtained by doing a calculation on the supermolecule, consisting of the surface and acetylene separated by > 100Å at their optimized geometries. E(complex) is the MRMP2 energy of the isomer in question. Thus, although MRMP2 is not size extensive, in this study, the size consistency errors [27] have been corrected for. At the FORS level the NOONs are exactly the same for the separated species and for the supermolecule. The energies are the same to 10^{-5} hartree. Thus, the FORS part of the calculation is size consistent, as expected for fully variational methods.

The adsorption energies presented in this study are all positive, and indicate stable structures (see Table 1). In the di-σ, endbridge, and cross species, the acetylene is dicoordinated, while the acetylene is tetracoordinated in the rbridge and pbridge species. The di-σ (dimerized) species is the most stable configuration for one acetylene molecule on the Si(100)–(2x1) surface (see Table 2), with an adsorption energy of 51.2 kcal·mol^{-1}. The endbridge is a very low energy isomer, only 4.5 kcal ·mol^{-1} less stable than the di-σ species.

The cross species is quite high in energy, 40.6 kcal·mol^{-1} above di-σ. The energy of pbridge relative to the di-σ isomer is 40.4 kcal·mol^{-1}, while that of rbridge is 30.3 kcal·mol^{-1}.

B. Local minima. Di-σ. In the di-σ configuration the acetylene is situated directly above a silicon dimer. Each carbon is sigma bonded to the corresponding silicon of the surface dimer. In the adsorbed acetylene unit, there is double bonding between the carbons and a bond length of 1.36Å, just slightly longer than the ethylene carbon-carbon bond length, 1.33Å. Because the acetylene is directly above the dimer, there is no strain between dimers in the row. Comparing the geometric parameters of the clean surface with those of the di-σ configuration, it is clear that there is very little perturbation of the remainder of the surface by the acetylene molecule. The interdimer distances are virtually identical, 3.84 Å in the bare surface and 3.83Å in di-σ. Similarly, the unsaturated silicon-silicon dimer bond distances are 2.25Å in both the clean surface and the di-σ structure. There is only a slight elongation of the Si-Si bond distance in the saturated dimer relative to the unsaturated dimer, 2.32Å and 2.25Å, respectively. Some elongation is expected since the dimer partial π bond has been broken. Examining the NOONs (see Fig. 5b) it is easy to see that there is very little interaction between the dimers in the same row. The π and π* orbitals on the unsaturated dimer and their NOONs are almost identical to those on the clean surface (Fig. 5a). This implies that there would be little advantage to adsorbing two acetylenes on adjacent dimers in the dimerized di-σ configuration relative to acetylenes being on dimers separated by a great distance. Adjacent dimers can be considered to be essentially noninteracting [7], and placing an acetylene on one of these dimers does not change that situation.

Endbridge. In the endbridge isomer (see Fig. 1), the acetylene is again di-coordinated, but now it is bridging two adjacent dimers, perpendicular to the dimer row. This leaves one silicon unsaturated on each dimer. This configuration is essentially a pure singlet diradical (see Fig. 5c), with HOMO and LUMO NOONs of 1.05 and 0.95, respectively. This isomer is therefore the most multi-reference of all isomers studied. Relative to the clean surface, in the endbridge species the intradimer Si-Si distance is lengthened by 0.12 Å (2.37Å vs. 2.25Å). The angle between the Si-C bond and the dimer bond (∠C-Si-Si) is 113°, 23° off normal. Each dimer partial π bond has been broken, and in addition, the unpaired electrons on the

unsaturated surface silicons and the π electrons on the acetylene are expected to repel each other. The interdimer Si-Si distances are shortened by 0.51Å and 0.21Å for the saturated and unsaturated silicons, respectively (3.33Å and 3.63 vs 3.84Å), having been pulled together due to the adsorption of the acetylene group directly above. The saturated distance undergoes a larger change, since these silicons are directly attached to the acetylene carbons.

Although the endbridge isomer is only slightly higher in energy than the di-σ species, the impact on the surface is quite different. As discussed above, in the di-σ isomer the addition of an acetylene molecule perturbs the rest of the surface very little, while the endbridge isomer has a significant effect on the geometry of the surface. Since the endbridge isomer is only slightly higher in energy than the di-σ isomer, the favorable interaction of the acetylene with the surface must nearly cancel the effect of disrupting the structure of the surface.

Cross. In the cross configuration (Fig. 1, 5d) the acetylene is again dicoordinated; however, the acetylene bridges opposite silicons in two adjacent dimers. This is an intermediate structure along the pathway that rotates the acetylene from the rbridge to the pbridge configuration (see following section). The cross isomer is also highly multiconfigurational, with NOONs of 1.148 and 0.851 for the HOMO and LUMO orbitals (Fig. 5d). Each dimer bond in this isomer is lengthened by 0.08Å from 2.25Å in the clean surface to 2.33Å. Because the acetylene bonds across two dimers, it pulls in the two adjacent dimers to give a shortened interdimer Si-Si distance of 3.56Å, 0.28Å shorter than the clean surface distance of 3.84Å. The orbitals and C-C bond length of 1.37Å indicate the presence of a C-C double bond. The C-Si bonds are single bonds, with bond lengths of 1.98 Å.

Rbridge and Pbridge. The rbridge and pbridge isomers each contain a tetracoordinated acetylene molecule, with the acetylene perpendicular and parallel to the silicon dimer bond, respectively. These are both higher energy isomers, due in part to the strain caused by coordinating to all four silicon atoms of the two dimers. The dimer-dimer distance is significantly reduced in both the rbridge and pbridge isomers. The Si-Si distance between two dimers in the same row is 3.84 Å on the bare surface, while for rbridge and pbridge it is 3.37Å and 3.01Å respectively, a significant perturbation.

C. Pathways connecting isomers. Now, consider the pathways by which the acetylene can move from one configuration to another on the surface. In the following discussion, the vibrational frequencies that are quoted should be used as a qualitative guide to the motions that occur in the cluster. Due to the large number of atoms present and the significant amount of coupling between modes, there can be significant delocalization of the normal modes throughout the molecule. See Table S1 in Supplementary Materials for a selection of important vibrational frequencies. Schematics of the transition state structures are given in Figure 1.

Di-σ to pbridge. In the di-σ to pbridge reaction path, the acetylene is moving parallel to the dimer row, from being dicoordinated with one dimer to being tetracoordinated with two dimers in the same dimer row. The vibrational frequencies of the di-σ normal modes (Fig. 6a) that correspond to this motion from di-σ to pbridge are 115 and 194 cm^{-1}. Starting from the other end, the analogous pbridge frequencies (Fig. 6b) that lead from pbridge to di-σ are 159 and 292 cm^{-1}. The forward barrier for the process is 59.2 $kcal \cdot mol^{-1}$, while the reverse barrier is 18.8 $kcal \cdot mol^{-1}$. The imaginary mode corresponding to the motion towards minima on the potential energy surface has a vibrational frequency of 386.0i cm^{-1} (Fig. 6c).

Pbridge to cross to rbridge. In addition to moving along the dimer row, the acetylene can also rotate with respect to the dimer rows. It is this motion that connects the pbridge, cross and rbridge configurations. The path from pbridge to rbridge will take the acetylene through a rotation of a full 90° in a plane roughly parallel to the plane of the surface. The acetylene begins parallel to the surface dimers and ends perpendicular to the dimers. The forward barrier going from pbridge to cross is 13.5 $kcal \cdot mol^{-1}$, while the reverse barrier is 12.3 $kcal \cdot mol^{-1}$. The vibrational frequency of the normal mode (Fig. 6d) at the pbridge minimum geometry corresponding to this motion is 279.7 cm^{-1}. The normal mode (Fig. 6e) at the transition state corresponding to motion towards reactants has a frequency of 535.8i cm^{-1}. At the cross species the twisting motion is spread over two normal modes (Fig. 6f) with frequencies of 395 cm^{-1} and 399 cm^{-1}.

Completing the rotation the acetylene goes from the cross intermediate through a second transition state to rbridge. The normal modes corresponding to rotation of the acetylene

parallel to the surface in rbridge, going back to cross, range from 433.2 cm^{-1} to 584.4 cm^{-1} (Fig. 6g). The cross to rbridge pathway has a 15.7 kcal·mol^{-1} barrier in the forward direction and an 18.2 kcal·mol^{-1} barrier in the reverse direction at the FORS(8,8) level. At the MRMP2 level, however, the forward barrier nearly goes to zero. Single point MRMP2 calculations were done at several points along the FORS(8,8) reaction path to locate the upper limit to the energy of the transition state. These single point calculations reveal an upper limit to the forward barrier of 1.3 kcal·mol^{-1}, and to the reverse barrier of 11.6 kcal·mol^{-1}. The normal mode corresponding to motion towards the minima is at 480.35i cm^{-1} (Fig. 6h).

Rbridge to Endbridge. The motion from rbridge to endbridge involves the acetylene moving perpendicular to the dimer row from a position in which it is coordinated to each of the four silicons in two dimers in the same row to one in which it is coordinated to one silicon per dimer, on the same side of the dimer row. The barrier in the forward direction is 5.2 kcal·mol^{-1}, while in the reverse direction, going from the more stable endbridge isomer to the rbridge, it is 31.1 kcal·mol^{-1}. The main endbridge vibrational frequencies going towards rbridge are 134.6 cm^{-1} and 145.0 cm^{-1} (Fig. 6i). The rbridge vibrational frequencies corresponding to motion towards endbridge are 229.0 cm^{-1} and 378.8 cm^{-1} (Fig. 6j). The imaginary normal mode corresponding to motion towards reactants is 508.10 cm^{-1} (Fig. 6k).

Comparison with Density Functional Theory Calculations. Now compare the MRMP2//FORS(8,8)/Mixed HW(d),6-31G(d) results with previous (spin polarized) density functional theory (DFT) results obtained by Sorescu and Jordan [10], employing the PW91 functional, plane wave basis sets, and slab models (including eight Si atoms per layer, allowing a c(4x2) arrangement of the dimers) with periodic boundary conditions. While the comparison is with their results at 0.25 monolayer coverage (except for cross which is at 0.5 ML coverage), the trends hold for all low coverages in their study. Fig. 7 presents a schematic of the potential energy surface with results from both studies, while the geometries are compared in Table 3. Consider, first, the two lowest energy species. Both theoretical approaches indicate that for one acetylene adsorbed on the Si(100)-(2x1) surface, the di-σ species is the most stable, while the endbridge species is only slightly less stable. Relative to di-σ, the two methods give rather significant differences in the energies of some of the less

stable isomers, over 17 kcal·mol^{-1} in some cases. While these are significant quantitative differences, it is important to note that the qualitative nature of the surface is the same in both studies. Except for the two highest energy isomers, pbridge and cross, the energetic ordering of the isomers is the same in both studies.

IV. Conclusions

The multireference results presented here predict that the lowest energy arrangement for acetylene adsorbed on the Si(100)-(2x1) surface is the di-σ on top dimerized configuration. The endbridge arrangement is only slightly higher in energy than the di-σ.

The calculations in this study confirm that when studying the Si(100)-(2x1) surface the PES will be quite multiconfigurational where there are unsaturated dimers present, but when dimers are fully saturated there is generally just one important configuration. In the latter cases, single-configuration methods are likely to be reliable.

Comparing the spin-polarized DFT and MRMP2 results for this system, the same trends are predicted. Both studies agree that the di-σ arrangement is the global minimum for adsorption of acetylene on the surface at low coverage. While DFT and MCSCF predict buckled and symmetric dimers, respectively, for the clean surface, the geometries of the saturated species in this study are quite similar for both methods. However, as discussed above, this system has a significant amount of multi-reference character. The parameterization of DFT makes difficult a detailed analysis of the origin of the differences in results that do exist. Because there are regions of the PES that are so clearly multireference, it is our assertion that when discrepancies occur between DFT and MRMP2, the MRMP2 results should be considered more reliable. It is likely that spin-restricted (e.g., RHF-like) DFT calculations on this system would be in much worse agreement with the multi-reference results.

The evidence in this paper does not support the theory that one of the tetracoordinated sites is more accessible, and traps an acetylene there, but it also does not definitively rule it out. Both tetracoordinated species involve a significant perturbation of the surface structure, and the formation of 4 bonds to the surface. Forming the pbridge structure must involve

pulling the dimers 0.83Å closer together than in the clean surface; forming rbridge pulls them 0.47Å closer than the clean surface. Without mapping out a pathway by which an acetylene reaches each of these sites, it is not possible to quantitatively describe how easy or difficult to access they are. Their structure indicates that they are not likely to be easy to access. In addition to those considerations, neither of these minima are trapped by large barriers from getting to a lower energy species. Pbridge must get over a maximum barrier of 12.3 $kcal \cdot mol^{-1}$ to get to a lower energy species, and eventually to endbridge. Rbridge is separated from endbridge by a barrier of only 5.2$kcal \cdot mol^{-1}$. Only at very low temperatures would those barriers be sufficient to trap an acetylene in a tetracoordinated minimum.

Acknowledgements. This work has been supported by a grant from the Basic Energy Sciences division of the U.S. Department of Energy, administered by the Ames Laboratory. The authors have benefited greatly from discussions with Drs. Mike Schmidt and Cheol Ho Choi. The authors are grateful for the hospitality of the Research School of Chemistry at the Australian National University.

References:

1 D. Qin, Y. N. Xia, J. A. Rogers, R. J. Jackman, X. M. Zhao, and G. M. Whitesides, Microsystem Technology in Chemistry and Life Science **194**, 1 (1998); R. Maboudian, Surface Science Reports **30** (6-8), 209 (1998); R. T. Howe, Journal of Vacuum Science & Technology, B: Microelectronics Processing and Phenomena **6** (6), 1809 (1988).

2 R. J. Hamers, S. K. Coulter, M. D. Ellison, J. S. Hovis, D. F. Padowitz, M. P. Schwartz, C. M. Greenlief, and J. N. Russell, Accounts of Chemical Research **33** (9), 617 (2000); S. F. Bent, Journal of Physical Chemistry B **106** (11), 2830 (2002).

3 R. A. Wolkow, Annual Review of Physical Chemistry **50**, 413 (1999).

4 R. J. Hamers and Y. J. Wang, Chemical Reviews **96** (4), 1261 (1996).

[5] M. S. Gordon, J. R. Shoemaker, and L. W. Burggraf, Journal of Chemical Physics **113** (20), 9355 (2000); A. Redondo and W. A. Goddard, Journal of Vacuum Science & Technology **21** (2), 344 (1982).

[6] J. Shoemaker, L. W. Burggraf, and M. S. Gordon, Journal of Chemical Physics **112** (6), 2994 (2000).

[7] Y. Jung, Y. Akinaga, K. D. Jordan, and M. S. Gordon, Theoretical Chemistry Accounts **109** (5), 268 (2003).

[8] C. Huang, W. Widdra, X. S. Wang, and W. H. Weinberg, Journal of Vacuum Science & Technology, A: Vacuum, Surfaces, and Films **11** (4), 2250 (1993); P. A. Taylor, R. M. Wallace, C. C. Cheng, W. H. Weinberg, M. J. Dresser, W. J. Choyke, and J. T. Yates, Journal of the American Chemical Society **114** (17), 6754 (1992).

[9] M. Nishijima, J. Yoshinobu, H. Tsuda, and M. Onchi, Surface Science **192** (2-3), 383 (1987).

[10] D. C. Sorescu and K. D. Jordan, Journal of Physical Chemistry B **104** (34), 8259 (2000).

[11] Q. Liu and R. Hoffmann, Journal of the American Chemical Society **117** (14), 4082 (1995).

[12] Y. Imamura, Y. Morikawa, T. Yamasaki, and H. Nakatsuji, Surface Science **341** (3), L1091 (1995).

[13] S. H. Xu, M. Keeffe, Y. Yang, C. Chen, M. Yu, G. J. Lapeyre, E. Rotenberg, J. Denlinger, and J. T. Yates, Physical Review Letters **84** (5), 939 (2000); S. Mezhenny, I. Lyubinetsky, W. J. Choyke, R. A. Wolkow, and J. T. Yates, Chemical Physics Letters **344** (1-2), 7 (2001); L. Li, C. Tindall, O. Takaoka, Y. Hasegawa, and T. Sakurai, Physical Review B **56** (8), 4648 (1997).

[14] F. Wang, D. C. Sorescu, and K. D. Jordan, Journal of Physical Chemistry B **106** (6), 1316 (2002).

[15] J. R. Shoemaker, L. W. Burggraf, and M. S. Gordon, Journal of Physical Chemistry A **103** (17), 3245 (1999).

[16] G. D. Fletcher, M. W. Schmidt, B. M. Bode, and M. S. Gordon, Computer Physics Communications **128** (1-2), 190 (2000); G. D. Fletcher, M. W. Schmidt, and M. S. Gordon, Advances in Chemical Physics **110**, 267 (1999); M. W. Schmidt, K. K. Baldridge, J. A. Boatz, S. T. Elbert, M. S. Gordon, J. H. Jensen, S. Koseki, N. Matsunaga, K. A. Nguyen, S. J. Su, T. L. Windus, M. Dupuis, and J. A. Montgomery, Journal of Computational Chemistry **14** (11), 1347 (1993).

[17] J. H. Lii and N. L. Allinger, Journal of the American Chemical Society **111** (23), 8566 (1989); J. H. Lii and N. L. Allinger, Journal of the American Chemical Society **111** (23), 8576 (1989); N. L. Allinger, Y. H. Yuh, and J. H. Lii, Journal of the American Chemical Society **111** (23), 8551 (1989).

[18] C. E. Kundrot, J. W. Ponder, and F. M. Richards, Journal of Computational Chemistry **12**, 402 (1991); J. W. Ponder and F. M. Richards, Journal of Computational Chemistry **8**, 1016 (1987).

[19] W. R. Wadt and P. J. Hay, Journal of Chemical Physics **82** (1), 284 (1985).

[20] P. C. Hariharan and J. A. Pople, Theoretica Chimica Acta **28**, 213 (1973).

[21] W. J. Hehre, R. Ditchfield, and J. A. Pople, Journal of Chemical Physics **56**, 2257 (1972).

[22] Y. S. Jung, C. H. Choi, and M. S. Gordon, Journal of Physical Chemistry B **105** (18), 4039 (2001).

[23] K. Ruedenberg, M. W. Schmidt, M. M. Gilbert, and S. T. Elbert, Chemical Physics **71** (1), 41 (1982); K. Ruedenberg and K. R. Sundberg, in *Quantum Science*, edited by J.-L. Calais, O. Goscenski, and J. Linderberg (Plenum, New York, 1976), pp. 505; L. M. Cheung, K. R. Sundberg, and K. Ruedenberg, International Journal of Quantum Chemistry **16** (5), 1103 (1979).

[24] D. G. Truhlar and M. S. Gordon, Science **249** (4968), 491 (1990).

[25] C. Gonzalez and H. B. Schlegel, Journal of Chemical Physics **90** (4), 2154 (1989).

[26] H. Nakano, Journal of Chemical Physics **99** (10), 7983 (1993).

[27] Calculations were done to probe the deviation of MRMP2 from size consistency for this system. The following size consistency errors were determined. E(surface)+E(acetylene)-E(surface+acetylene)=21.9kcal·mol-1; E(surface)+2E(acetylene)-E(surface+2acetylene)=49.1kcal·mol-1; 2E(acetylene)-E(2acetylene)=2.2kcal·mol-1. This issue will be addressed more fully by examining a representative set of molecules in a later paper.

Table 1. Adsorption Energies (kcal·mol-1)

isomer	MRMP/FORS(8,8)	DFT†
Di-σ	51.2	62.2
Endbridge	46.7	60.1
Pbridge	11.2	30
Rbridge	20.8	49.3
Cross*	10.6	38.1*

† DFT adsorption energies are taken from Sorescu and Jordan, ref. 5, at a coverage of 0.25 monolayers, except *Cross for which the 0.5 ML coverage adsorption energy is used, because that for 0.25 ML is not available

Table 2. Relative energies (kcal·mol-1)

MRMP/Mixed//FORS(8,8)/Mixed	
Minima	
Di-σ	0.0
Endbridge	4.5
Pbridge	40.0
Rbridge	30.3
Cross	40.6
Transition States	
Di-σ to Pbridge	59.2
Endbridge to Rbridge	35.5
Pbridge to Cross	52.9
Cross to Rbridge	39.2

Table 3. Vibratonal Frequencies

Due to delocalization of vibrational motion and coupling of normal modes, some cluster motions have more than one vibrational frequency associated with them. In these cases, the normal mode with the largest contribution to the relvant motion is listed in the first column

vibration	frequency		
di-σ			
C_2H_2 perp to dimer row	112.41		
C_2H_2 parallel to dimer row	114.58	193.67	185.89
cluster breathing	149.21		
dimer seesaw	157.65		
dimer row in plane twist	193.38	257.09	
both dimers, in plane twist	531.94		
acetylene in plane torsion	341.68	359.13	
unsaturated dimer buckling	220.98		
saturated dimer buckling	243.80		
unsaturated dimer stretch	503.96		
saturated dimer stretch	508.05		
acetylene/dimer C-Si symmetric stretch	720.29		
acetylene/dimer C-Si antisymmetric stretch	753.53	760.00	
H-C-Si Bend	732.01		
acetylene C-H antisymmetric wag	1020.80		
acetylene C-H symmetric wag	766.99		
acetylene C-H symmetric wag in-palne (of acetylene)	1171.14		
acetylene C-H asymmetric wag in-plane (of acetylene)	1396.38		
C-C Stretch	1575.81		
C-H Stretch antisymmetric	3302.35		
C-H Stretch symmetric	3324.75		
endbridge			
C_2H_2 perp to dimer row	134.62	144.98	
C_2H_2 parallel to dimer row	342.72	163.86	200.6
C_2H_2 parallel to dimer row + surface buckle	247.67		
symmetric buckle	261.68	458.17	
acetylene quasi in plane torsion	363.66		
acetylene quasi in plane torsion/surface buckle	435.52	475.67	
dimer stretch	479.81	499.23	
acetylene/dimer C-Si symmetric stretch	635.66		
acetylene/dimer C-Si antisymmetric stretch	739.55	760.53	
acetylene C-H antisymmetric wag	1026.27		
acetylene symmetric in-plane wag	1241.86		

acetylene antisymmetric in-plane wag	1432.08		
C-C stretch	1565.77		
C-H Stretch antisymmetric	3288.63		
C-H Stretch symmetric	3313.04		
pbridge			
C_2H_2 parallel to dimer row	159.18	291.69	350.12
C_2H_2 perp to dimer row	168.07		
surface + acetylene twist	279.70		
symmetric surface + acetylene buckle	264.38		
antisymmetric surface buckle	279.70		
acetylene/dimer C-Si symmetric stretch	581.78	535.76	602.79
acetylene/dimer C-Si antisymmetric stretch/parallel to dimer row	543.72		
acetylene/dimer C-Si antisymmetric stretch	620.83	663.43	678.58
C-C stretch	891.72		
acetylene symmetric wag	1024.11		
acetylene antisymmetric wag	1024.77	1027.36	1040.16
acetylene C-H symmetric in-plane wag	1160.83		
acetylene antisymmetric in-plane wag	1315.94		
C-H Stretch antisymmetric	3262.93		
C-H Stretch symmetric	3276.02		
rbridge			
asymmetric in-plane dimer slide	146.75		
symmetric in-plane dimer slide	154.13		
dimer buckle asynmmetric	154.79	259.62	
dimer buckle synmmetric	162.13		
C_2H_2 parallel to dimer row	344.41	378.22	
C_2H_2 perp to dimer row	378.80	229.04	
acetylene in plane torsion/surface buckle	528.79	584.41	433.21
acetylene/dimer C-Si symmetric stretch	450.28	460.03	641.71
acetylene/dimer C-Si antisymmetric stretch	536.91	681.60	742.40
acetylene/dimer C-Si antisymmetric stretch/parallel to dimer row	571.46		
C-C Stretch	946.73		
acetylene symmetric wag	991.36		
acetylene antisymmetric wag	996.92		
acetylene C-H symmetric in-plane wag	1227.64		
acetylene antisymmetric in-plane wag	1351.97		
C-H Stretch antisymmetric	3296.60		
C-H Stretch symmetric	3316.88		

cross			
acetylene moving diagonal to dimer row, perpendicular to C-C bond	146.65	203.57	206.37
acetylene moving diagonal to dimer row, in direction of C-C bond	171.37	521.39	
dimer buckle asymmetric	269.39		
dimer buckle symmetric	294.97		
acetylene in plane torsion	395.45	443.84	364.55
Acetylene torsion, symmetric surface buckle	562.44		
acetylene out of plane wag	646.22		
C-Si antisymmetric stretch	716.63	671.02	682.88
out of plane twist	1000.94		
in plane scissoring	1242.57		
in plane rocking	1417.31		
C-C stretch	1508.84		
C-H Stretch antisymmetric	3285.83		
C-H Stretch symmetric	3308.29		

Table 4. Important Geometrical Parameters. Bond lengths in Å.

Minima	Bare Surface	Free Acetylene	Dimerized		Endbridge		Pbridge		Rbridge		Cross
			FORS	DFT[a]	FORS	DFT[a]	FORS	DFT[a]	FORS	DFT[a]	FORS
Si-Si unsaturated	2.25		2.25		-		-		-		
Si-Si saturated	-		2.32	2.36	2.37	2.39	2.30	2.36	2.27	2.29	2.33
						2.46		2.36		2.29	
Si-Si interdimer	-		3.83		-		-		-		3.56
Si-Si interdimer saturated	-		-		3.33		3.01		3.37		
Si-Si interdimer unsaturated	3.84		-		3.63		-		-		
C-C	-	1.21	1.36	1.35	1.36	1.36	1.60	1.56	1.57	1.51	1.37
C-Si	-		1.93	1.90	1.94	1.92	2.05	2.06	2.00	2.00	1.98
				1.92		1.92		2.06		2.01	

Transition States	Dim2p	P2cross	Cross2r	End2r
Si1-Si2	2.31	2.32	2.27	2.27
Si3-Si4	2.36	2.32	2.26	2.26
Interdimer Si1-Si3	3.41	3.25	3.48	3.56
Interdimer Si2-Si4	3.10	3.25	3.52	3.40
C-C	1.49	1.47	1.44	1.47
C-Si1	1.95	1.99	1.96	2.65
C-Si2	2.01	2.67	2.73	1.95
C-Si3	3.15	2.66	2.41	2.35
C-Si4	2.28	1.99	1.97	1.95

[a] DFT geoemetries are taken from ref 5, Sorescu and Jordan

Figure 1. Stationary points

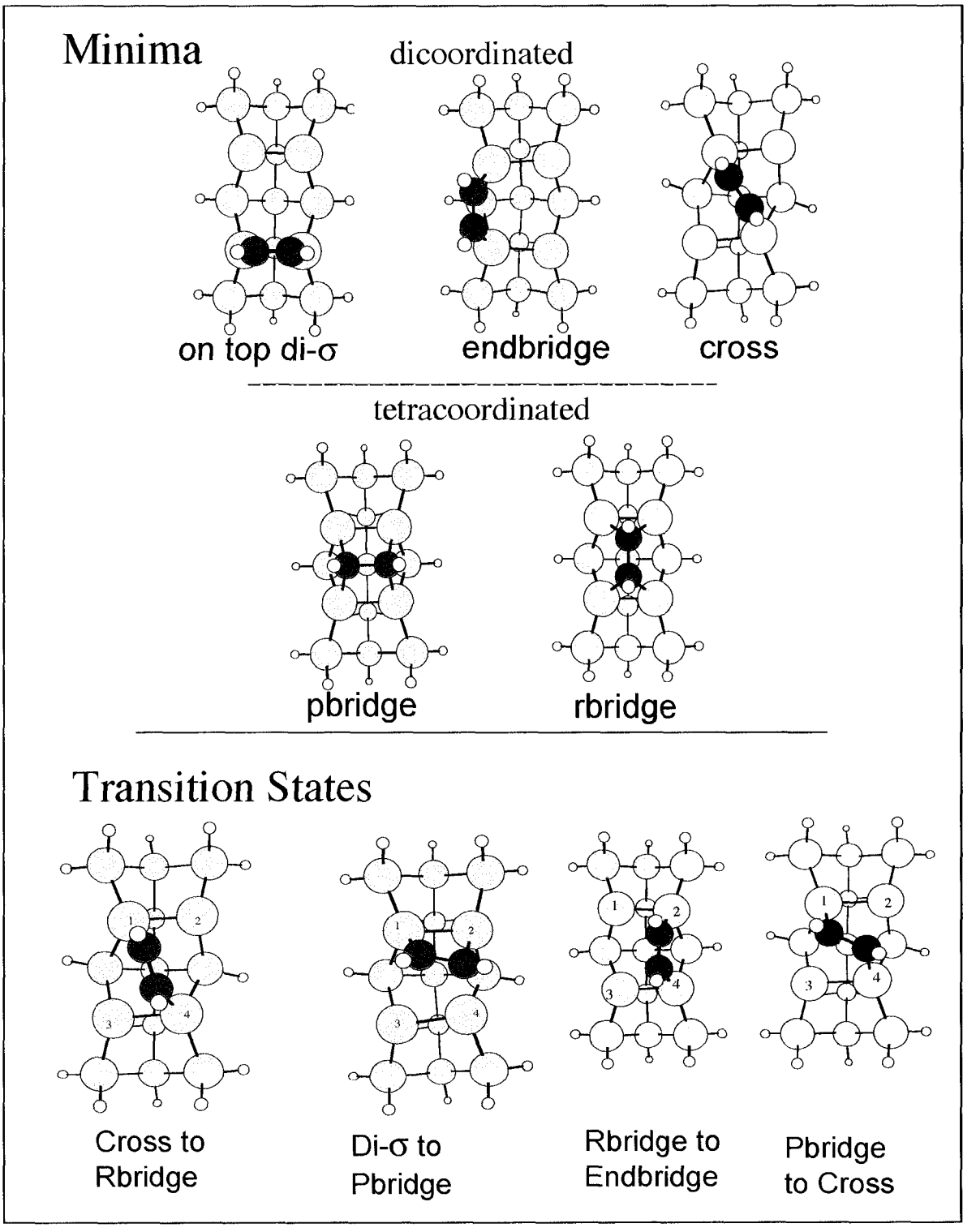

Figure 2. One and two dimer clusters

dimer silicons are colored purple

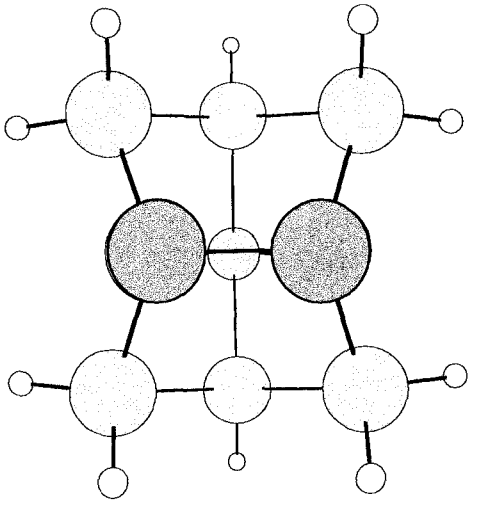

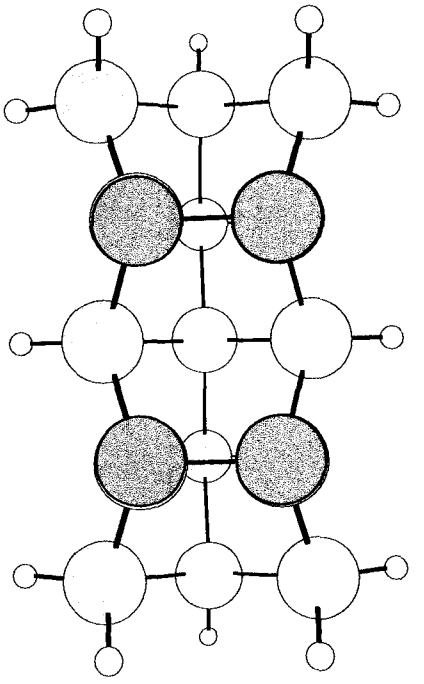

Si_9H_{12}:

One dimer cluster

Si_9H_{12}:

Two dimer cluster

Figure 3. Bulk model

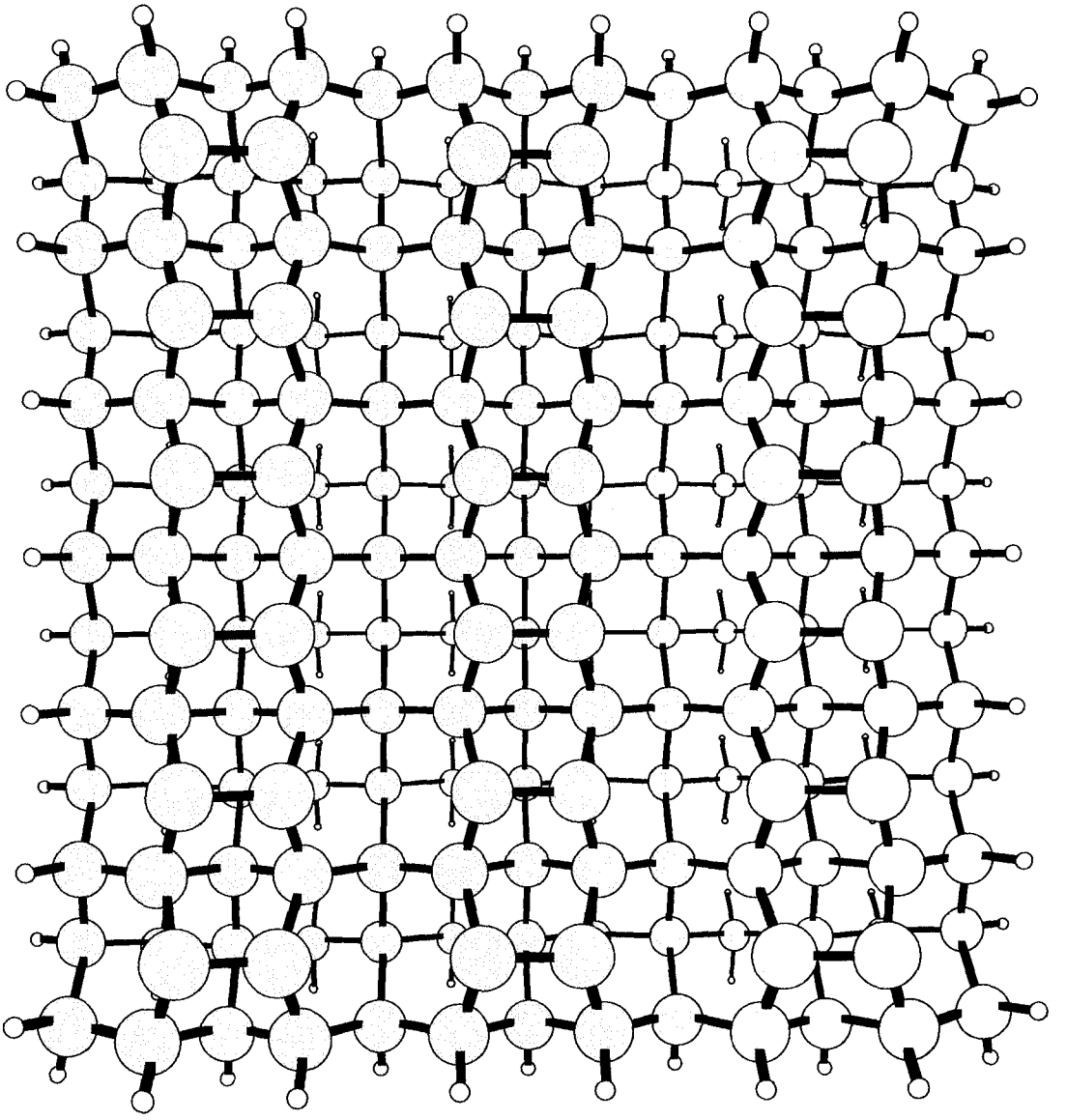

Figure 4. Active space

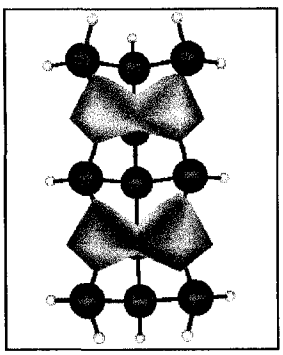
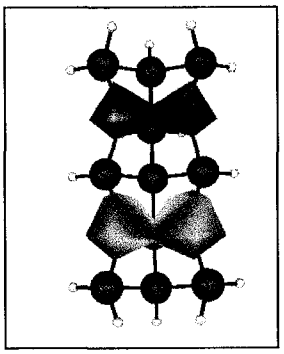

Dimer π
bonding orbitals

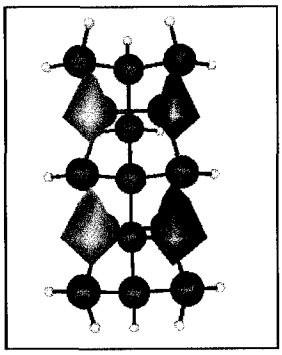
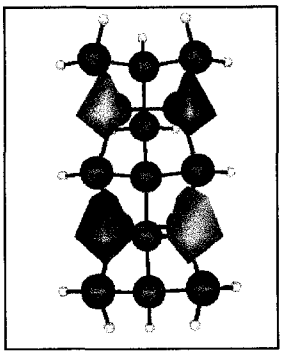

Dimer π^* anti-
bonding orbitals

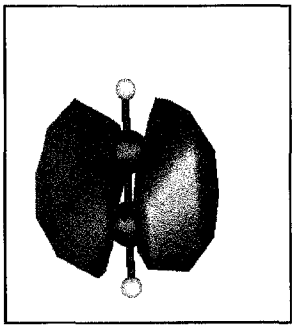
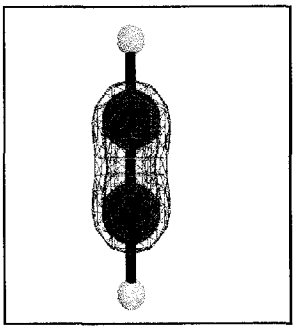

Acetylene π
bonding orbitals

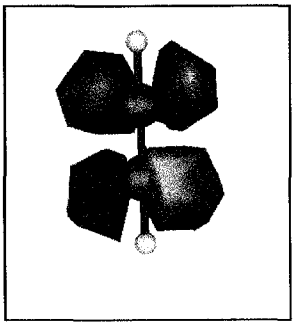
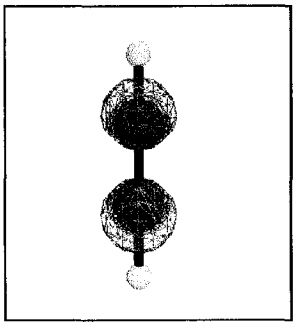

Acetylene π^*
anti-bonding
orbitals

Figure 5. Orbitals

Numbers below orbitals are Natural Orbital Occupation Numbers that represent the number of electrons in that orbital

(a) Bare Surface:

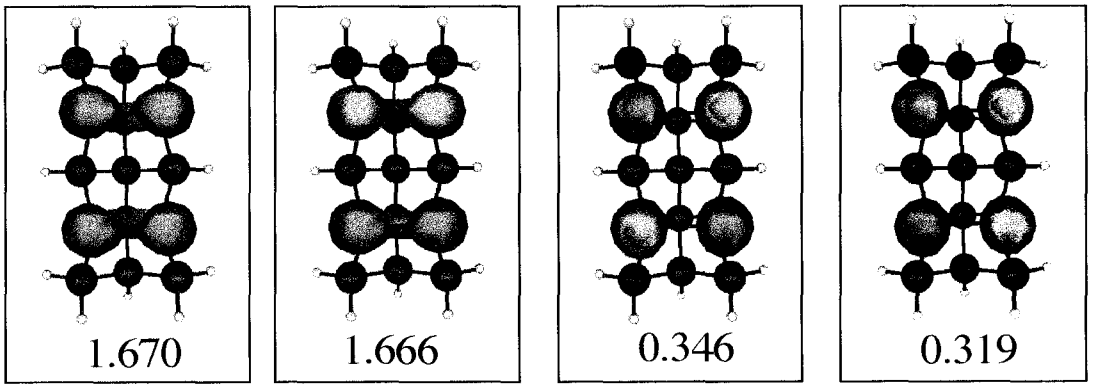

(b) Di-σ:

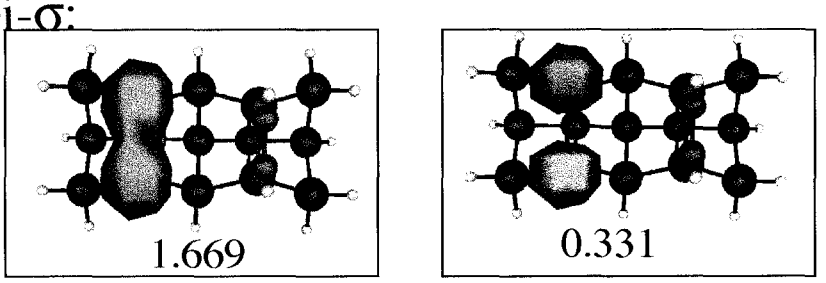

(c) Endbridge:

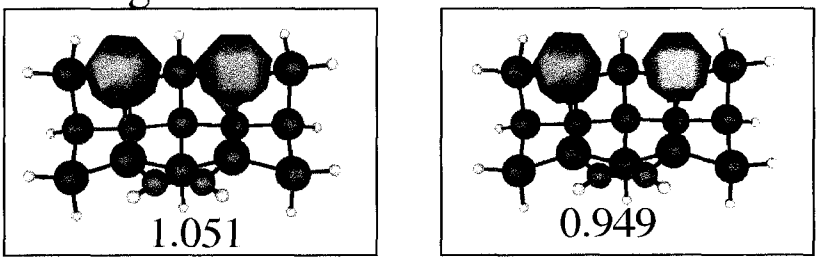

(d) Cross:

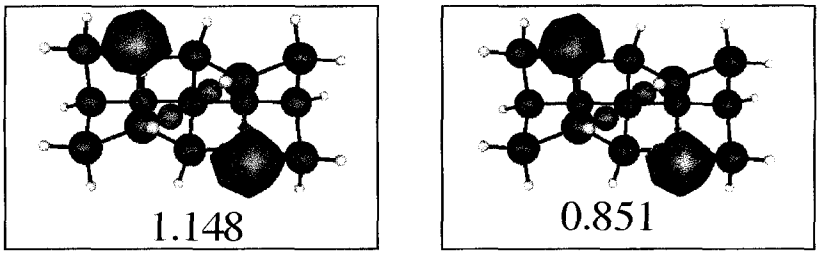

Figure 6. Normal modes

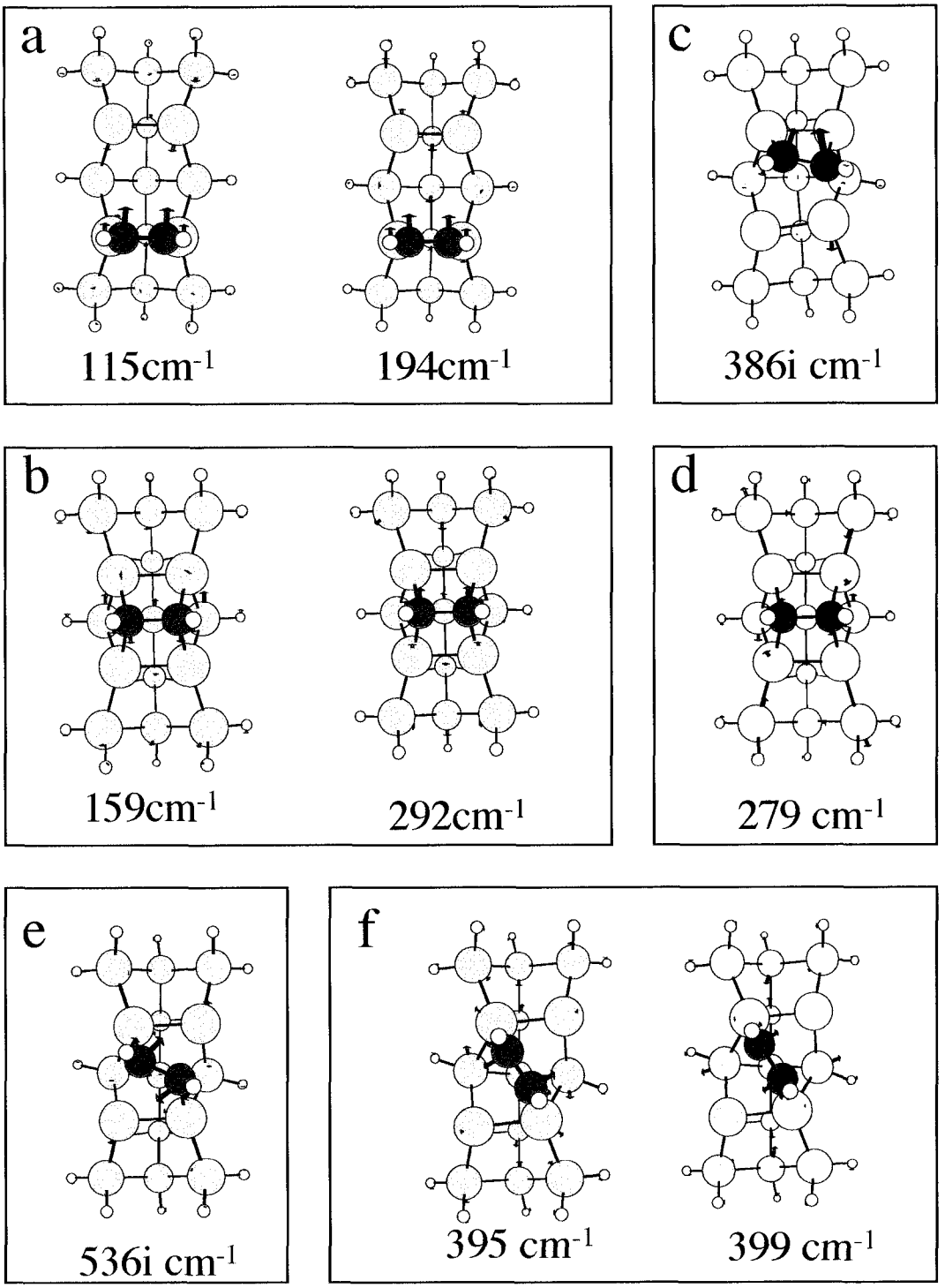

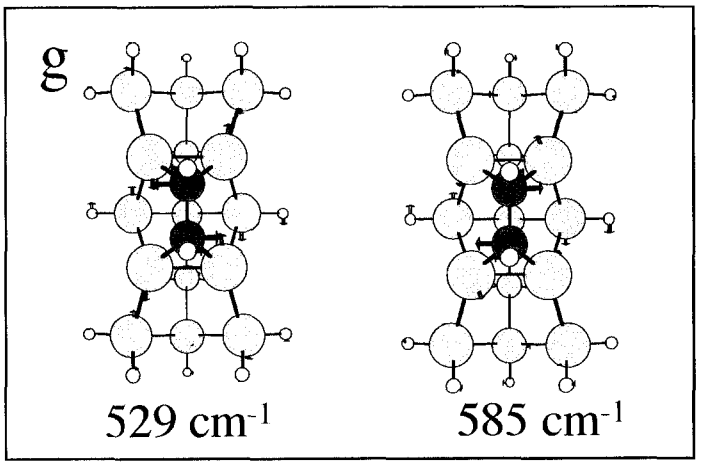
g
529 cm-1
585 cm-1

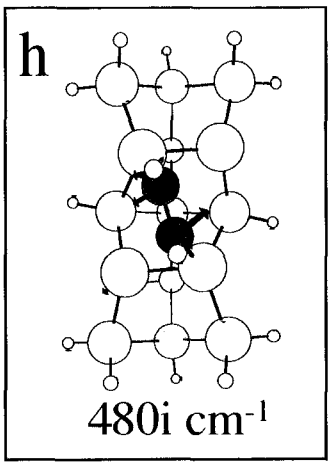
h
480i cm-1

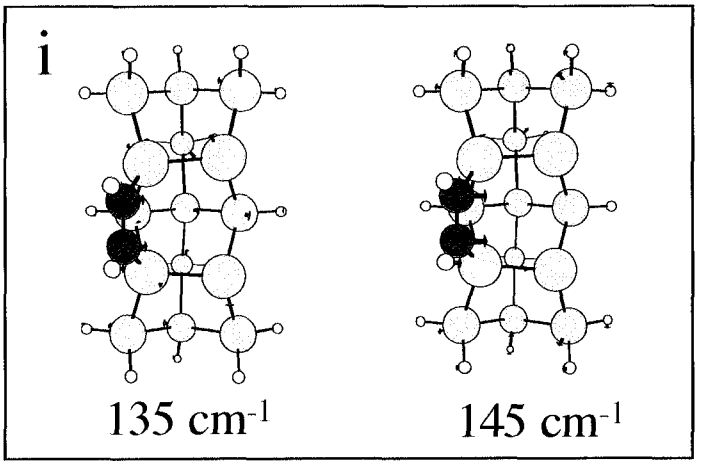
i
135 cm-1
145 cm-1

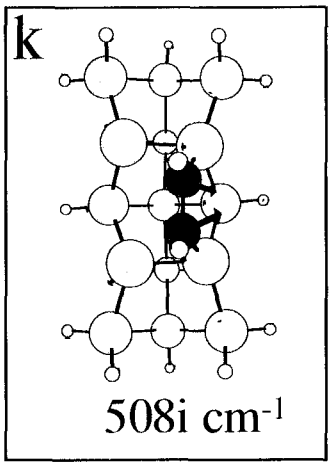
k
508i cm-1

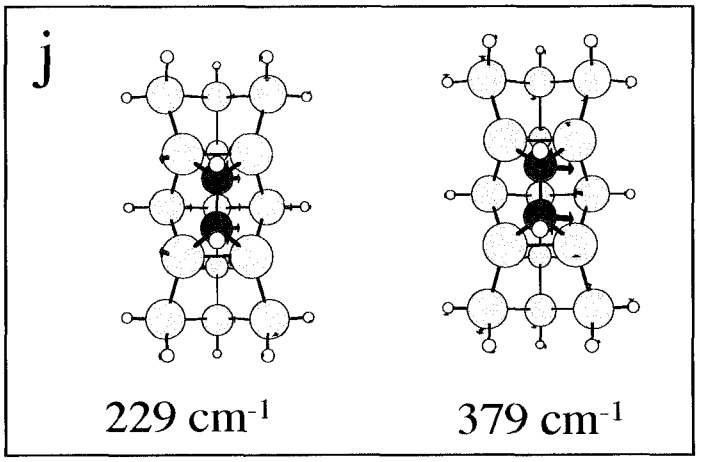
j
229 cm-1
379 cm-1

Figure 7. Composite minimum energy path

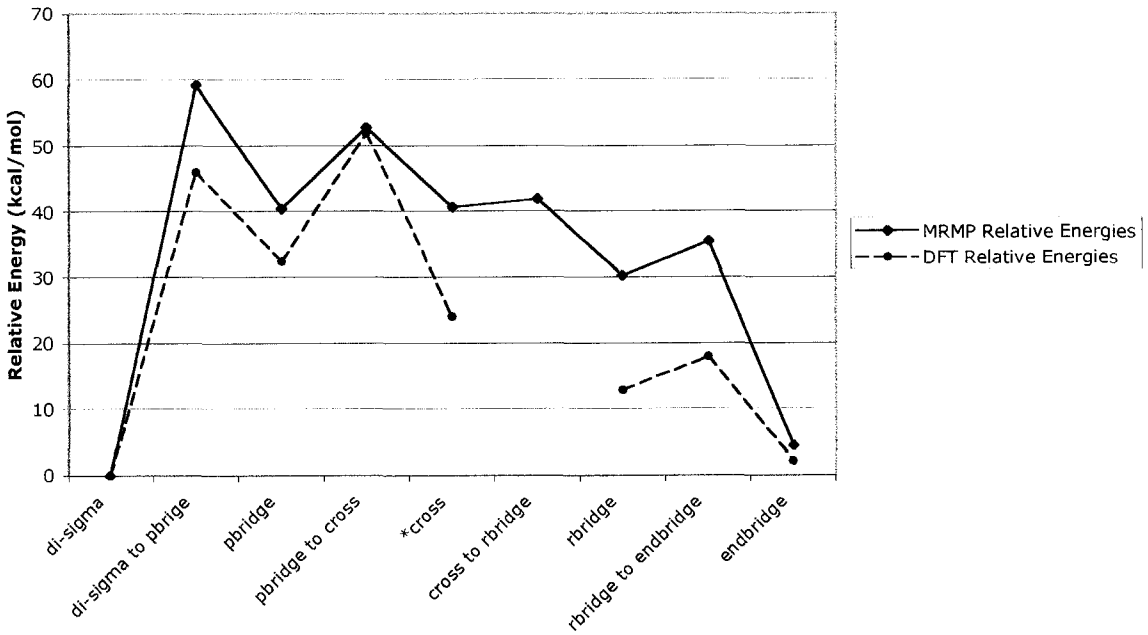

DFT relative energies are taken from Sorescu and Jordan, ref. 5, at a coverage of 0.25 monolayers, except *Cross for which the 0.5 ML coverage adsorption energy is used, because that for 0.25 ML is not available

CHAPTER 4: MULTI-REFERENCE SECOND-ORDER PERTURBATION THEORY: HOW SIZE CONSISTENT IS "ALMOST SIZE CONSISTENT"?

Jamie M. Rintelman[∞], Ivana Adamovic[∞], Mark S. Gordon[∞]

Abstract.

A systematic study of the deviation from size consistency of the MRMP2 multi-reference second order pertubation theory method is presented. The size consistency error is shown to depend on the number of monomers in a supermolecule calculation, size of basis set, number of correlated valence electrons, and size of active space. HF, F_2, and N_2 are used as test cases, with stretched bonds, to include simple, well-defined multi-reference character. This is essential in ensuring that MRMP2 is being tested as a multi-reference method.

Introduction.

Among his set of criteria for what constitutes an acceptable "model chemistry", Professor John Pople had *size consistent* high on the list. For a method to be size consistent, at minimum the energy of a supermolecule A---B, with fragments A and B separated by a long distance must be the sum of the energies computed separately for A and B. Indeed, a major reason for the great popularity of second order Moller-Plesset perturbation theory (MP2)[1], as opposed to other perturbation theory formulations, is the fact that MP2 is size consistent[2]. On the other hand, truncated configuration interaction (CI) wave functions, such as the popular singles and doubles method (CISD) are not size consistent.

[∞] The work presented in this study was performed equally by Jamie Rintelman and Ivana Adamovic under the supervision of Prof. Mark Gordon.

The increased flexibility that comes with multi-configurational self-consistent field (MCSCF) wave functions is critical to the description of many chemical phenomena, especially those that involve near degeneracies, such as one encounters as bonds are being broken or formed. If an MCSCF wave function is formulated using the complete active space (CASSCF)[3] or equivalently, a fully optimized reaction space (FORS)[4], and one uses a consistent active space, the resulting wave function is properly size consistent. However, a simple MCSCF wave function, like its Hartree-Fock (HF) analog, does not account for the so-called 'dynamic' correlation effects. For HF-based methods, dynamic correlation is incorporated using a variety of approaches, including MP2 (size-consistent) and CISD (not size-consistent). If one is starting from a FORS MCSCF wave function, the analogous methods would be multi-reference second order perturbation theory (MRPT2) or multi-reference CI (MRCI). The most common implementation MRCI is the singles and doubles analog of CISD, called MR(SD)CI. As is the case for CISD, MR(SD)CI is known to be size *in*consistent. Fortunately, for both CISD and MR(SD)CI there are simple corrections to approximately correct for the size-consistent error by estimating the contributions from higher excitations[5].

The MRPT2 approach for recovering dynamic correlation starting from an MCSCF wave function has become popular because, like its single-reference analog MP2, it is computationally efficient when compared with the alternative of MR(SD)CI. Unlike its closed-shell single reference counterpart, MRPT2 is not uniquely defined. Consequently, thus, there have been several alternative implementations, including CASPT2[6] of Roos' group, MROPT[7] of Davidson's group, Hirao's MRMP2[8], and Nakano's MCQDPT2[9]. Unlike MRCI, for which the lack of size-consistency is clear, the error in MRPT2 methods depends on the choice of the zeroth order Hamiltonian. This study focuses on MCQDPT2 and MRMP2, which are equivalent when the multi-state MCQDPT2 theory is applied to a single state.

While the various flavors of MRPT have seen wide application, its size extensivity and size consistency properties have received surprisingly little attention. In a recent paper, Witek, Nakano and Hirao[10] used Ne dimer as a test of size-consistency, or lack thereof, and concluded that their methods are "almost size consistent; the largest deviation from size-consistency is 0.18 kcal/mol. Very large errors from size-consistency are observed for the MRCI method..." However, Ne and Ne_2 are essentially closed shell, and therefore do not have the very property for which the method was developed. Thus, the multi-reference nature of MRPT is not being tested, and their study is essentially a comparison of the single reference MP2 (known to be size-consistent) and CISD (known to be size-inconsistent) methods.

Presented herein is a systematic study of size-consistency errors in MRMP2, and the factors that affect the magnitude of these errors.

Method.

The size consistency error (SCE) is defined as the difference between the sum of the energies obtained from the separate monomer calculations and the energy obtained from a calculation in which all the monomers are present but separated by distances sufficient to guarantee no interactions between them (the "super-molecule" calculation). Thus, for the A---B system discussed above,

$$SCE=|E(A)+E(B)-E(A\text{---}B)|. \qquad (1)$$

The above notion of size consistency can be impacted by several parameters that define the size of the model system in different senses, including:

1) number of monomers
2) size of the basis set
3) number of electrons

4) size of the active space

The aim of the present study is to examine the impact of each parameter in turn, on the SCE. The details of each study are given below.

Because MRMP2 is a multireference method, it is important to include test cases that are multireference in nature. This is accomplished here by choosing molecules well suited to testing the four size criteria, and then stretching bond lengths to ensure that there is significant occupation outside the single reference. Bond lengths and natural orbital occupation numbers (NOONs) are listed in Table 1 for HF, F_2 and N_2, the three test molecules chosen for this study. NOONs indicate the number of electrons present in an orbital. N_2 is the least multireference of the set, with σ and σ^* occupation number close enough to closed shell to be described with a single reference wave function, but with occupation numbers for the π and π^* orbitals well outside the range in which a single reference wave function would be appropriate.

Now consider the following points:

1) To study the dependence of the SCE on the number of monomers, up to six HF molecules are considered, using an active space for each HF that consists of two electrons occupying the σ and σ^* orbitals. The active space will be denoted (2,2). The presence of well-defined, yet simple, multi-reference character is guaranteed by stretching the H-F bond to 1.6Å. The choice of HF simultaneously facilitates the second study, on the effect of basis set, described below.

2) To study the basis set effect on the SCE, a system that can be described by a wide range of basis sets and remain computationally tractable is needed. The HF molecule is described by two basis sets due to Pople and co-workers, the 6-31G(d,p)[11,12] and 6-311G(d,p)[13], and three correlation consistent basis sets, cc-pVDZ, cc-pVTZ, and cc-pVQZ, by Dunning and coworkers[14]. In addition, the latter three basis sets facilitate an extrapolation[15] of the one-particle basis to the approximate complete basis set (CBS)

limit. Furthermore, we combine the first two studies so that the effects of one may be removed from the other. Thus, calculations using all five basis sets are carried out on one to six HF molecules.

3) In examining the effect of increasing the number of electrons the comparison of systems with many subtle chemical differences is unavoidable. First, it is sensible to choose HF since data on effects 1 and 2, above, will be available should their influence become important. Then, given the constraints of tractability, the (2,2) active space, and the desire to increase the number of chemically relevant *valence* electrons (rather than inactive *core* electrons), a natural choice is F_2. Since the active space is the same as that used for HF, the additional valence electrons test the impact that an increase in the valence dynamic correlation (i.e. the MP2 part of the calculation) has on the SCE. As for HF, the single bond of F_2 is stretched to ensure multi-reference character. The cc-pVTZ basis is used for F_2.

4) N_2 is chosen to examine the impact of increasing the active space since its triple bond permits three well defined spaces: (2,2) including σ and σ^*, (4,4) including both π and π^* orbitals, and (6,6) including σ, σ^*, π, and π^*. The cc-pVTZ basis is used for these tests.

Finally, several of the above factors are combined in an example to illustrate that the magnitude of the size consistency error is significant in 'real world' applications. This example is taken from a study on the reaction of acetylene on the Si(100)-(2x1)[16]surface, and includes the $Si_{15}H_{16}$ cluster with one and two acetylenes, and the Si_9H_{12} cluster with one acetylene. The silicon atoms have the Hay-Wadt[17] effective core potential basis set supplemented with d functions from the 6-31G(d)[12] basis. The 6-31G(d)[11] basis is employed for C and H. The GAMESS program was used for all calculations[18].

Results/Analysis.

The dependence of the SCE on the number of monomers and the basis set is shown in Figures 1-3, and Tables 2-4, for all cases. The SCE grows rapidly with the number of monomers in the supermolecule calculation. Figures 4 and 5 show that the *error per monomer* is approximately linear. This suggests that the SCE can be characterized as a many-body effect. Assuming the error for two monomers is the two-body error, the SCE can be approximated by scaling this two-body interaction by the number of unique monomer pairs. That is,

$$(SCE)_n = (SCE)_2 \times n(n-1)/2 \qquad (1)$$

where n is the number of monomers. Plots of equation (1) using the CBS $(SCE)_2$ for HF and the cc-pVTZ $(SCE)_2$ for F_2 are compared with the exact SCE in Figures 1 and 2, and found to match reasonably well. Note that deviations begin at n=4, the range at which there are now a significant number of 3-body and greater interactions; even so, at n=6 the two-body approximation still recovers 84% and 87% of the total error for HF and F_2, respectively.

Now consider the effect of basis set size. Each of the five basis sets is used to calculate the MRMP2 energy for 1 to 6 HFs. The shape of the curve is qualitatively the same for each number of HFs (Fig 6), which indicates that the many-body effect described above is independent of the chosen atomic basis set. While HF has 20 basis functions with both the 6-31G(d,p) basis and the cc-pVDZ basis, the 6-31G(d,p) lies slightly off the curve. This is most likely simply due to the fact that the basis sets are slightly different.

Although the *shape* of the curve is similar for all of the basis sets, there are important quantitative changes as the basis set is increased. As an example, consider the error in size consistency for n = 3 as the basis set is increased. For the smallest, 6-31G(d,p) basis set, the SCE is ~ 3 kcal/mol. For the largest basis set, cc-pVQZ, this increases to ~ 5 kcal/mol, and at the CBS limit, the SCE is ~ 6 kcal/mol. So, the SCE approximately doubles as one

increases the basis set from a modest one to the CBS limit. This is a substantial basis set effect.

Since the basis set effect has been demonstrated for HF, the analysis of F_2 was limited to one basis set, cc-pVTZ (Figure 2 and Table 3). F_2 shows a significant increase in SCE over HF. HF and F_2 are analogous molecules, in which H and F each have one unpaired valence electron being shared to form a single bond. However, F_2 has nearly twice the number of "observer" valence electron pairs that are included in the MRMP2 (dynamic correlation) step. The fact that the SCE increases dramatically when H is replaced by F suggests that the additional valence electrons that are correlated in the perturbation step exacerbates the problem. While the absolute error is much larger for F_2 than HF, the SCE divided by the total energy is also larger.

The MRMP2 energy was calculated for N_2 with three different active spaces, using the cc-pVTZ basis set, to examine the active space effect on the SCE. The results are presented in Table 4 and Figure 3. The factorial scaling of FORS-SCF with the size of the active space limits the range over which investigations of active space dependence are practical. In order to see a trend the smaller active space must be a subset of any larger active space in order to sensibly compare the two. There are two important observations to note. For a given active space, the increase in the SCE is qualitatively similar to that illustrated earlier for HF and F_2; a greater than linear increase with the number of N_2 molecules. Second, for a fixed number (2) of N_2 molecules, the SCE decreases as the active space is increased. This is almost certainly because a larger part of the correlation problem is being treated in a size consistent manner for the larger active space, i.e. Full-CI within the active space.

Acetylene on Si(100).

The possibility that size consistency for the MRMP2 method could be a serious issue was first discovered during a study of the adsorption of acetylene molecules on the Si(100)-(2x1)

surface[16]. In order to determine the adsorption energy of one, two or more acetylenes on the surface, one must compare the energies of the complex and of the separated reactants. It is the computation of the energy of the separated reactants that involves the issue of MRMP2 size consistency. The surface models employed were Si_9H_{12} and $Si_{15}H_{16}$. The SCEs for $Si_{15}H_{16}$ plus one and two acetylenes, and Si_9H_{12} plus one acetylene, are shown in Table 5. The errors are sizeable, as is the case with the test systems discussed above, and cannot be neglected without disastrous effects on reported adsorption energies.

Note, as well, that the error for $Si_{15}H_{16}$ + 2 C_2H_2 can be reasonably approximated as the sum of the two-body errors: $2(Si_{15}H_{16} + C_2H_2) + (C_2H_2 + C_2H_2) = 2*21.9 + 2.2 = 46.0$ kcal·mol^{-1} with 49.1 kcal·mol^{-1} for the exact error. This 3.1 kcal·mol^{-1} difference is too large to recommend the use of the two-body approximation for quantitatively estimating the exact size consistency error.

Conclusions.

The calculations presented here emphasize the importance of knowing the limitations of a method when using it. While MRMP2 can be quite accurate and useful for relative energies, in contrast to MRCI, there is currently no simple way to estimate the MRMP2 SCE. It is therefore important that supermolecule calculations be done when necessary to eliminate any size consistency errors. This should never be prohibitively expensive, since, if one can afford a calculation of the complex, the calculation of the supermolecule should be no more expensive. Of course, if the expense of computing the complex stresses the limits of resources at ones disposal, it may be difficult to do an equally expensive supermolecule calculation.

The many body effect present in the growth of this error with respect to the number of separated reactants is quite startling. While one mediating factor may be that most applications are likely to involve no more than two separated reactants, the error can still be on the order of several kcal/mol, as illustrated with the test cases in this study.

The authors suggest that the phrase "almost size consistent" is an inappropriate and misleading characterization of the MRMP2 method.

Acknowledgements. The authors are grateful to Dr. Michael Schmidt for several illuminating discussions. This work was supported by grants from the Air Force Office of Scientific Research (MSG, IA) and the Department of Energy via the Ames Laboratory (JMR). The calculations were performed on an cluster of Power3 and Power4 workstations made possible by SUR grants from IBM and funding from AFOSR and DOE.

References:

1 C. Moller and S. Plesset, Phys. Rev. **46**, 618 (1934).

2 N. S. Ostlund and M. F. Bowen, Theoretica Chimica Acta **40** (2), 175 (1975).

3 B. O. Roos, P. Taylor, and P. E. Siegbahn, Chemical Physics **48**, 157 (1980).

4 K. Ruedenberg, M. W. Schmidt, M. M. Gilbert, and S. T. Elbert, Chemical Physics **71** (1), 41 (1982).

5 M. Robb, Molecular Physics **44**, 173 (1981); S. R. Langhoff and E. R. Davidson, International Journal of Quantum Chemistry **8**, 61 (1974).

6 B. O. Roos, K. Andersson, M. K. Fulscher, P.-A. Malmqvist, L. Serrano-Andres, K. Pierloot, and M. Merchan, Advances in Chemical Physics **93**, 219 (1996).

7 P. M. Kozlowski and E. R. Davidson, Journal of Chemical Physics **100**, 3672 (1994).

8 K. Hirao, Chemical Physics Letters **190**, 374 (1992); K. Hirao, Chemical Physics Letters **196**, 397 (1992); K. Hirao, International Journal of Quantum Chemistry **S26**, 517 (1992); K. Hirao, Chemical Physics Letters **201**, 59 (1993).

9 H. Nakano, Journal of Chemical Physics **99** (10), 7983 (1993); H. Nakano, Chemical Physics Letters **207**, 372 (1993).

[10] H. A. Witek, H. Nakano, and K. Hirao, Journal of Chemical Physics **118** (18), 8197 (2003).

[11] W. J. Hehre, R. Ditchfield, and J. A. Pople, Journal of Chemical Physics **56**, 2257 (1972).

[12] R. Ditchfield, W. J. Hehre, and J. A. Pople, Journal of Chemical Physics **54**, 724 (1971); P. C. Hariharan and J. A. Pople, Theoretica Chimica Acta **28**, 213 (1973).

[13] R. Krishnan, J. S. Binkley, R. Seeger, and J. A. Pople, J. Chem. Phys. **72**, 650 (1980).

[14] T. H. Dunning Jr., Journal of Chemical Physics **90** (2), 1007 (1989).

[15] T. Y. Yan, W. L. Hase, and C. Doubleday, Journal of Chemical Physics **120** (19), 9253 (2004); D. Feller, Journal of Chemical Physics **111** (10), 4373 (1999); D. Feller and J. A. Sordo, Journal of Chemical Physics **113** (2), 485 (2000); A. Halkier, T. Helgaker, P. Jorgensen, W. Klopper, H. Koch, J. Olsen, and A. K. Wilson, Chemical Physics Letters **286** (3-4), 243 (1998); G. A. Petersson and M. J. Frisch, Journal of Physical Chemistry A **104** (11), 2183 (2000).

[16] J. M. Rintelman and M. S. Gordon, Journal of Physical Chemistry B **108** (23), 7820 (2004).

[17] W. R. Wadt and P. J. Hay, Journal of Chemical Physics **82** (1), 284 (1985).

[18] G. D. Fletcher, M. W. Schmidt, B. M. Bode, and M. S. Gordon, Computer Physics Communications **128** (1-2), 190 (2000); M. W. Schmidt, K. K. Baldridge, J. A. Boatz, S. T. Elbert, M. S. Gordon, J. H. Jensen, S. Koseki, N. Matsunaga, K. A. Nguyen, S. J. Su, T. L. Windus, M. Dupuis, and J. A. Montgomery, Journal of Computational Chemistry **14** (11), 1347 (1993).

Table 1. Natural Orbital Occupation Numbers

HF - bond distance 1.60Å

6-31G(d,p)	6-311G(d,p)	cc-pVDZ	cc-pVTZ	cc-pVQZ
1.7623, 0.2377	1.7662, 0.2338	1.7645, 0.2355	1.7731, 0.2269	1.7756, 0.2244

F_2 - bond distance 1.50Å

cc-pVTZ
1.7662, 0.2338

N2 - bond distance 1.50Å

	cc-pVTZ		
	(2,2)	(4,4)	(6,6)
σ,σ^*	1.9564, 0.0436	n/a	1.9323, 0.0681
π,π^*	n/a	1.7539,0.2461	1.8042, 0.1956

Table 2. size consistency error (hartree) for HF as a function of basis set and number of HF monomers

#HFs	6-31G(d,p)	6-311G(d,p)	cc-pVDZ	cc-pVTZ	cc-pVQZ	CBS	two-body SCE
1	0.00000	0.00000	0.00000	0.00000	0.00000	0.00000	0.00000
2	0.00169	0.00174	0.00159	0.00234	0.00266	0.00284	0.00284
3	0.00518	0.00536	0.00487	0.00724	0.00826	0.00884	0.00000
4	0.01058	0.01100	0.00996	0.01496	0.01719	0.01839	0.00000
5	0.01837	0.01883	0.01698	0.02582	0.02991	0.03200	0.00000
6	0.02769	0.02911	0.02614	0.04028	0.04727	0.05053	0.00000

Table 3. Size consistency error (hartree) as a function of number of F_2 monomers per calculation

#F_2s	F_2 (cc-pVTZ)	two-body approximate SCE
1	0.000000	0.000000
2	0.005307	0.005307
3	0.016401	0.015921
4	0.033874	0.031842
5	0.058484	0.053070
6	0.091235	0.079605

Table 4. Size consistency error (hartree) as a function of active space and number of N_2s per calculation

#N_2s	(2,2) active space	(4,4) active space	(6,6) active space
1	0.000000	0.000000	0.000000
2	0.016575	0.015733	0.011497
3	0.051809	0.053651	
4	0.108261		
5	0.189039		

Figure 1. Size consistency error as a function of the number of HFs in the supermolecule

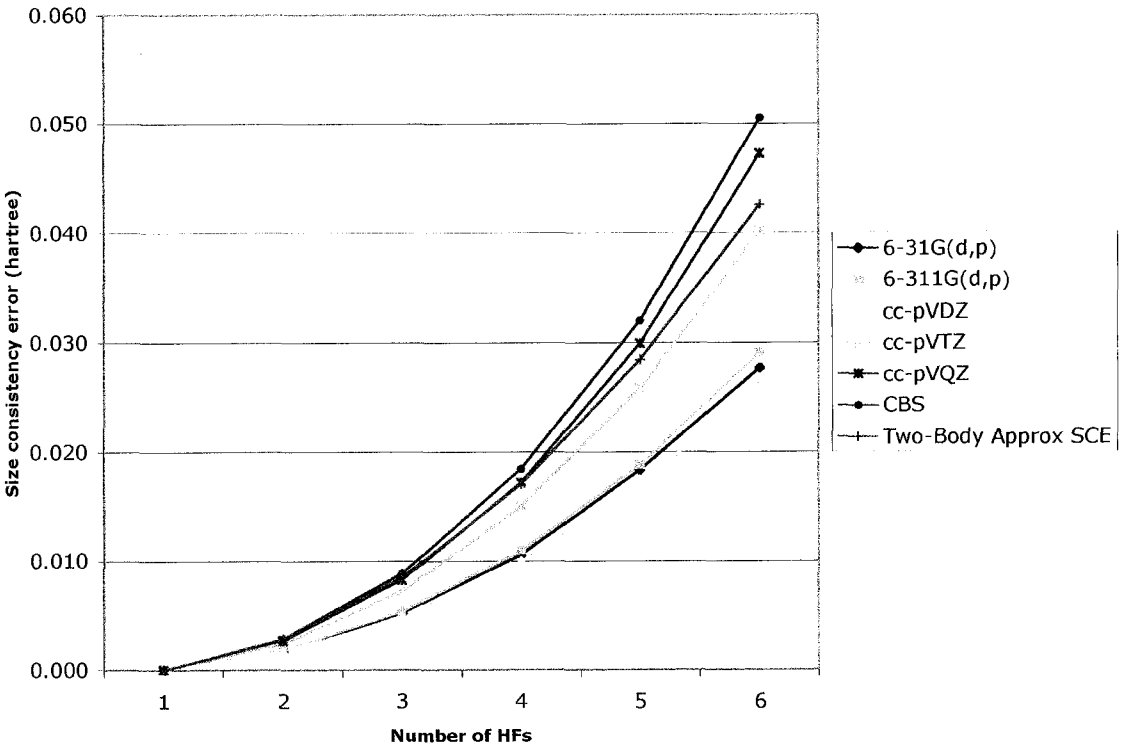

Figure 2. Size consistency error as a function of the number of F_2 molecules

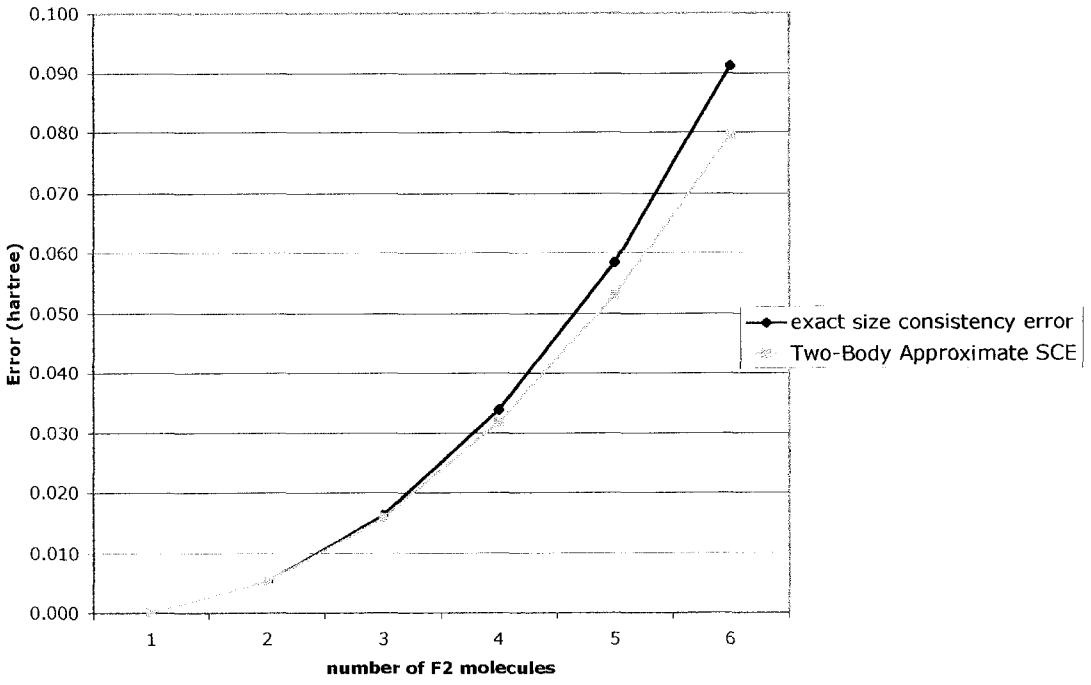

Figure 3. Size consistency error as a function of the number of N_2 molecules

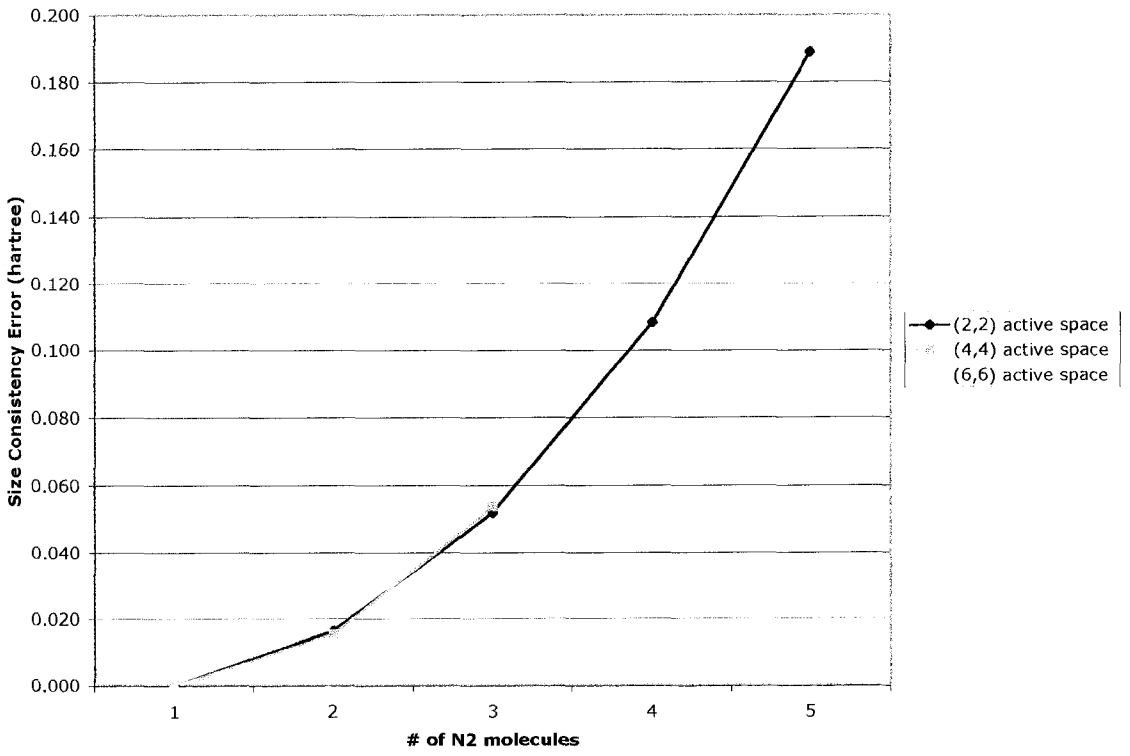

Figure 4. Size consistency error per HF as a function of the number of HFs

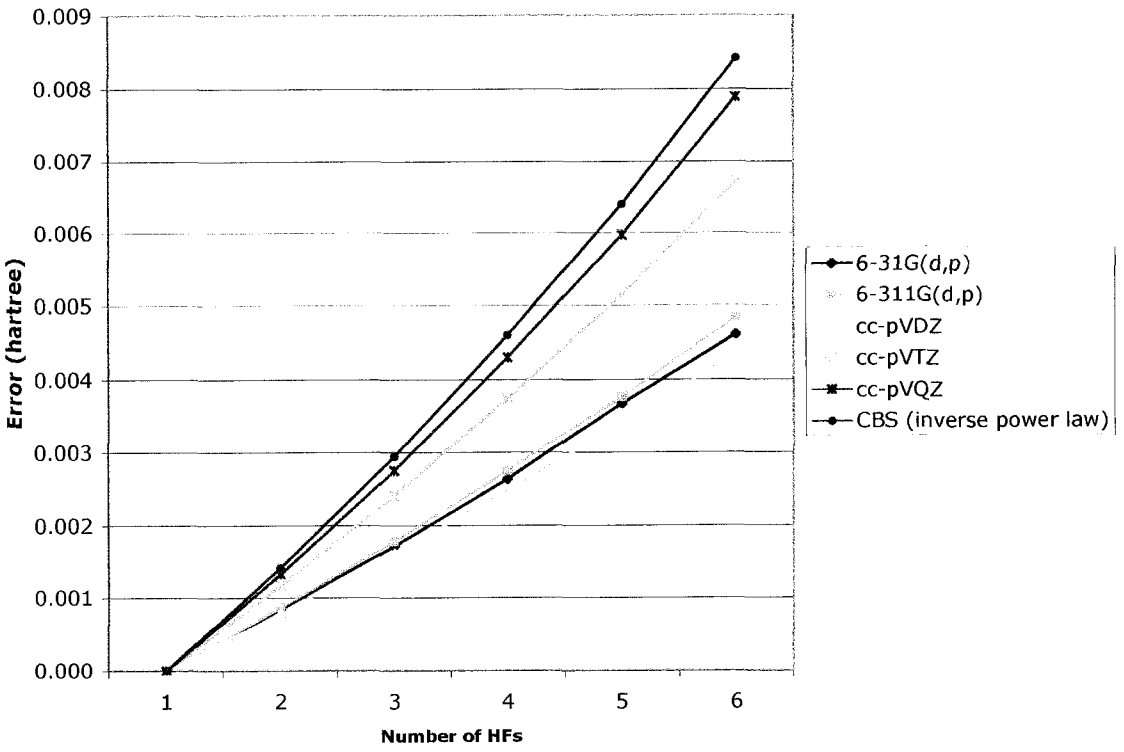

Figure 5. Size consistency error per F_2 molecule as a function of the number of F_2s

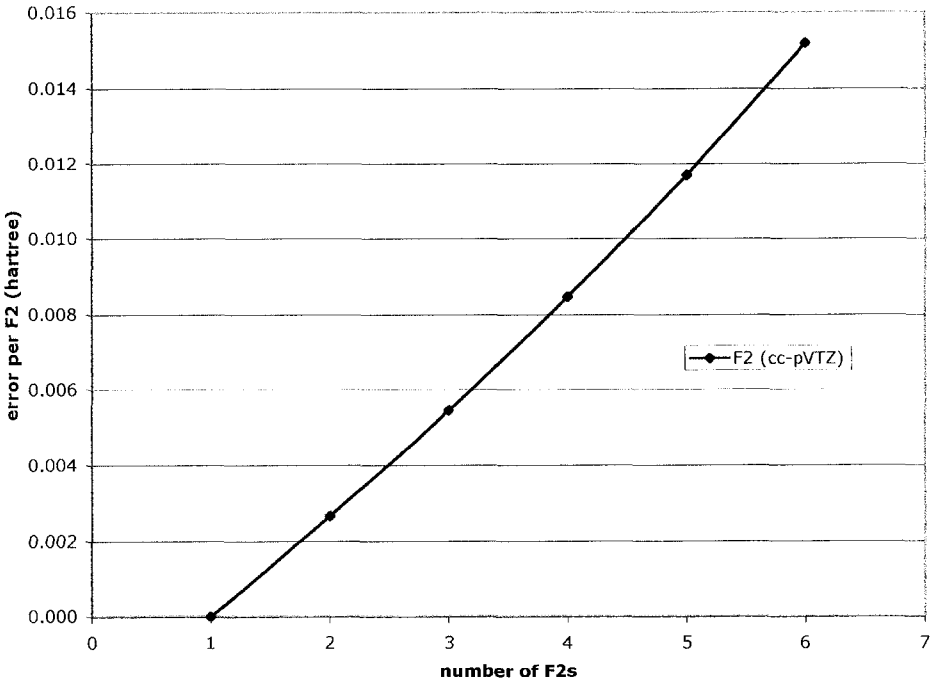

Figure 6. Size consistency error as a function of the number of basis functions per HF

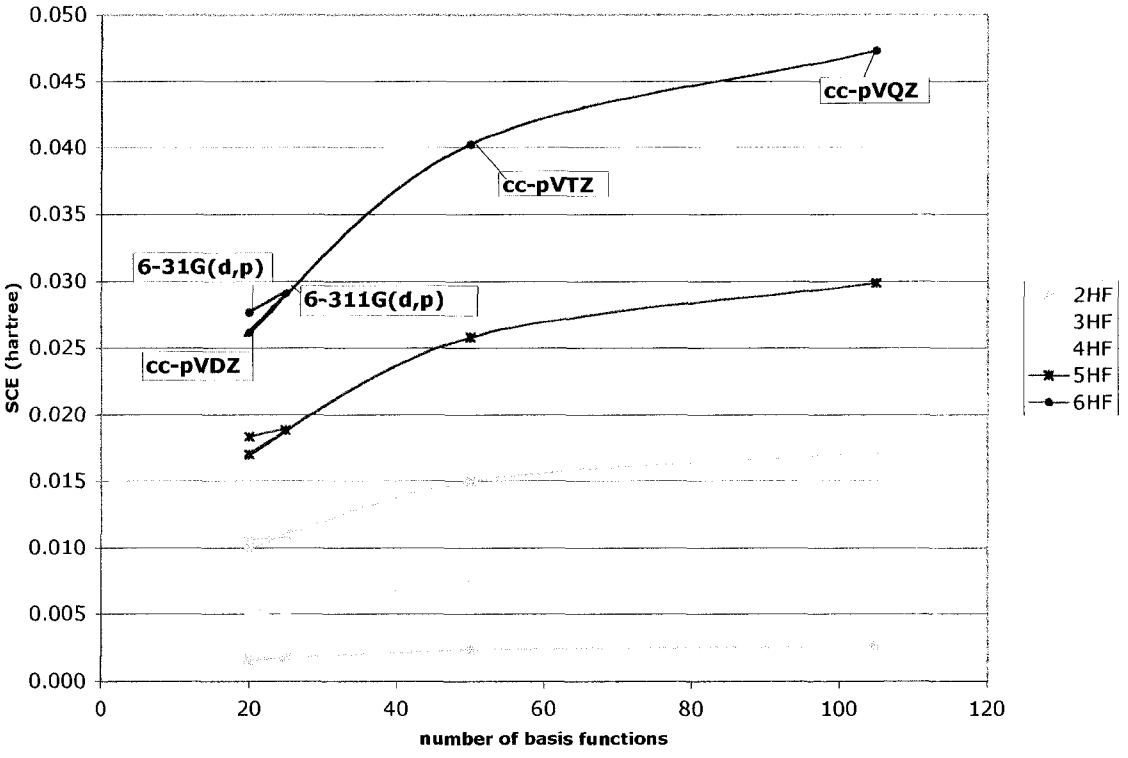

CHAPTER 5: EXCHANGE REPULSION IN THE GENERAL EFFECTIVE FRAGMENT POTENTIAL (EFP) METHOD

Jamie M. Rintelman and Mark S. Gordon

Abstract

Presented herein are energy and gradient expressions for the ab initio-EFP exchange repulsion interaction in the effective fragment potential method. The effective fragment potential method contains terms representing Coulomb, polarization, and exchange repulsion + charge transfer effects included as one-electron terms in the ab initio Hamiltonian. In the original implementation, the exchange repulsion + charge transfer term is fitted to a potential derived from calculations on the water dimer. The analytical exchange repulsion energy and gradient expressions presented here represent a step towards eliminating this fitted term. Without the fitted term a potential can be generated for any solvent in a single ab inito calculation. Approximations are made to the two-electron terms and some of the one-electron terms to produce an efficient analytical approach to evaluating the exchange repulsion energy and gradient.

I. Introduction.

The majority of chemical reactions occur in solution. In many areas, such as biochemistry, the natural solvent is water. However, many other solvents are common in organic and inorganic chemistry. It is no surprise then that quantum chemists are increasingly motivated to develop and utilize methods that enable the treatment of solvent effects, as they can significantly alter the character and mechanism of a reaction.

Solvent models belong to one of two classes: continuum or discrete. Continuum solvent models present an efficient approach to simulating the presence of a bulk solvent. They reproduce the behavior of the bulk well by surrounding the solute with a dielectric

continuum. However, continuum models do not include the interactions between the solute and individual solvent models.

Discrete solvent models replace each individual solvent molecule with a potential derived or obtained from quantum mechanics for that particular molecule. This is a more expensive approach, but can explicitly treat the direct interaction between the solute and solvent, which is more robust than the continuum approach. For a large number of solvent molecules, discrete methods have the complication of requiring adequate sampling of the configuration space. With a small number of solvent molecules this can be done using chemical intuition or simply placing the solvent molecules in every possible coordination; however, with a larger number of solvent molecules this is nearly impossible, and a simulation method like Monte Carlo or molecular dynamics is required. The greater complexity of the discrete approach to solvation over continuum approaches is usually outweighed by the greater accuracy achieved with discrete solvent models. It may be that the best approach involves a combination of continuum and discrete methods[1].

II. Overview of the effective fragment potential (EFP) method

The EFP[2] method is a discrete solvent/liquid model that was originally developed for water. The system is divided into two regions, ab initio and EFP. The ab intio region includes the solute or reaction of interest and perhaps a small number of ab intio solvent molecules directly involved in the reaction. The EFP region includes all of the additional solvent molecules represented by EFPs.

The original implementation[3-5] of the EFP method was based on the Hartree-Fock (HF) approximation, and includes (1) Coulomb (2) polarization and (3) exchange repulsion, and charge transfer. These interactions occur between the EFP and ab initio regions and between pairs of effective fragments. The EFP interactions with the ab intio region are added as one electron terms to the ab initio Hamiltonian. The interactions within the EFP region are simple potentials, since the EFPs themselves are classical potentials. The Coulomb and

polarizability terms are based on properties of the solvent monomer and can be generated by a single ab initio calculation on that monomer. In the original EFP implementation, henceforth referred to as EFP1, the third term is a 'remainder' term containing all effects from HF not included in the first two terms. The remainder term is fitted to a functional form, based on the water dimer potential.

The success of the EFP1 method has led to the desire to remove the inconvenience of fitting the third term, so that the methods can be easily and generally extended to any solvent or liquid. For a general model that includes additional contributions, such as dispersion, this remainder term would require additional analytic functions to include all of the effects that it would have to model, thereby making the fitting process more complex. The alternative approach is to derive general expressions, from first principles, for each interaction that is represented in the EFP1 remainder term. First among these is the exchange repulsion. This requires the derivation of expressions that accurately account for the exchange repulsion interaction between EFPs and between an EFP and the ab initio region. The EFP-EFP exchange repulsion interaction has been developed and implemented by Jensen and coworkers[6,7], and an expression for the ab initio/EFP energy[8] has been reported.

III. Ab-Initio/EFP Exchange Repulsion Energy.

Each ab initio/EFP pair can be defined as a bimolecular system in which the RHF wave function of each isolated molecule A and B is expressed in terms of orthonormal molecular orbitals (MOs), for which the intermolecular overlap is nonzero. This allows one to express the total energy in terms of the energies of the isolated molecules plus intermolecular coulomb and exchange repulsion energies[2]. The exchange repulsion energy can then be expressed in terms of the intermolecular overlap, through second order.

The exchange repulsion energy between the ab initio region and an EFP[8], is given by

$$E^{XR} = -2\sum_i^A \sum_j^B \langle ij|ij\rangle - 2\sum_i^A \sum_j^B S_{ij}\left[2\left(V_{ij}^A + G_{ij}^A\right) + \sum_l^B F_{jl}^B S_{li}\right] + 2\sum_i^A \sum_j^B S_{ij}\left[\sum_k^A S_{kj}\left(F_{ik}^A + V_{ik}^B + J_{ik}^B\right) + S_{ij}\left(V_{jj}^A + J_{jj}^A\right) - \sum_k^A S_{kj}\langle ik|jj\rangle\right] \quad (1)$$

where the convention, here and throughout this paper, is that A signifies the ab initio piece and B signifies an EFP. For two-electron integrals a superscript of A or B denotes a hidden sum over obitals on that piece

i.e. $J_{ij}^A = \sum_{n\in A} \langle ij|nn\rangle$

$K_{ij}^B = \sum_{l'\in B} \langle il'|kl'\rangle$,

$G_{ij}^A = 2J_{ij}^A - K_{ij}^A$

and $\langle \mathrm{ij}|\mathrm{kl}\rangle = \int d\mathbf{r}_1 d\mathbf{r}_2 \psi_i^*(\mathbf{r}_1)\psi_j(\mathbf{r}_1) r_{12}^{-1} \psi_k^*(\mathbf{r}_2)\psi_l(\mathbf{r}_2)$

additionally, throughout the paper a primed index i.e. n', is always on the EFP region, as is j. Unprimed indices are in the ab intio region.

For potential energy integrals a superscript A or B indicates that piece over which the sum over nuclear centers occurs;

i.e. $V_{ik}^B = \sum_{J\in B} \left\langle i \left| \frac{-Z_J}{\mathbf{r}_{1J}} \right| k \right\rangle$

The orbitals on the ab initio piece are optimized, and will be discussed later in this section. The EFP orbitals on the other hand are localized molecular orbitals (LMOs), calculated using the Boys localization procedure[9] which are determined during the initial EFP construction process and then frozen throughout the subsequent calculations. The LMOs, as well as the Fock matrix and other properties, for each EFP are generated with a single separate ab initio calculation, and then are included as input data. The internal geometry of the EFP is defined by the user in this calculation, and frozen thereafter. The EFP data needs to be generated only one time, and can then be stored and reused. Likewise, an EFP needs to be generated only once for each type of solvent molecule, since the EFP is based on the properties of the isolated monomer.

Now consider the ab initio orbitals. The variational derivative of Eq. (1) gives an exchange repulsion Fock matrix.

$$
\begin{aligned}
V_{mi}^{XR} = & -\sum_j^B \langle mj|ij\rangle - \tfrac{1}{2}\sum_j^B S_{mj}\left[2\left(V_{ij}^A + G_{ij}^A\right) + \sum_l^B F_{jl}^B S_{li}\right] \\
& - \tfrac{1}{2}\sum_j^B S_{ij}\left[2\left(V_{mj}^A + G_{mj}^A\right) + \sum_l^B F_{jl}^B S_{lm}\right] \\
& - \sum_k^A \sum_j^B S_{kj}\left(4\langle kj|mi\rangle - \langle km|ji\rangle - \langle ki|jm\rangle\right) \\
& + \sum_j^B S_{mj}\left[\sum_k^A S_{kj}\left(F_{ik}^{A'} - \langle ik|jj\rangle\right) + S_{ij}\left(V_{jj}^A + J_{jj}^A\right)\right] \\
& + \sum_j^B S_{ij}\left[\sum_k^A S_{kj}\left(F_{mk}^{A'} - \langle mk|jj\rangle\right)\right] \\
& + \tfrac{1}{2}\sum_n^A \sum_j^B \sum_k^A S_{k'j} S_{kj}\left\{4\langle nk|im\rangle - \langle nm|ik\rangle - \langle ni|mk\rangle\right\} + \sum_k^A \sum_j^B S_{kj}^2 \langle jj|mi\rangle
\end{aligned}
\qquad (2)
$$

where $F_{ik}^{A'} = F_{ik} + V_{ik}^B + J_{ik}^B$.

When V_{mi}^{XR} is added to the ab initio Fock matrix during the orbital optimization procedure, the ab initio orbitals are optimized with respect to the ab initio/EFP exchange repulsion interaction. Using these orbitals to evaluate E^{XR} in Eq. (1) gives the ab initio/EFP exchange repulsion energy.

This exchange repulsion Fock matrix is important for later formulation of gradients. Having optimized orbitals ensures that the Lagrangian is symmetric, that matrix elements between occupied and virtual orbitals are zero. This greatly simplifies the derivation and implementation of the derivative expression by allowing the replacement of derivatives of coefficient matrices with derivatives of overlap matrices[10].

IV. Ab Initio / EFP E^{XR} approximations.

Both Eqs (1) and (2) contain two-electron terms which would be too expensive to evaluate exactly. A number of approximations are made to reduce the expense of these two-electron terms, as well as some of the one-electron terms in these expressions. The approximations

used here are based on either a multipole expansion[11] or a spherical Gaussian overlap(SGO) approximation[12], and have been previously reported [8]. They are explained below.

Previous applications of the SGO approximation have used localized orbitals to maximize the accuracy of this approximation, and have shown that errors with canonical orbitals are unacceptably large[7]. Here, the ab initio orbitals cannot be localized, since localizing the orbitals after each orbital optimization step would be prohibitively expensive. Instead the SGO approximation is applied to the integrals in the atomic orbital (AO) basis, taking advantage of the inherently localized nature of AOs. The integrals are then transformed to the MO basis.

Two-electron terms.

There are three types of two-electron integrals that must be considered, depending upon the number and combination of orbitals from the ab initio and EFP pieces. These three types are $\langle AB|AB\rangle$, $\langle AB|AA\rangle$, and $\langle AA|BB\rangle$, where A denotes an ab initio orbital and B denotes an EFP orbital.

•$\langle AB|AB\rangle$ integrals. The integral $\langle ij|ij\rangle$ is first rewritten with the ab initio MOs expanded in the AO basis, $\sum_{\mu\in A}\sum_{\nu\in A} C_{\mu i}C_{\nu i}\langle \mu j|\nu j\rangle$. The SGO approximation is then applied directly to $\langle \mu j|\nu j\rangle$ as follows.

$$\psi_i\psi_j = \sum_{\mu} C_{\mu i}\chi_{\mu}\psi_j$$

$$\approx \sum_{\mu} C_{\mu i}\left(\frac{2\alpha_{\mu j}}{\pi}\right)^{\frac{3}{2}} S_{\mu j}e^{-2\alpha_{\mu j}\left|\mathbf{r}-\frac{1}{2}\left(\mathbf{R}_{\mu}-\mathbf{R}_j\right)\right|^2}$$

$$\langle \mu j | \nu j \rangle = \frac{2}{\sqrt{\pi}} \sqrt{\frac{2\alpha_{\mu j}\alpha_{\nu j}}{\alpha_{\mu j}+\alpha_{\nu j}}} S_{\mu j} S_{\nu j} F_0 \left[\tfrac{1}{4} \frac{2\alpha_{\mu j}\alpha_{\nu j}}{\alpha_{\mu j}+\alpha_{\nu j}} R_{\mu\nu}^2 \right] \tag{3}$$

$$\text{where } \alpha_{\mu j} = -\frac{2}{R_{\mu j}} \ln |S_{\mu j}|$$

F_0 is the incomplete gamma function of order 0, and can be evaluated using the relationship:

$$F_0[t] = \tfrac{1}{2}\left(\tfrac{\pi}{t}\right)^{\frac{1}{2}} erf\left(t^{\frac{1}{2}}\right)$$
$$F_0[0] = 1$$

One need not be concerned with a possible discontinuity as t approaches zero, since t will never be very close to zero without being identically equal to zero, and this will only occur in the case that $\mathbf{R}_\mu = \mathbf{R}_\nu$.

• $\langle AB | AA \rangle$ integrals will be also be expanded in the AO basis, i.e. $\langle ij | nn \rangle = \sum_{\mu,\lambda,\sigma} C_{\mu i} C_{\lambda n} C_{\sigma n} \langle \mu j | \lambda\sigma \rangle$. These integrals must be approximated first with a multipole expansion, then with the SGO approximation, since applying the SGO approximation directly would lead to singularities for $\mathbf{R}_\lambda = \mathbf{R}_\sigma$, when the AOs are on the same atomic center.

$$\begin{aligned} \langle \mu j | \lambda\sigma \rangle &\approx S_{\lambda\sigma} \left\langle \mu \left| R_{1Q_{\lambda\sigma}}^{-1} \right| j \right\rangle \\ &\approx \left(\frac{8\alpha_{\mu j}}{\pi} \right)^{\frac{1}{2}} S_{\mu j} S_{\lambda\sigma} F_0 \left[2\alpha_{\mu j} R_{P_{\mu j} Q_{\lambda\sigma}}^2 \right] \equiv I_{\mu j}^{\lambda\sigma, SGO} \end{aligned} \tag{4}$$

where the multipole expansion is always applied to the pair of ab initio orbitals and $\mathbf{R}_P$ and $\mathbf{R}_Q$ are Gaussian product centers

$$\begin{aligned} \mathbf{R}_{P_{\mu j}} &= \frac{\alpha_\mu \mathbf{R}_\mu + \alpha_j \mathbf{R}_j}{\alpha_\mu + \alpha_j}, \text{ where } \alpha_\mu = \alpha_j = \alpha_{\mu j}, \text{ due to the SGO approximation} \\ &= \frac{\alpha_{\mu j}\mathbf{R}_\mu + \alpha_{\mu j}\mathbf{R}_j}{\alpha_{\mu j} + \alpha_{\mu j}} = \frac{\mathbf{R}_\mu + \mathbf{R}_j}{2} \end{aligned} \tag{5}$$

$$\mathbf{R}_{Q_{\lambda\sigma}} = \frac{\alpha_\lambda \mathbf{R}_\lambda + \alpha_\sigma \mathbf{R}_\sigma}{\alpha_\lambda + \alpha_\sigma}$$

In cases for which the AOs are not primitive Gaussians, but basis functions constructed from a contraction of several primitives, $\mathbf{R}_Q$ is not well-defined, since a contracted Gaussian function does not have just one, but several exponents. The multipole expansion must, therefore, be applied either to the integrals over primitive Gaussians or a further approximation must be made. The $\mathbf{R}_{Q_{\lambda\sigma}}$ term can be approximated with the dipole integral $\langle\lambda|\mathbf{r}|\sigma\rangle$, removing the need to apply the approximation to primitive Gaussians[13]. The utility of this further approximation depends upon the degree of contraction of the basis set.

• $\langle AA|BB\rangle$ integrals are simplified using a multipole expansion applied to the EFP LMOs:

$$\langle ik|jj\rangle \approx \left\langle i\left|\frac{1}{|\mathbf{r}_1 - \mathbf{R}_j|}\right|k\right\rangle = V_{ik}^j \qquad (6)$$

These integrals are evaluated in a manner that is analogous to the evaluation of electron-nuclear attraction integrals; here the nuclear charge is replaced with the electronic charge of –1.

<u>One-electron terms</u>.

• V_{ij}^A, the electron – nuclear attraction integral between the ab initio nuclei and orbitals on both the ab initio and the EFP parts, can be simplified using the SGO approximation:

$$\langle i|\hat{V}^A|j\rangle = \sum_{\mu\in A} C_{\mu i}\langle \mu|\hat{V}^A|j\rangle$$
$$\langle \mu|\hat{V}^A|j\rangle = -\left(\frac{8\alpha_{\mu j}}{\pi}\right)^{\frac{1}{2}} S_{\mu j}\sum_{l\in A} Z_l F_0\left[2\alpha_{\mu j}R_{Pl}^2\right] \equiv V_{\mu j}^{A,SGO} \qquad (7)$$

• V_{jj}^A is treated with a multipole expansion, and replaced with

$$V_{jj}^A = \sum_{l\in A}\frac{-Z_l}{R_{jl}}$$

$F_{ik}^{A'}$ is replaced with $F_{ik}^{A} + V_{ik}^{EFP,B}$, where $V_{ik}^{EFP,B}$, the ab initio/EFP intermolecular coulomb interaction, is evaluated using a distributed multipolar analysis, as implemented in EFP1[3,5].

V. Gradients

Geometry optimizations of ab initio/EFP complexes to find energy minima requires the derivative of the energy with respect to the atomic positions. Ab initio and EFP atomic centers will be treated separately, because the internal fragment geometries are frozen, and the fragment LMOs are frozen. Thus, the derivation is presented in two steps: (1) derivatives with respect to ab initio atomic centers and (2) derivatives with respect to EFP atomic centers.

(1) Derivatives with respect to ab initio atom centers. The first term is used to illustrate each step in the derivation process; the result is then summarized for the entire energy expression. First, consider the derivative of each term, using the chain rule, showing the explicit and implicit dependence of the integrals on the atomic positions. This is made clearer by expanding the MOs in the AO basis.

$$\frac{\partial\langle ij|ij\rangle}{\partial x_a} = \frac{\partial \sum_{\mu,\nu\in A} C_{\mu i}C_{\nu i}\langle \mu j|\nu j\rangle}{\partial x_a} = \sum_{\mu,\nu\in A}\begin{Bmatrix} C_{\mu i}^{a}C_{\nu i}\langle \mu j|\nu j\rangle + C_{\mu i}C_{\nu i}^{a}\langle \mu j|\nu j\rangle \\ +C_{\mu i}C_{\nu i}\langle \mu^{a} j|\nu j\rangle + C_{\mu i}C_{\nu i}\langle \mu j|\nu^{a} j\rangle \\ +C_{\mu i}C_{\nu i}\langle \mu j^{a}|\nu j\rangle + C_{\mu i}C_{\nu i}\langle \mu j|\nu j^{a}\rangle \end{Bmatrix} \tag{8}$$

The superscript a indicates a derivative with respect to a coordinate on center a. The last two terms are equal to zero, because the EFP LMOs are frozen, and the first and second pair of terms can be combined, due to symmetry, to give only two terms.

$$\frac{\partial\langle ij|ij\rangle}{\partial x_a} = \sum_{\mu,\nu\in A}\left\{2C_{\mu i}^{a}C_{\nu i}\langle \mu j|\nu j\rangle + 2C_{\mu i}C_{\nu i}\langle \mu^{a} j|\nu j\rangle\right\} = \sum_{\mu,\nu\in A}\left\{2C_{\mu i}^{a}\langle \mu j|ij\rangle + 2\langle i^{a} j|ij\rangle\right\} \tag{9}$$

This expression cannot be used as written, because the $C_{\mu i}$ are matrices of numbers, and therefore $C^a_{\mu i}$ would require solution of the time-consuming coupled perturbed Hartree-Fock equations. However, Eq. (9) can be rewritten using the orbital response term, which allow us to replace the derivatives of coefficient matrices with derivatives of overlap matrices[10].

$$\begin{aligned}
\frac{\partial\langle ij|ij\rangle}{\partial x_a} &= \sum_{\mu\in A}\sum_{i\in A}\sum_{j\in B}\left\{2C^a_{\mu i}\langle \mu j|ij\rangle + 2\langle i^a j|ij\rangle\right\} \\
&= \sum_{\mu\in A}\sum_{i,m\in A}\sum_{j\in B}\left\{2C_{\mu m}U^a_{mi}\langle \mu j|ij\rangle + 2\langle i^a j|ij\rangle\right\} \\
&= \sum_{i,m\in A}\sum_{j\in B}\left\{2U^a_{mi}\langle mj|ij\rangle + 2\langle i^a j|ij\rangle\right\} \\
&= \sum_{i,m\in A}\sum_{j\in B}\left\{U^a_{mi}\left(\langle mj|ij\rangle + \langle ij|mj\rangle\right) + 2\langle i^a j|ij\rangle\right\} \\
&= \sum_{j\in B}\left\{\sum_{m,i\in A}U^a_{mi}\langle mj|ij\rangle + \sum_{m,i\in A}U^a_{mi}\langle ij|mj\rangle + 2\langle i^a j|ij\rangle\right\}
\end{aligned} \tag{10}$$

In the second sum, interchange i and m, and recombine sums

$$= \sum_{j\in B}\left\{\sum_{m,i\in A}\left(U^a_{mi}+U^a_{im}\right)\langle mj|ij\rangle + 2\langle i^a j|ij\rangle\right\}$$

where $C^a_{\mu i} = \sum_{m\in A} C_{\mu m}U^a_{mi}$

The derivative of the orthonormality constraint

$$\begin{aligned}
&\sum_{\mu,\nu\in A} C_{\mu m}S_{\mu\nu}C_{i\nu} = \delta_{mi} \\
&U^a_{mi} + S^a_{im} + U^a_{im} = 0 \\
&U^a_{mi} + U^a_{im} = -S^a_{im}
\end{aligned} \tag{11}$$

can now be used to eliminate $U^a_{mi} + U^a_{im}$:

$$\frac{\partial\langle ij|ij\rangle}{\partial x_a} = \sum_{j\in B}\left\{\sum_{m,i\in A} -S_{im}\langle mj|ij\rangle + 2\langle i^a j|ij\rangle\right\} \tag{12}$$

giving an expression containing terms that are all straightforward to evaluate.

Carrying out each of these steps on the entire energy expression gives the following expression for the derivative of the energy with respect to the ab initio atomic positions.

$$
\begin{aligned}
\frac{\partial E^{XR}}{\partial x_a} = & -2\sum_i^A \sum_j^B \langle ij|ij\rangle^a - 2\sum_i^A \sum_j^B S_{ij}^a \left[2\left(V_{ij}^A + G_{ij}^A\right) + \sum_l^B F_{jl}^B S_{li} \right] \\
& -2\sum_i^A \sum_j^B S_{ij} \left[2\left(V_{ij}^{A^a} + G_{ij}^{A^a}\right) + \sum_l^B F_{jl}^B S_{li}^a \right] \\
& +2\sum_i^A \sum_j^B S_{ij}^a \left[\sum_k^A S_{kj} F_{ik}^{A'} + S_{ij}\left(V_{jj}^A + J_{jj}^A\right) - \sum_k^A S_{kj} \langle ik|jj\rangle \right] \\
& +2\sum_i^A \sum_j^B S_{ij} \left[\begin{array}{l} \sum_k^A S_{kj}^a F_{ik}^{A'} + S_{kj} F_{ik}^{A'a} + S_{ij}^a \left(V_{jj}^A + J_{jj}^A\right) + S_{ij}\left(V_{jj}^{A^a} + J_{jj}^{A^a}\right) \\ -\sum_k^A S_{kj}^a \langle ik|jj\rangle + S_{kj} \langle ik|jj\rangle^a \end{array} \right] \\
& +\sum_{m,i}^A \sum_j^B S_{mi}^a \left\{ \begin{array}{l} \langle mj|ij\rangle + S_{mj}\left[2\left(V_{ij}^A + G_{ij}^A\right) + \sum_l^B F_{jl}^B S_{li} \right] \\ +S_{ij}\left[2\left(V_{mj}^A + G_{mj}^A\right) + \sum_l^B F_{jl}^B S_{lm} \right] \\ -S_{mj}\left[\sum_k^A S_{kj} F_{ik}^{A'} + S_{ij}\left(V_{jj}^A + J_{jj}^A\right) - \sum_k^A S_{kj} \langle ik|jj\rangle \right] \\ -S_{ij}\left[\sum_k^A S_{kj} F_{mk}^{A'} + S_{mj}\left(V_{jj}^A + J_{jj}^A\right) - \sum_k^A S_{kj} \langle mk|jj\rangle \right] \end{array} \right\} \\
& +\sum_{m,i,n}^A \sum_j^B S_{mn}^a S_{ij} \left\{ \begin{array}{l} 2\left[4(ij|mn) - (im|jn) - (in|jm) \right] \\ -\sum_k^A S_{kj} \left[4(ik|mn) - (im|kn) - (in|km) \right] \end{array} \right\} \\
& -\sum_{m,i,k}^A \sum_j^B S_{mk}^a S_{ij} \left\{ S_{mj} F_{ik}^{A'} + S_{kj} F_{im}^{A'} + 2S_{ij}(jj|mk) - S_{mj}(ik|jj) - S_{kj}(im|jj) \right\}
\end{aligned}
\tag{13}
$$

(2) Derivatives with respect to EFP centers. A similar procedure is used to obtain the derivative of E^{XR} with respect to EFP atomic positions. Many of the terms are equal to zero in this case, because the EFP LMOs are frozen. Again, the first term is used to illustrate the procedure.

$$
\begin{aligned}
& -2\sum_i^A \sum_j^B \frac{\partial \langle ij|ij\rangle}{\partial x_b} \\
& \quad = -2\sum_i^A \sum_\mu^A \sum_j^B \sum_{\nu'}^B \left\{ \langle ij|ij\rangle^b + 2C_{\nu' j}^b \langle i\nu'|ij\rangle + 2C_{\mu i}^b \langle \mu j|ij\rangle \right\}
\end{aligned}
\tag{14}
$$

The C^b on EFPs are equal to zero, because the EFP LMOs are frozen, giving

$$= -2\sum_i^A \sum_\mu^A \sum_j^B \sum_{\nu'}^B \left\{ \langle ij|ij\rangle^b + 2C_{\mu i}^b \langle \mu j|ij\rangle \right\}$$

Derivatives of coefficient matrices are replaced with orbital response terms, U^b (cf., Eq. (11))

$$= -2\sum_{i,m}^A \sum_\mu^A \sum_j^B \sum_{\nu'}^B \left\{ \langle ij|ij\rangle^b + 2C_{\mu m} U_{mi}^b \langle \mu j|ij\rangle \right\}$$
$$= -2\sum_{i,m}^A \sum_j^B \sum_{\nu'}^B \left\{ \langle ij|ij\rangle^b + 2U_{mi}^b \langle mj|ij\rangle \right\}$$

Orbital response terms are then replaced with derivatives of overlap matrices

$$= -2\sum_{i,m}^A \sum_j^B \sum_{\nu'}^B \left\{ \langle ij|ij\rangle^b + \left(U_{mi}^b + U_{im}^b\right) \langle mj|ij\rangle \right\}$$
$$= -2\sum_{i,m}^A \sum_j^B \sum_{\nu'}^B \left\{ \langle ij|ij\rangle^b - S_{mi}^b \langle mj|ij\rangle \right\}$$

However, the $S_{mi}^b = 0$, since the basis functions, and therefore MOs on A, do not depend upon the positions of the EFP atoms. Therefore, the expression is simply

$$\begin{aligned} -2\sum_i^A \sum_j^B \frac{\partial \langle ij|ij\rangle}{\partial x_b} &= -2\sum_i^A \sum_j^B \langle ij|ij\rangle^b \\ = -2\sum_i^A \sum_j^B \sum_{\nu'}^B 2C_{\nu' j} \langle i\nu'^b | ij\rangle & \end{aligned} \tag{15}$$

The full derivative of E^{XR} with respect to EFP positions is:

$$\begin{aligned} \frac{\partial E^{XR}}{\partial x_b} = & -4\sum_i^A \sum_j^B \langle ij^b|ij\rangle + \\ & -2\sum_i^A \sum_j^B S_{ij}^b \left[2\left(V_{ij}^A + G_{ij}^A\right) + \sum_l^B F_{jl}^B S_{li} \right] \\ & -2\sum_i^A \sum_j^B S_{ij} \begin{bmatrix} 2\left(\left\langle i\middle|\hat{V}^A\middle|j^b\right\rangle + G_{ij}^{A^b}\right) \\ +\sum_l^B S_{li} + F_{jl}^B S_{li}^b \end{bmatrix} \\ & +2\sum_i^A \sum_j^B S_{ij}^b \left[\sum_k^A S_{kj} F_{ik}'^A + S_{ij}\left(V_{jj}^A + J_{jj}^A\right) - \sum_k^A S_{kj} \langle ik|jj\rangle \right] \\ & +2\sum_i^A \sum_j^B S_{ij} \begin{bmatrix} \sum_k^A S_{kj}^b F_{ik}'^A + S_{kj} \left(\left\langle i\middle|\sum_J^B \frac{Z_J\left(x_1 - x_J\right)}{\mathbf{r}_{1J}^3}\middle|k\right\rangle \right. \\ \left. +2\sum_{n'}^B \langle ik|n'^b n'\rangle \right) \\ +S_{ij}^b\left(V_{jj}^A + J_{jj}^A\right) + S_{ij} V_{jj}^{A^b} - \sum_k^A S_{kj}^b \langle ik|jj\rangle \end{bmatrix} \end{aligned} \tag{16}$$

VI. Gradient Approximations

As in the energy expression, there are terms in the gradient expressions that are too expensive to compute exactly, most notably the two electron terms. These terms are replaced with approximations similar to those used in the energy expression, with additional approximations needed for the derivative terms.

Two electron ab intio derivative integrals. Similar approximations for derivative integrals to those employed for regular integrals can be used. This is because the derivative of an AO with angular momentum l is simply the sum of one orbital with angular momentum l+1, and one with angular momentum l-1. For an s orbital the derivative generates just one p orbital. This simple relationship allows for the application of the previously used approximations with little modification.

The ab initio derivative two-electron integrals are divided into four classes: $\langle A^a B|AB\rangle$, $\langle A^a A|AB\rangle$, $\langle AA|A^a B\rangle$, and $\langle A^a A|BB\rangle$

• $\langle A^a B|AB\rangle$ integrals.

$$\langle i^a j|ij\rangle = \sum_{\mu,\lambda}^{A} C_{\mu i} C_{\lambda i} \langle \mu^a j|\lambda j\rangle = \sum_{\mu,\lambda}^{A} C_{\mu i} C_{\lambda i} \left(\langle \mu_{-1} j|\lambda j\rangle + \langle \mu_{+1} j|\lambda j\rangle\right)$$

$$\approx \sum_{\mu,\lambda}^{A} C_{\mu i} C_{\lambda i} \left(\langle \mu_{-1} j|\lambda j\rangle + \langle \mu_{+1} j|\lambda j\rangle\right)^{SGO}$$

$$\left(\langle \mu_{-1} j|\lambda j\rangle + \langle \mu_{+1} j|\lambda j\rangle\right)^{SGO} = \frac{2}{\sqrt{\pi}} S_{vj} \left(\sqrt{\frac{2\alpha_{\mu_{-1}j}\alpha_{vj}}{\alpha_{\mu_{-1}j}+\alpha_{vj}}} S_{\mu_{-1}j} F_0\left[\frac{1}{4}\frac{2\alpha_{\mu_{-1}j}\alpha_{vj}}{\alpha_{\mu_{-1}j}+\alpha_{vj}} R_{\mu v}^2\right] + \sqrt{\frac{2\alpha_{\mu_{+1}j}\alpha_{vj}}{\alpha_{\mu_{+1}j}+\alpha_{vj}}} S_{\mu_{+1}j} F_0\left[\frac{1}{4}\frac{2\alpha_{\mu_{+1}j}\alpha_{vj}}{\alpha_{\mu_{+1}j}+\alpha_{vj}} R_{\mu v}^2\right] \right)$$

$$\equiv I_{\lambda j}^{\mu^a j SGO} \qquad (17)$$

where $\alpha_{\mu_{-1}j} = -\frac{2}{R_{\mu j}} \ln\left|S_{\mu_{-1}j}\right|$

and ± 1 subscripts refer to the higher or lower angular momentum component to the derivative

• $\langle A^a A | AB \rangle$ integrals:

$$\langle n^a n | ij \rangle = \sum_{\mu,\nu} C_{\mu n} C_{\nu n} \langle \nu^a \lambda | \mu j \rangle$$

$$\langle \nu^a \lambda | \mu j \rangle = \langle \nu_{l\pm1} \lambda | \mu j \rangle \approx S_{\nu_{l\pm1}\lambda} \langle \mu | R_{1Q}^{-1} | j \rangle \tag{18}$$

$$\approx \left(\frac{8\alpha}{\pi}\right)^{1/2} S_{\mu j} \left(S_{\nu_{l+1}\lambda} + S_{\nu_{l-1}\lambda}\right) F_0\left[2\alpha R_{PQ}^2\right] \equiv I_{\mu j}^{\nu^a \lambda, SGO}$$

• $\langle AA | A^a B \rangle$ integrals:

$$\langle nn | i^a j \rangle = \sum_{\mu,\nu,\lambda \in A} C_{\nu n} C_{\lambda n} C_{\mu i} \langle \nu\lambda | \mu^a j \rangle$$

$$\langle \nu\lambda | \mu^a j \rangle = \langle \nu\lambda | \mu_{\pm1} j \rangle \approx S_{\nu\lambda} \langle \mu_{\pm1} | R_{1Q}^{-1} | j \rangle \tag{19}$$

$$\approx \left(\frac{8}{\pi}\right)^{1/2} S_{\nu\lambda} \begin{pmatrix} \alpha_{\mu_{-1}j}^{\frac{1}{2}} S_{\mu_{-1}j} F_0\left[2\alpha_{\mu_{-1}j} R_{P_{\mu j} Q_{\nu\lambda}}^2\right] \\ +\alpha_{\mu_{+1}j}^{\frac{1}{2}} S_{\mu_{+1}j} F_0\left[2\alpha_{\mu_{+1}j} R_{P_{\mu j} Q_{\nu\lambda}}^2\right] \end{pmatrix} \equiv I_{\mu^a j}^{\nu\lambda, SGO}$$

• $\langle A^a A | BB \rangle$ integrals:

$$\langle n^a n | jj \rangle = \sum_{\mu \in A} C_{\mu n} \langle \mu^a n | jj \rangle$$

$$\langle \mu^a n | jj \rangle \approx \left\langle \mu_{l-1} \left| |\mathbf{r_i} - \mathbf{R_j}|^{-1} \right| n \right\rangle + \left\langle \mu_{l+1} \left| |\mathbf{r_i} - \mathbf{R_j}|^{-1} \right| n \right\rangle = V_{\mu^a n}^{j} \tag{20}$$

<u>One electron ab initio derivative integrals:</u> $V_{i^a j}^{A}$

$$\langle \mu^a | \hat{V}^A | j \rangle = -\left(\frac{8\alpha_{\mu_{-1}j}}{\pi}\right)^{\frac{1}{2}} S_{\mu_{-1}j} \sum_{I \in A} Z_I F_0\left[2\alpha_{\mu_{-1}j} R_{P_{\mu_{-1}j} I}^2\right]$$

$$-\left(\frac{8\alpha_{\mu_{+1}j}}{\pi}\right)^{\frac{1}{2}} S_{\mu_{+1}j} \sum_{I \in A} Z_I F_0\left[2\alpha_{\mu_{+1}j} R_{P_{\mu_{+1}j} I}^2\right] \tag{21}$$

$$\equiv V_{\mu^a j}^{A, SGO}$$

Two electron EFP derivative integrals. EFP derivatives are of the following types: $\langle AB^b|AB\rangle$, $\langle AA|AB^b\rangle$ and $\langle AA|B^bB\rangle$.

• $\langle AB^b|AB\rangle$ integrals:

$$\begin{aligned}\langle ij^b|ij\rangle &= \sum_{\mu,\lambda}^{A}\sum_{\nu'}^{B} C_{\mu i}C_{\lambda i}C_{\nu' j}\langle \mu\nu'^b|\lambda j\rangle \\ &= \sum_{\mu,\lambda}^{A}\sum_{\nu'}^{B} C_{\mu i}C_{\lambda i}C_{\nu' j}\left(\langle \mu\nu'_{-1}|\lambda j\rangle + \langle \mu\nu'_{+1}|\lambda j\rangle\right) \\ &\approx \sum_{\mu,\lambda}^{A} C_{\mu m}C_{\lambda i}C_{\nu' j}\left(\langle \mu\nu'_{-1}|\lambda j\rangle + \langle \mu\nu'_{+1}|\lambda j\rangle\right)^{SGO}\end{aligned}$$

$$\langle \mu\nu'^b|\lambda j\rangle^{SGO} = \frac{2}{\pi}S_{\lambda j}\left(\begin{array}{l}\sqrt{\dfrac{2\alpha_{\mu\nu'_{-1}}\alpha_{\lambda j}}{\alpha_{\mu\nu'_{-1}}+\alpha_{\lambda j}}}S_{\mu\nu'_{-1}}F_0\left[\dfrac{2\alpha_{\mu\nu'_{-1}}\alpha_{\lambda j}}{\alpha_{\mu\nu'_{-1}}+\alpha_{\lambda j}}R^2_{P_{\mu\nu'}Q_{\lambda j}}\right] \\ +\sqrt{\dfrac{2\alpha_{\mu\nu'_{+1}}\alpha_{\lambda j}}{\alpha_{\mu\nu'_{+1}}+\alpha_{\lambda j}}}S_{\mu\nu'_{+1}}F_0\left[\dfrac{2\alpha_{\mu\nu'_{+1}}\alpha_{\lambda j}}{\alpha_{\mu\nu'_{+1}}+\alpha_{\lambda j}}R^2_{P_{\mu\nu'}Q_{\lambda j}}\right]\end{array}\right) \equiv I^{\mu\nu'^b}_{\lambda j} \qquad (22)$$

where $\alpha_{\nu'_{-1}j} = -\dfrac{2}{R_{\nu j}}\ln|S_{\nu'_{-1}j}|$

and ± 1 subscripts refer to the higher or lower angular momentum component of the derivative

• $\langle AA|AB^b\rangle$ type integrals.

$$\langle ij^b|nn\rangle = \sum_{\mu,\lambda,\sigma\in A}\sum_{\nu'\in B} C_{\mu i}C_{\nu' j}C_{\lambda n}C_{\sigma n}\langle \mu\nu'^b|\lambda\sigma\rangle$$

$$\begin{aligned}\langle \mu\nu'^b|\lambda\sigma\rangle &= \langle \mu\nu'_{\pm 1}|\lambda\sigma\rangle \approx S_{\lambda\sigma}\langle \mu|R^{-1}_{1Q}|\nu'_{\pm 1}\rangle \qquad (23)\\ &\approx \left(\frac{8}{\pi}\right)^{1/2} S_{\lambda\sigma}\left(\begin{array}{l}\alpha^{\frac{1}{2}}_{\mu\nu_{-1}}S_{\mu\nu_{-1}}F_0\left[2\alpha_{\mu\nu_{-1}}R^2_{P_{\mu\nu}Q_{\lambda\sigma}}\right] \\ +\alpha^{\frac{1}{2}}_{\mu\nu_{+1}}S_{\mu\nu_{+1}}F_0\left[2\alpha_{\mu\nu_{+1}}R^2_{P_{\mu\nu}Q_{\lambda\sigma}}\right]\end{array}\right) \equiv I^{\lambda\sigma,SGO}_{\mu\nu'^b}\end{aligned}$$

• $\langle AA|B^bB\rangle$ type integrals.

$$\langle ik|n'n'\rangle = \sum_{\mu,\nu\in A}\sum_{\lambda'\in B} C_{\mu i}C_{\nu k}C_{\lambda' n'}\langle \mu\nu|\lambda'^b n'\rangle$$

$$\langle \mu\nu|\lambda_b' n'\rangle \approx S_{\mu\nu}\langle \lambda'^b|R_{1Q}^{-1}|n'\rangle \qquad (24)$$

$$\approx S_{\mu\nu}\left(\frac{8}{\pi}\right)^{\frac{1}{2}}\begin{pmatrix}\alpha_{\lambda_{-1}' n'}^{\frac{1}{2}}S_{\lambda_{-1}' n'}F_0\left[2\alpha_{\lambda_{-1}' n'}R^2_{P_{\lambda' n'}Q_{\mu\nu}}\right]\\ +\alpha_{\lambda_{+1}' n'}^{\frac{1}{2}}S_{\lambda_{+1}' n'}F_0\left[2\alpha_{\lambda_{+1}' n'}R^2_{P_{\lambda' n'}Q_{\mu\nu}}\right]\end{pmatrix}\equiv I^{\mu\nu,SGO}_{\lambda'^b n'}$$

<u>One electron EFP derivative integrals:</u> $V^A_{ij^b}$

$$\langle i|\hat{V}^A|j^b\rangle = \sum_{\nu\in A}\sum_{\mu'\in B} C_{\nu i}C_{\mu' j}\langle \nu|\hat{V}^A|\mu'^b\rangle$$

$$\langle \nu|\hat{V}^A|\mu'^b\rangle \approx -\left(\frac{8\alpha_{\nu\mu_{-1}'}}{\pi}\right)^{\frac{1}{2}}S_{\nu\mu_{-1}'}\sum_{I\in A}Z_I F_0\left[2\alpha_{\nu\mu_{-1}'}R^2_{P_{\nu\mu_{-1}'}I}\right] \qquad (25)$$

$$-\left(\frac{8\alpha_{\nu\mu_{+1}'}}{\pi}\right)^{\frac{1}{2}}S_{\nu\mu_{+1}'}\sum_{I\in A}Z_I F_0\left[2\alpha_{\nu\mu_{+1}'}R^2_{P_{\nu\mu_{+1}'}I}\right]$$

$$\equiv V^{A,SGO}_{\nu\mu'^b}$$

Application of these approximations gives the following expressions for derivatives of E^{XR} with respect to ab initio and EFP atomic centers.

Ab Initio Derivative:

$$\frac{\partial E_{exch}}{\partial x_a} \approx -2\sum_i^A \sum_{\mu,\nu}^A \sum_j^B 2C_{\mu i}C_{\nu i} I_{\nu j}^{\mu^a j,SGO} + \sum_{m,i}^A \sum_{\mu,\nu}^A \sum_j^B S_{mi}^a C_{\mu i} C_{\nu i} I_{\nu j}^{\mu j,SGO}$$

$$-2\sum_i^A \sum_\nu^A \sum_j^B S_{ij}^a \left[2\left(C_{\nu i} V_{\nu j}^{A,SGO} + G_{ij}^{A,SGO} \right) + \sum_l^B F_{jl}^B S_{li} \right]$$

$$-2\sum_i^A \sum_j^B S_{ij} \left[2\left(\begin{array}{l} \sum_\mu^A C_{\mu i} V_{\mu^a j}^{A,SGO} + \sum_l^A \left\langle i \left| \frac{Z_I (x_1 - x_I)}{R_{1I}^3} \right| j \right\rangle \\ +\sum_{\mu,\nu,\lambda}^A C_{\mu i} \frac{1}{2} P_{\nu\lambda} \left\{ \begin{array}{l} 4I_{\mu j}^{\nu^a \lambda,SGO} + 2I_{\mu^a j}^{\nu\lambda,SGO} \\ -\left(I_{\lambda j}^{\nu^a \mu,SGO} + I_{\nu^a j}^{\mu\lambda,SGO} \right) - I_{\lambda j}^{\nu\mu^a,SGO} \end{array} \right\} \end{array} \right) + \sum_l^B \sum_\mu^A F_{jl}^B S_{li}^a \right]$$

$$+\sum_{m,i,\mu}^A \sum_\mu^A \sum_j^B S_{mi}^a \left\{ \begin{array}{l} S_{mj} \left[2\left(\sum_\mu^A C_{\mu i} V_{\mu j}^{A,SGO} + G_{ij}^{A,SGO} \right) + \sum_l^B F_{jl}^B S_{li} \right] \\ +S_{ij} \left[2\left(C_{\mu m} V_{\mu j}^{A,SGO} + G_{mj}^{A,SGO} \right) + \sum_l^B F_{jl}^B S_{lm} \right] \end{array} \right\}$$

$$+\sum_{m,i,n}^A \sum_{\mu,\nu,\lambda}^A \sum_j^B C_{\mu i} C_{\nu m} C_{\lambda n} S_{mn}^a S_{ij} \left\{ 2\left[4I_{\mu j}^{\nu\lambda,SGO} - I_{\lambda j}^{\mu\nu,SGO} - I_{\nu j}^{\lambda\mu,SGO} \right] \right\}$$

$$+2\sum_i^A \sum_j^B S_{ij}^a \left[\sum_k^A S_{kj} F_{ik}^{A'} + S_{ij} \left(\sum_I^A \frac{-Z_I}{R_{jI}} + \sum_n^A V_{nn}^j \right) - \sum_k^A S_{kj} V_{ik}^j \right]$$

$$+2\sum_i^A \sum_j^B S_{ij} \left[\begin{array}{l} \sum_k^A S_{kj}^a F_{ik}^{A'} + S_{kj} \left(F_{ik}^{A^a} + \sum_{\mu,\nu \in A} C_{\mu i} V_{\mu^a j}^{B,SGO} + 2C_{\mu i} V_{\mu^a k}^j \right) F_{ik}^{A'a} \\ +\sum_\mu^A \left[S_{ij}^a \left(\sum_I^A \frac{-Z_I}{R_{jI}} + \sum_n^A V_{nn}^j \right) + S_{ij} \left(\sum_I^A \frac{Z_I (x_j - x_I)}{R_{jI}^3} + \sum_n^A 2C_{\mu n} V_{\mu^a n}^j \right) \right] \\ -\sum_k^A \sum_\mu^A \left[S_{kj}^a V_{ik}^j + S_{kj} \left(C_{\mu i} V_{\mu^a k}^j + C_{\mu k} V_{\mu^a i}^j \right) \right] \end{array} \right]$$

$$+\sum_{m,i}^A \sum_j^B S_{mi}^a \left\{ \begin{array}{l} -S_{mj} \left[\sum_k^A S_{kj} F_{ik}^{A'} + S_{ij} \left(\sum_I^A \frac{-Z_I}{R_{jI}} + \sum_n^A V_{nn}^j \right) - \sum_k^A S_{kj} V_{ik}^j \right] \\ -S_{ij} \left[\sum_k^A S_{kj} F_{mk}^{A'} + S_{mj} \left(\sum_I^A \frac{-Z_I}{R_{jI}} + \sum_n^A V_{nn}^j \right) - \sum_k^A S_{kj} V_{mk}^j \right] \end{array} \right\}$$

$$+\sum_{m,i,n}^A \sum_j^B S_{mn}^a S_{ij} \left\{ -\sum_k^A S_{kj} \left[4(ik|mn) - (im|kn) - (in|km) \right] \right\}$$

$$-\sum_{m,i,k}^A \sum_j^B S_{mk}^a S_{ij} \left\{ S_{mj} \left(F_{ik}^{A'} - V_{ik}^j \right) + S_{kj} \left(F_{im}^{A'} - V_{im}^j \right) + 2S_{ij} V_{mk}^j \right\}$$

EFP Derivative:

$$\frac{\partial E^{XR}}{\partial x_b} = -4\sum_i^A \sum_j^B \sum_{\mu,\lambda}^A \sum_{\nu'}^B C_{\mu i} C_{\lambda i} C_{\nu' j} I_{\lambda j}^{\nu' b\ \mu,SGO}$$

$$-2\sum_i^A \sum_j^B S_{ij}^b \left[2\left(\sum_\mu^A C_{\mu i} V_{\mu j}^{A,SGO} + G_{ij}^{A,SGO} \right) + \sum_l^B F_{jl}^B S_{li} \right]$$

$$-2\sum_i^A \sum_j^B S_{ij} \left[\begin{array}{l} 2\left(\sum_\mu^A \sum_{\nu'}^B C_{\mu i} C_{\nu' j} V_{\mu \nu'^b}^{A,SGO} + G_{ij}^{A^b,SGO} \right) \\ +\sum_l^B S_{li} + F_{jl}^B S_{li}^b \end{array} \right]$$

$$+2\sum_i^A \sum_j^B S_{ij}^b \left[\sum_k^A S_{kj} F_{ik}^{'A} + S_{ij} \left(\sum_l^A \frac{-Z_l}{R_{jl}} + \sum_n^A V_{nn}^j \right) - \sum_k^A S_{kj} V_{ik}^j \right]$$

$$+2\sum_i^A \sum_j^B S_{ij} \left[\begin{array}{l} \sum_k^A S_{kj}^b F_{ik}^{'A} + S_{kj} \left(\begin{array}{l} \left\langle i \left| \sum_J^B \frac{Z_J (x_1 - x_J)}{\mathbf{r}_{1J}^3} \right| k \right\rangle \\ +2\sum_{n'}^B \sum_{\mu,\nu}^A \sum_{\lambda'}^B C_{\mu l} C_{\nu k} C_{\lambda' n'} I_{\lambda'^b\ n'}^{\mu\nu} \end{array} \right) \\ +S_{ij}^b \left(\sum_l^A \frac{-Z_l}{R_{jl}} + \sum_n^A V_{nn}^j \right) + S_{ij} V_{jj}^{A^b} - \sum_k^A S_{kj}^b V_{ik}^j \end{array} \right]$$

where

$$G_{ij}^{A,SGO} = \sum_{n \in A} \sum_{\mu,\nu,\lambda \in A} C_{\mu i} C_{\nu n} C_{\lambda n} \left(2I_{\mu j}^{\lambda\sigma,SGO} - I_{j\lambda}^{\mu\nu,SGO} \right)$$

and

$$G_{ij}^{A^b,SGO} = \sum_{n \in A} \sum_{\mu,\lambda,\sigma \in A} \sum_{\nu' \in B} C_{\mu i} C_{\lambda n} C_{\sigma n} C_{\nu' j} \left(2I_{\mu \nu'^b}^{\lambda\sigma,SGO} - I_{\nu'^b\ \sigma}^{\mu\lambda,SGO} \right)$$

VII. Optimizing internally frozen EFP geometries.

The internal geometries of EFPs are frozen, therefore the derivative of E^{XR} with respect to EFP atomic positions cannot be applied directly. Instead, this derivative is used to determine the total translational and rotational forces on the EFP as a whole [3,7]. There are six geometrical degrees of freedom associated with each EFP including three translational and three rotational components (torques). The translational force is simply the sum of each of the Cartesian forces described by Eq (27) to give a net force on each EFP.

$$\mathbf{F}^{B} = \sum_{b \in B} \left(-\nabla_b E\right) \tag{28}$$

Calculation of the torques is more involved, and is described below.

$$\mathbf{F}_{\theta}^{B} = \sum_{b \in B} \left(\mathbf{R}_b - \mathbf{R}_{COM}\right) \times \left(-\nabla_b E\right) + \sum_{b \in B} \tau_b \tag{29}$$

where b is an atomic center on EFP B, and τ_b is the point torque on b.

The first part of Eq (29) is a straightforward cross product with the Cartesian gradient. The second part , τ_b is the point torque correction about an AO center due to the anisotropy of p,d, etc. orbitals; the torque on B about point b.

$$\tau_b = (\mathbf{r}_b - \mathbf{r}_a) \times (\nabla_b E^{XR}) = \mathbf{r}_{ba} \times (\nabla_b E^{XR}) \tag{30}$$

The first term of Eq (26), the derivative of E^{XR} with respect to EFP atomic centers, is used to illustrate this procedure.

$$\begin{aligned} &\mathbf{r}_{ba} \times \left(\nabla_b \langle ij|ij\rangle\right) = \mathbf{r}_{ba} \times \left(\langle i\nabla_b j|ij\rangle + \langle ij|i\nabla_b j\rangle\right) = 2\mathbf{r}_{ba} \times \left(\langle i\nabla_b j|ij\rangle\right) \\ &= \sum_{v' \in b} 2C_{v'j}\mathbf{r}_{ba} \times \left(\langle i\nabla_b v'|ij\rangle\right) \\ &= \sum_{v',\sigma' \in b} \sum_{a \in A} \sum_{\mu,\lambda \in a} 2C_{\mu i}C_{v'j}C_{\lambda i}C_{\sigma' j}\mathbf{r}_{ba} \times \langle \mu\nabla_b v'|\lambda\sigma'\rangle \end{aligned} \tag{31}$$

$\mathbf{r}_{ba} \times \langle \mu\nabla_b v'|\lambda\sigma'\rangle$ has the following Cartesian components:

$$\begin{aligned} \left[\mathbf{r}_{ba} \times \langle \mu\nabla_b v'|\lambda\sigma'\rangle\right]_x &= (y_b - y_a)\left\langle \mu\frac{\partial v'}{\partial z_b}\middle|\lambda\sigma'\right\rangle - (z_b - z_a)\left\langle \mu\frac{\partial v'}{\partial y_b}\middle|\lambda\sigma'\right\rangle \\ \left[\mathbf{r}_{ba} \times \langle \mu\nabla_b v'|\lambda\sigma'\rangle\right]_y &= (z_b - z_a)\left\langle \mu\frac{\partial v'}{\partial x_b}\middle|\lambda\sigma'\right\rangle - (x_b - x_a)\left\langle \mu\frac{\partial v'}{\partial z_b}\middle|\lambda\sigma'\right\rangle \\ \left[\mathbf{r}_{ba} \times \langle \mu\nabla_b v'|\lambda\sigma'\rangle\right]_z &= (x_b - x_a)\left\langle \mu\frac{\partial v'}{\partial y_b}\middle|\lambda\sigma'\right\rangle - (y_b - y_a)\left\langle \mu\frac{\partial v'}{\partial x_b}\middle|\lambda\sigma'\right\rangle \end{aligned} \tag{32}$$

The integrals in the torque expression are approximated as in the Cartesian gradient expressions.

VIII. Conclusions.

An expression has been derived and coded for the ab initio-EFP exchange repulsion interaction which is evaluated using optimized orbitals obtained by including the ab initio-EFP exchange repulsion Fock operator in the orbital optimzation procedure. This use of this operator has allowed us to derive an efficient gradient expression without resorting to the use of expensive coupled perturbed Hartree Fock type equations. This gradient expression has been derived and presented here. Also reported is an approximate ab intio-EFP exchange repulsion gradient, which utilizes the approximations established in the energy evaluation. This should provide a cheap, but accurate alternative to fully ab intio solvent studies, especially in cases where continuum models or simple potentials lack sufficient accuracy.

Acknowledgments. The authors have benefited greatly from a number of useful discussions with Prof. Jan Jensen and Dr. Mike Schmidt. JR is grateful to Dr. Graham Fletcher for invaluable advice on derivation and coding. This work was supported by grants from the Air Force Office of Scientific Research (MSG) and the Department of Energy via the Ames Laboratory (JMR).

References:

1 P. Bandyopadhyay, M. S. Gordon, B. Mennucci, and J. Tomasi, Journal of Chemical Physics **116** (12), 5023 (2002); P. Bandyopadhyay and M. S. Gordon, Journal of Chemical Physics **113** (3), 1104 (2000).

2 M. S. Gordon, M. A. Freitag, P. Bandyopadhyay, J. H. Jensen, V. Kairys, and W. J. Stevens, Journal of Physical Chemistry A **105** (2), 293 (2001).

3 P. N. Day, J. H. Jensen, M. S. Gordon, S. P. Webb, W. J. Stevens, M. Krauss, D. Garmer, H. Basch, and D. Cohen, Journal of Chemical Physics **105** (5), 1968 (1996).

4 J. H. Jensen, P. N. Day, M. S. Gordon, H. Basch, D. Cohen, D. R. Garmer, M. Kraus, and W. J. Stevens, ACS Symposium Series **569** (Modeling the Hydrogen Bond), 139 (1994).

5 W. Chen and M. S. Gordon, Journal of Chemical Physics **105** (24), 11081 (1996).

[6] J. H. Jensen and M. S. Gordon, molecular physics **89** (5), 1313 (1996).

[7] J. H. Jensen and M. S. Gordon, Journal of Chemical Physics **108** (12), 4772 (1998).

[8] J. H. Jensen, Journal of Chemical Physics **114** (20), 8775 (2001).

[9] S. F. Boys, in *Quantum science of atoms, molecules, and solids*, edited by P. O. Lowdin (Academic Press, New York, 1966), pp. 253.

[10] M. W. Schmidt; Y. Yamaguchi, Y. Osamura, J. D. Goddard, and H. F. Schaefer III, *A new dimension to quantum chemistry: Analytic derivative methods in ab initio.* (Oxford University Press, New York, 1994).

[11] A. J. Stone, *The Theory of Intermolecular Forces.* (Oxford University Press, Oxford, 1996).

[12] J. H. Jensen, Journal of Chemical Physics **104** (19), 7795 (1996).

[13] J. H. Jensen.

CHAPTER 6: GENERAL CONCLUSIONS

In studying a chemical problem with electronic structure theory the method must be well matched to the chemistry of the system. The two applications projects in this thesis focused on locating equilibrium geometries of multireference systems using FORS-MCSCF wave functions. Both SiC_3 and Si_2C_2 have low energy linear and rhombic structures, with the SiC_3 linear structure slightly more stable than the most stable rhombic structure; the reverse is true for the Si_2C_2 system. A similar study of the SiC_3 and Si_2C_2 anions would enable further comparisons with photoelectron spectroscopy studies of these species.

The Si(100)-(2x1) system is shown to range from nearly closed shell to very multi-reference, depending upon its location on the potential energy surface. The degree of multi-reference character is closely related to the number of under-coordinated surface dimer silicons. When the surface is saturated these dimer silicons are no longer under-coordinated. Comparisons with DFT-based calculations on the surface indicate that the MRMP2 and DFT results are similar when the surface is adequately described with a single-reference wave function. Both levels of theory predict the most favorable adsorption geometry to involve the acetylene directly on top of and parallel to a single surface dimer.

The most stable adsorption geometry of acetylene on the Si(100)-(2x1) surface is presented; however, it remains of interest to determine the pathway by which acetylene reacts with the surface. Likewise, the favored adsorption configuration of several acetylenes near each other on the surface could shed further light on experimental studies of this system, and the discrepancy between theory and experiment.

Examination of the size consistency of MRMP2 serves as a reminder of the importance of understanding the limitations of any computational method, not simply treating it as a black box. It also should serve to caution against dismissing small size consistency errors as unimportant, as these errors grow as the size of the system grows and often in a greater than linear fashion.

Finally, an ab initio/EFP exchange repulsion energy is implemented for the EFP method, which evaluates the energy using optimized molecular orbitals. It will replace the fitted term which currently includes the exchange repulsion interaction. Energy gradients are

derived with respect to both ab intio and EFP atomic positions, as well as approximate expressions for each of these gradients. This will allow an efficient gradient to be implemented for a general EFP method. Coding this gradient is the next logical step; having an available code is necessary requisite to using this method to study reactions in interesting non-aqueous solvents.

The range of topics included in this thesis spans quantum chemistry quite broadly, indicating not a lack of focus, but a breadth of interest in the many subjects encompassed by the field of quantum chemistry.

ACKNOWLEDGMENTS

This is probably the only shot I will get at an Oscar speech, so I make no attempt to be brief. There are too many people in my life who I have relied on and learned from that I could not possibly name them all, but this is my best attempt.

First chronologically, and in many other ways, is my family. My parents, Linda and Jim Rintelman, have been an unflagging source of encouragement throughout my life. They always thought that I could do anything, even or especially when I was not so sure. My two sisters, Jodi and Michelle, have become my best friends, as my mother always said they would. These four people have always been my home in that fairy tale sense of being that place in the world where everything is always okay, no matter where that place is. The positive influence of having a foundation this strong cannot be overstated.

Mary Jane and Ben will always carry a good share of the blame for the abrupt end of my career as a waitress. So much for "slinging baskets".

We all owe a debt of gratitude to the teachers we have had throughout our lives. I am no exception. Unfortunately, I will never be able to thank the most influential educator in my life. Mr. Otto Phansteil, my high school chemistry teacher for two years, passed away several years ago.

Mark Gordon has been a great mentor and great friend throughout my years in graduate school. He has been influential in many ways, both in my education in chemistry and other unrelated areas, most notably (to he and I, at least) in a sharp reversal of my political leanings and my nascent love for New York City.

Some of the most interesting conversations in my life have been with Mike Schmidt, often over lunch at Bali Satay House, or one of the other campus town restaurants in the weekly lunch rotation. It is impossible to summarize what I have learned from Mike, the subjects are too many and too varied.

There are very few problems that could not be figured out talking to Mark and Mike sitting in the entrance way to their offices.

I have never had that "we're in this together" feeling as I have had with Heather Netzloff and Ivana Adamovic, especially over the last year. It has been invaluable.

Immediately upon arriving at ISU, Tuan Nguyen and I became good friends. He has been a great friend to me ever since, especially during those months (years?) when there didn't seem to be much else in Ames.

Debbie Zorn has been a constant source of encouragement to me to always be getting ready for swim-suit season, and I hope I have been the same to her. Unfortunately, I seldom was able to keep up with the daily cake-eating regimen she recommended.

Bub, I honestly do not know if I would have made it through this without you. You have so selflessly been there whenever I needed you. I am not sure I will ever be able to return the favor. Thank you.

Since my arrival at ISU Kris Hinders has been the expert on all things non-chemistry. I cannot think of a single question she could not answer or a single problem she could not fix. On top of this she is as friendly and pleasant as a person can be. I am lucky to have gotten to know and become friends with Kris and her beautiful family.

I spent nearly four months of 2003 in Canberra with the *Gordon Group: Australia.* Our experience at the Research School of Chemistry at Australian National University was one I will always remember. It was one of the most fun times of my life. Nowhere else is there a more welcoming group of people. Thank you to Leo Radom, Geoff and the rest of the Radom Group; Adam, Chris, Kelly and the gang at the RSC.

Eraka Soder has been a great best friend to me, and has brought a great deal of joy (and at times heartbreaking sadness) to my life in Ames. She has been the best friend a friend could be. She so sympathized and empathized with my triumphs and (mini-)tragedies, I think that she felt them as strongly as I did.

Ryan McCulla, I hope that we will always be practicing.

Graham Fletcher, the love of my life. I have been extremely lucky to find someone to share my life with who knows my work so well, better than I do. I cannot thank you enough for the help you have been to me, and for enduring me while I wrote up my thesis. Thank you.